UNIVERSITY OF BELGRADE

FACULTY OF MECHANICAL ENGINEERING

RADZEYA MFTAH A. EDGENI ZAIDI

APPLICATION OF FRACTURE MECHANICS PARAMETERS TO RESIDUAL LIFE ASSESSMENT OF WELDED PIPES EXPLOITATION UNDER FATIGUE LOADING

DOCTORAL DISSERTATION

BELGRADE 2021

УНИВЕРЗИТЕТ У БЕОГРАДУ

МАШИНСКИ ФАКУЛТЕТ

RADZEYA MFTAH A. EDGENI ZAIDI

ПРИМЕНА ПАРАМЕТАРА МЕХАНИКЕ ЛОМА НА ПРОЦЕНУ ПРЕОСТАЛОГ ВЕКА ЗАВАРЕНИХ ЦЕВИ У УСЛОВИМА ЗАМОРНОГ ОПТЕРЕЋЕЊА

Докторска дисертација

БЕОГРАД, 2021

Mentor of Doctoral Dissertation

Prof. Dr. Aleksandar Sedmak

University of Belgrade, Faculty of Mechanical Engineering

Members of Committee

Prof. Dr. Zoran Radaković

Faculty of Mechanical Engineering, Belgrade

Prof. Dr. Aleksandar Grbović

Faculty of Mechanical Engineering, Belgrade

Prof. Dr. Gordana Bakić

Faculty of Mechanical Engineering, Belgrade

Dr. Snežana Kirin, senior scientist

Innovation Center of Faculty of Mechanical Engineering, Belgrade

Date of Defense:

ACKNOWLEDGEMENT

I wish to express my thanks to my supervisor and mentor Dr. Aleksandar Sedmak for his comprehensive and informative discussions valuable guidance and support. Blagoj Petrovski and Dr. Aleksandar Grbović, who was generous with me in their time, and their guidance's. The appreciation is extended to Dr.Mohamed Swei for his time and efforts and my Libyan colleagues for their support. I sincerely thank my sisters for their devoted love, encouragement, and support. Finally, I am grateful to my husband Asaad, my son Abdallah, for their love, encouragement, and understanding throughout my long endeavor.

ABSTRACT:

Thesis presents a study of the fatigue life of welded steel tubes made of API J55 steel, using the parameters of the fracture mechanics obtained on the basis of experimental research. At the same time, analyses the integrity using a FAD diagram and estimates the remaining life of welded tubes made of API J55 steel, based on experimental data, using the extended finite element method (XFEM) as one of the new calculation techniques integrated into the Abaqus software package. For simple geometries analytical methods are developed and applied.

Keywords: Fracture mechanics, Fatigue crack growth, FAD, Risk matrix

Rezime

Teza predstavalja studiju procene zamornog veka zavarenih cevi napravljenih od API J55 čelika, koristeći parametre i svojstva mehanike loma, određenih eksperimentalno. Integritet cevi je određen primenom FAD dijagrama, na osnovu koga je procenjen i rizik od loma, koristeći originalnu metodu preko matrice rizika. Preostali vek je određen takođe na osnovu eksperimentalnih podataka o koeficijnetima Parisov zakona za čelik API J55, primenom relativno nove numeričke metode, tzv. proširene Metode Konalnih Elemenata (pMKE), ugrađene u ABAQUS softver. Za slučaj jednostavne geometrije razrađena je i primenjena analitička metoda.

Ključne reči:

Mehanika loma, Zamorni rast prsline, Dijagram analize loma, Matrica rizika

Content

LIST OF FIGURES:

LIST OF TABLES:

1 Introduction

In general, cracks pose a threat to structural integrity, including pipelines. Evaluation of the defects is important for pipeline companies because some defects pipelines maybe make it defective during service periods, the more the pipeline ages, the more integrity assessment is required.

Welded pressure pipes are very sensitive to cracks and their stable or unstable growth, Cracks in welded vessels often arise in welded joints, although Errors can also occur in the base material. For safety can be avoided causes of failure of welded pipes in the oil industry and represented in the wrong choice of materials and welding effect technology, deviation from the predicted properties of materials and welded joints, the wrong method of calculating the pipe (pipeline), and deviation from the foreseen conditions of exploitation (load, temperature, working medium). Thus, defects and damage that occurs in-service must be understood and controlled, to ensure structural integrity.

We know today that variable load can trigger the fatigue mechanism in the material, starting from a microscopic formation of a crack, its growth to a critical size, and extremely to the final breakage of the construction. One of the first engineer's Researches of relevance in fatigue was performed by Wöhler. He is noticed that the application of a load cycle that is far below the static strength structure does not affect its damage at all, but if this load is repeated many times, it may lead to a complete breakdown. Therefore, pipelines as pressure equipment must be designed and constructed to guarantee safety and security in the exploitation. For this reason, a number of standards have been developed, which are introduced as mandatory, and relate to the selection of materials, construction, production, and testing in accordance with the purpose of the facility and dangerous to the environment in case of failure.

Welded pipes in oil and gas wells fall high responsible construction, so it is important to know the resistance to fracture (the residual strength) of pipes or pipelines in exploitation when there are cracks or other damage that can lead to their cancellation. Within the thesis, a study of the fatigue life of welded steel tubes was carried out strength. Using the parameters of the fracture mechanics obtained on the basis of experimental research, an estimate of the remaining life of protective welded tubes with an external is made an axial surface crack, made of API J55 steel. At the same time, range of amplitude stress and crack size effects on the remaining fatigue life are analyzed. It is also using the extended finite element method (XFEM) as one of the new calculation techniques in the crash growth-modeling domain structure, which was created as a result of numerous researches in the last

ten years. This technique enables presentation discontinuity independent of the network of finite elements, and that using enhancement features as a means of displaying all of the discounted behaviors.

2 Pipeline

Pipelines transport and distribute fluids. Small diameter gathering lines collect the product (crude oil, liquefied petroleum products,) from where it is extracted, after moving to a gathering facility, it moves to feeder pipelines with relatively large diameters which transports the product to refineries. Pipelines can have seam or seamless pipes and their specifications defined by the API standard [1][2]. Typical pipelines in oil and gas industry are shown in ***Figure. 2.1***.

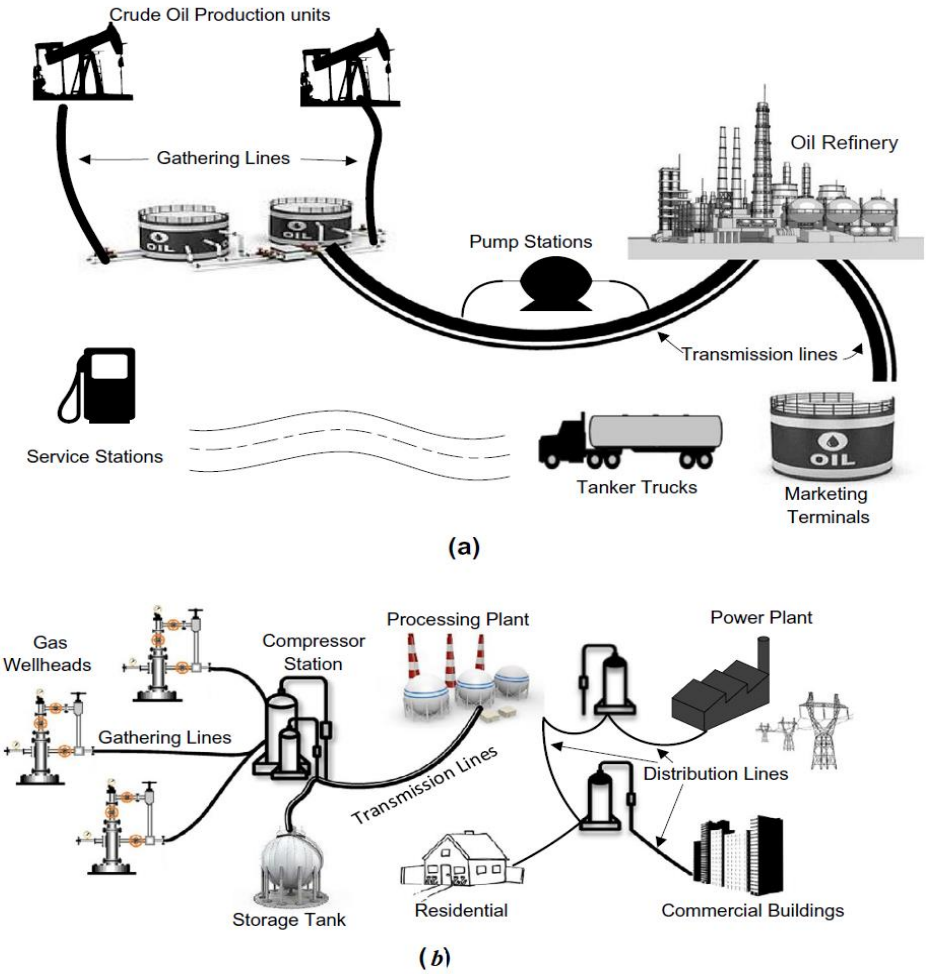

Figure 2-1: Oil and gas pipeline system: (a) Oil pipeline system (b) Gas pipeline system, adopted from Natural Gas Pipelines (2015).

2.1 Hazard of Pipelines

Transmission pipelines, that carrying natural gas are hazard to people and properties. Their failure rate depends on many factors, like design, construction, maintenance and environment, ***Figure 2.2***. [3]

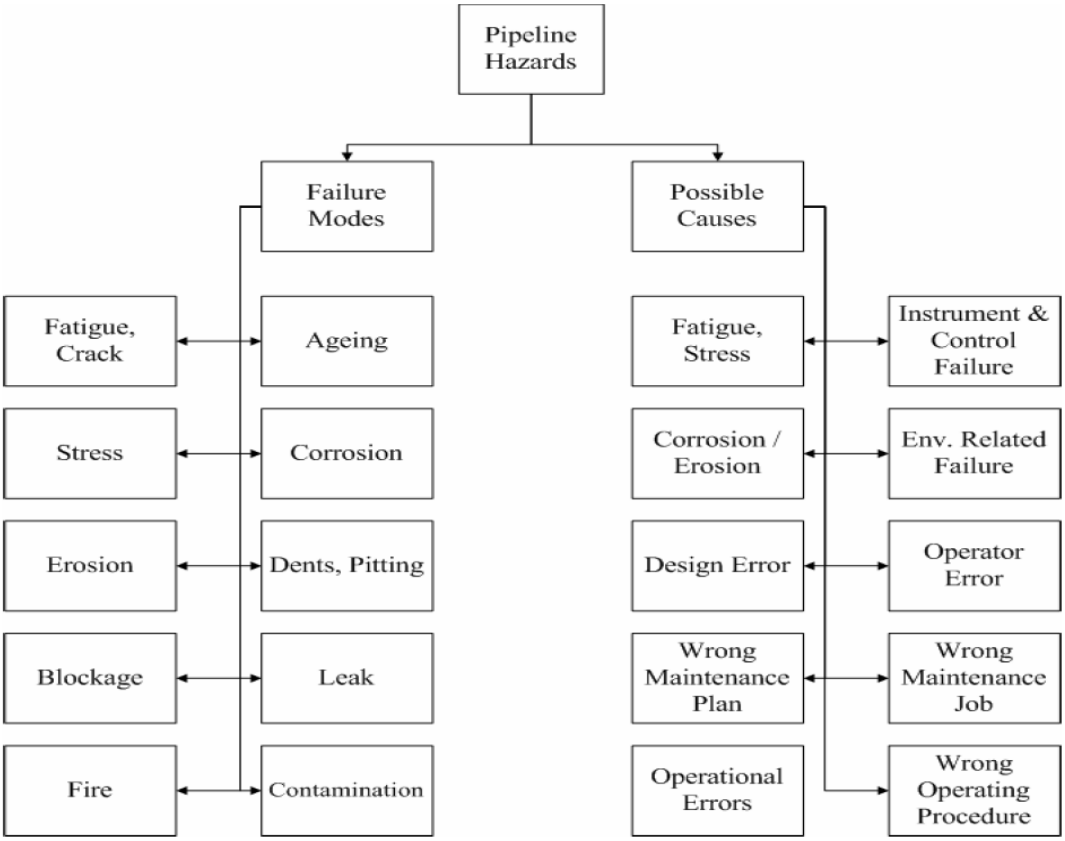

Figure 2-2: Hazard classification for pipelines

2.2 Pipeline Integrity

Structural integrity assessment of pipelines is very important for safe exploitation and prevention of possible failure.

2.2.1 Failure Types in Pipeline

Pipeline failures mostly occur due to effects of environment and stresses, as well as material properties and defects. Categorizes the failure types that can occur in oil and gas pipelines into five groups [4]:

i. Mechanical: This failure results from a material defect or construction fault. Failure typically occurs by an external force acting on overloads the pipe to the point where failure occurs, or when a pipeline presence on a rock causes a hole dent, and the damage that occurs when the pipe is struck by earthmoving equipment, [5].

ii. Environmentally induced failures include internal and external corrosion, stress corrosion cracking, chemical attacks, weld seam corrosion, as well as internal erosion.

iii. Material, construction, and fabrication failures occur due to errors such as are seam and girth weld errors, laminations, hard spots, and weld pinholes, [6].

iv. Operational failure is a result of errors from operator inaccuracy/error, break down or insufficiency of safeguarding systems.

v. Natural hazard results from flooding, lightning strikes, shifting land, earthquakes, hurricanes, and volcanoes.

2.3 Steel Weldments

Today, with the requirement of strength in design, the risk of fracture, which is large, must also be considered depends on the characteristics of welded joints. Local properties of welded joints and the danger of the existing errors are two basic factors for safety construction. It is important to be good weld ability of the selected material for making constructs, in order to obtain compounds of suitable properties, with little chance of occurrence of errors. Steel pipes must have adequate strength, ductility, impact toughness, and rigid for special applications Corrosion and oxidation resistance and deformation resistance crawling at working temperature. Different alloying elements are added to achieve different required properties. For this reason, it is ideal to work in complex conditions to choose the composition that gives it optimal combination of properties for a specific purpose. In doing so, the price must be taken into account, the choice of steel should be directed to the cheapest solution with the corresponding properties.

Recently, the choice of materials for equipment in the exploitation of oil has significantly expanded gas. Carbon, low alloy, alloyed and high alloy steels are used, as well non-ferrous alloys. Materials are classified into classes according to tensile strength, and the minimum value which is stated in the manufacturer's documentation represents the lower limit of tensile strength. Today, in the world, the biggest issue is the production of pipes for the petroleum industry use the American Petroleum Institute (API) standards. These norms standardized steel quality, pipe length, diameter and wall thickness, joints and threads.

2.3.1 Welding Steel Pipe Classification

Steel pipelines for the transmission of gas and oil may extend thousands of kilometers and they represent one of the most sophisticated engineering achievements of the modern era. There are two main types of pipes for industrial use. One is the seamless pipe and the other is produced in the form of a pipe by welding. Some of the steel tubes are manufactured from plates that are formed into an appropriate shape and then seam welded. An efficient and high productivity process for achieving this involves high-frequency welding in which the abutting surfaces are forged together following localized heating.[7]. The most widely used categories of welding methods for pipe making are gas

metal / submerged arc welding and electric resistance / induction welding, [8][9], as shown in ***Figures. 2.3-2.4.***

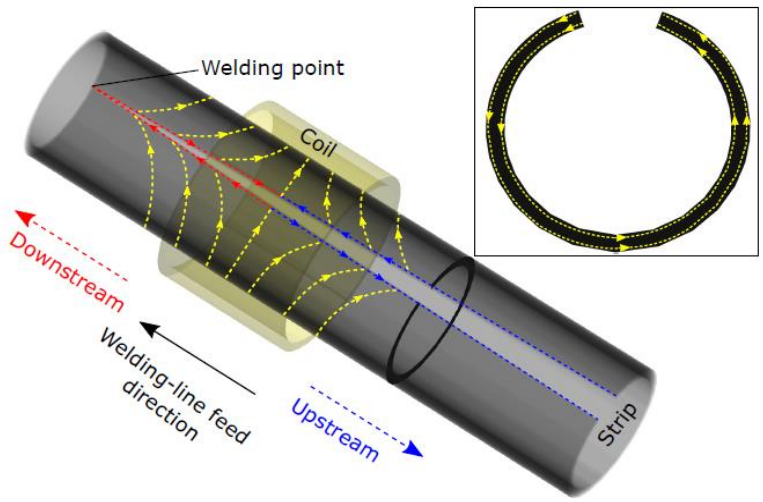

Figure 2-3: Schematic current path in the tube

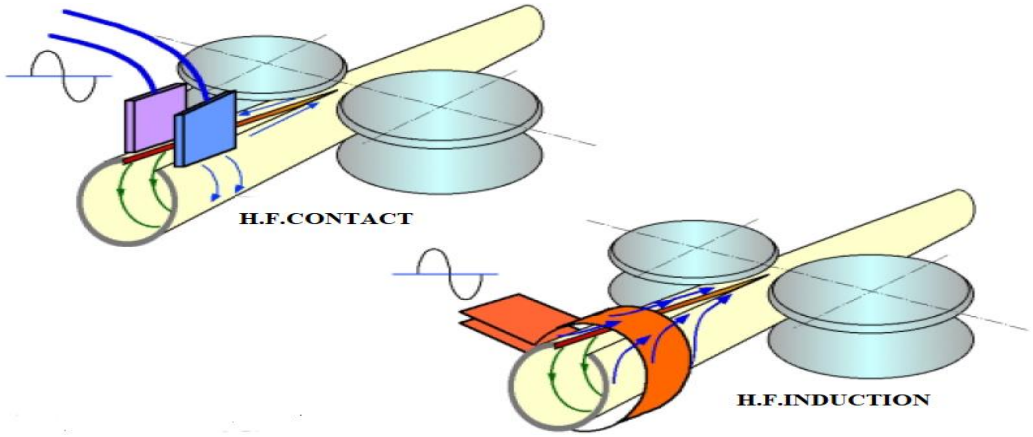

Figure 2-4: High Frequency Welding

2.3.2 HF Induction Welding

High-frequency induction welding is shown in ***Figures.*** **2.5**

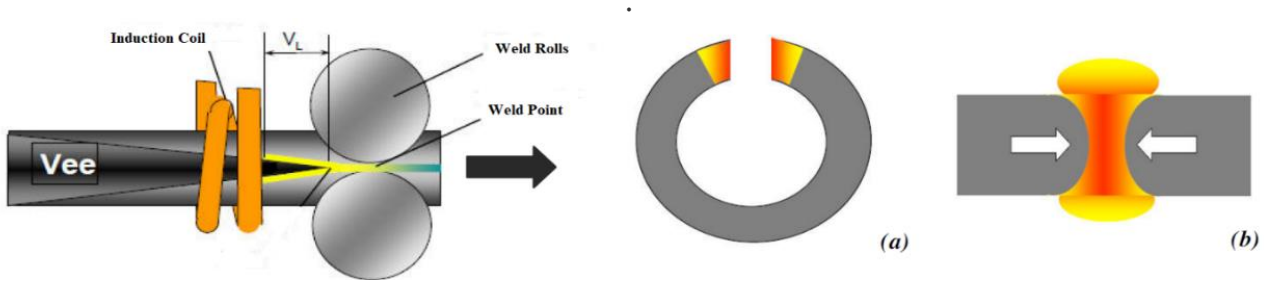

Figure 2-5: HF induction welding (a) heating of coil edges (b)forging during HFI welding for pipe production

The HF weld has no filler metal and, if done properly, no molten or oxidized metal is left on the bond line. ***Figure 2.6*** shows that all of the molten thin layer and metal oxides and other inclusions are squeezed out of the weld toward the outside and inside surfaces as the edges pass between the weld rolls. The high frequency current follows a "Vee" shaped path down one edge of the "Vee" and up the other, from one sliding contact (A) to the other (B), completing electrical circuit, ***Figure 2.7.*** During high frequency heating, high frequency current enters the strip edge from the top and the side of the edge. The parent metal melting occurs in butting (roughness) surfaces and this molten layer formed is squeezed out from the edges together with the oxide films. Heat penetration produced by high frequency current into the edges of the parent metal is greater at the top and bottom corners and less at the middle wall thickness, ***Figure 2.8***

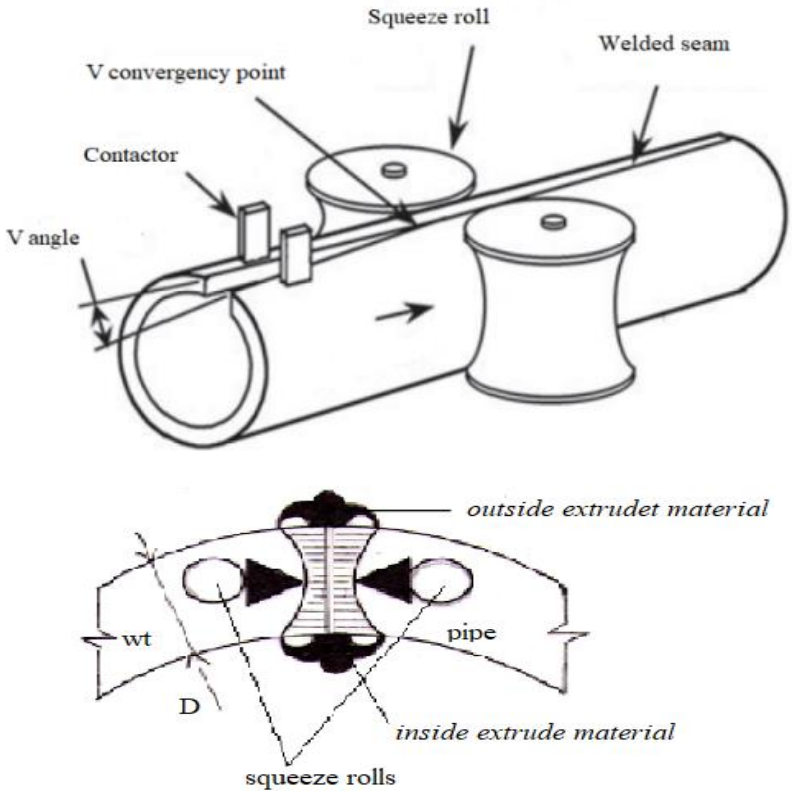

Figure 2-6: HF electric resistance forge weld

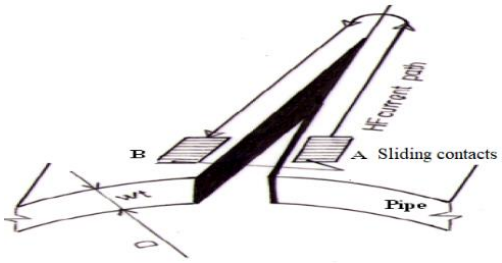

Figure 2-7: Sliding contacts of HF current

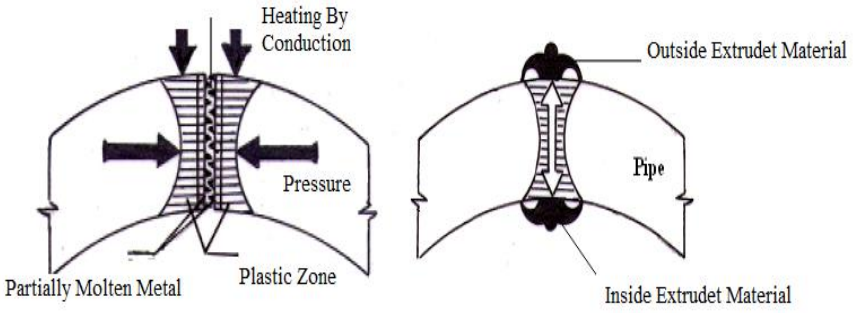

Figure 2-8: Schematic sequence of HFERW

From the metallurgical point of view, high frequency electric resistance welding (HFERW) is characterized by extremely rapid heating and cooling over a very short period combined with forging pressure. This specific thermal cycles combined with forging pressure are important metallurgical factors. As a result of these metallurgical factors some complex microstructure changes can occur.[10]

Cold Cracks

Cold cracks form in the weld at some point in time after the weld has cooled[11]. ***Figure 2.9a.***

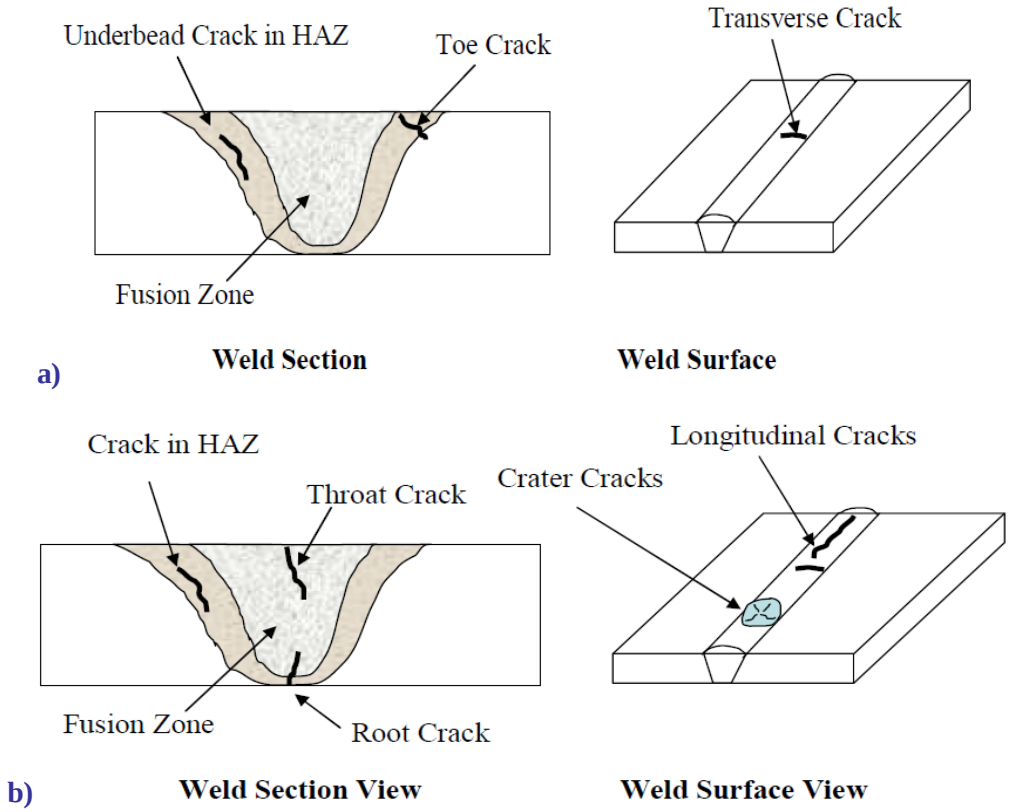

Figure 2-9: Showing locations of typical (a) cold cracks (b) hot cracks in welds

Fatigue and corrosion Cracks

Fatigue and corrosion cracks are shown in ***Figure 2-10***

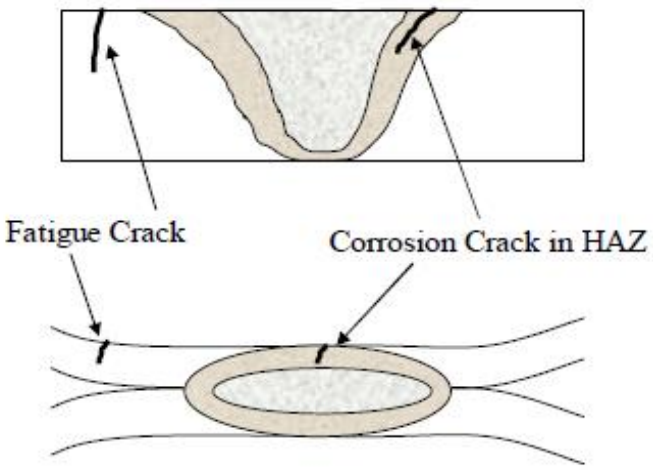

Figure 2-10: Schematic showing locations of fatigue and corrosion crack in and near the welds

Pipeline Cracks are shown in ***Figure 2-11***

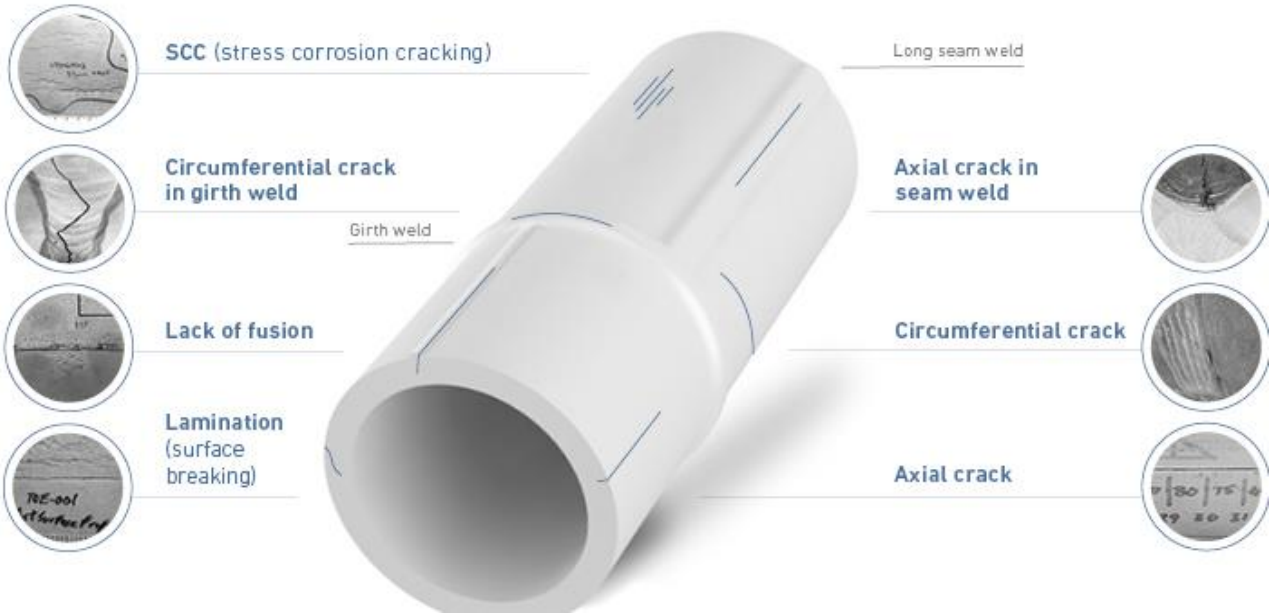

Figure 2-11: Some examples of pipeline cracks

2.4 Pipeline Inspection Management and Safety

Figure 2.12 shows based on EGIG data the distribution of the causes of the accidents occurred between 2004 and 2013 [3]. Inspection techniques and tools are shown in ***Figure 2.13***, **2.14** respectively.

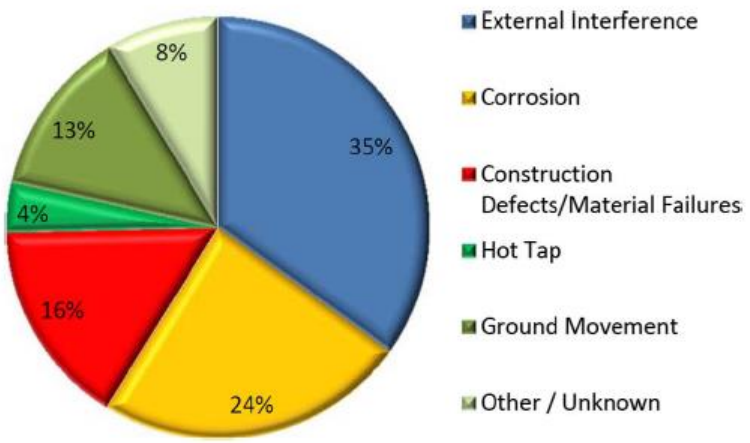

Figure 2-12: The causes of the damages occurred in gas pipelines[12]

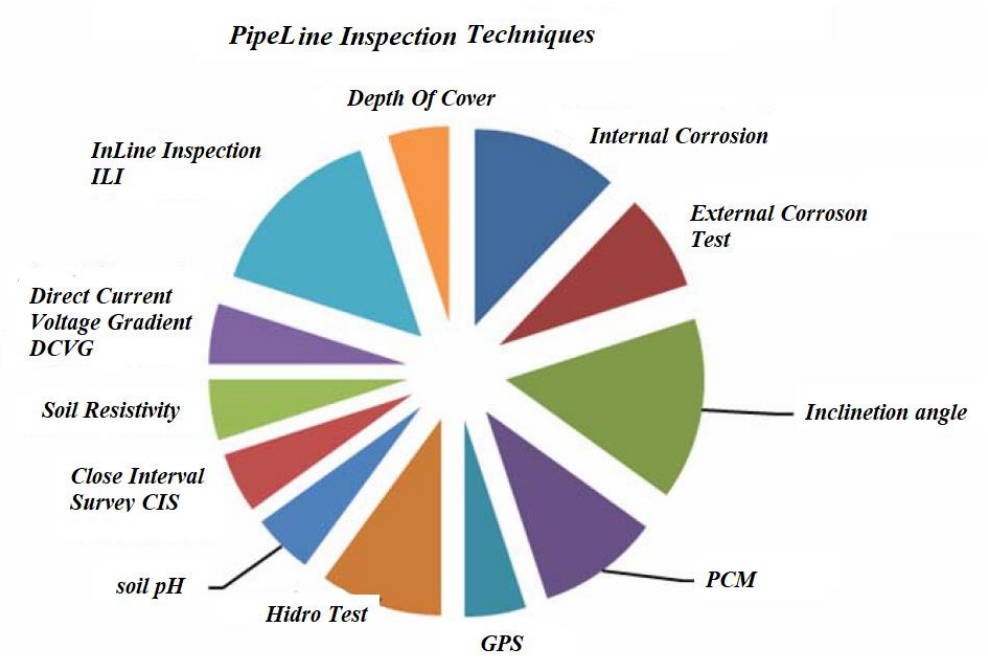

Figure 2-13: Pipeline inspection techniques

a ***b***

Figure 2-14: Inspection tool (a) Crack inspection tool (Results cracking) (b) Flux leakage tool

3 Fracture Mechanics

3.1 Fundamentals of Fracture Mechanics

To improve the performance of mechanical components, Fracture mechanics plays a big role in modern material science and mechanical engineering, a field dealing with crack propagation under loading in a material of a structure, by correlates analytical investigation of crack propagation with related experimental work and characterizes material resistance to fracture, ***Figure 3.1***. Such analytical investigation is done by calculating parameters like the stress intensity factor at the crack tip is further used to determine the crack growth rate under cyclic loading, i.e. fatigue. Each applied cyclic load causes an increase in crack length. Fracture mechanics is divided into linear elastic fracture mechanics (LEFM) and elastic plastic fracture mechanics (EPFM). LEFM is a design methodology applicable under elastic conditions to deal with brittle-elastic materials such as high-strength steel, glass, ice, and concrete, [14]. On the other hand, EPFM is valid for materials that exhibit non-linear stress-strain behavior, as for example low-carbon steel, stainless steel, and certain aluminum alloys (Anderson 2005), [13],[15],[16].

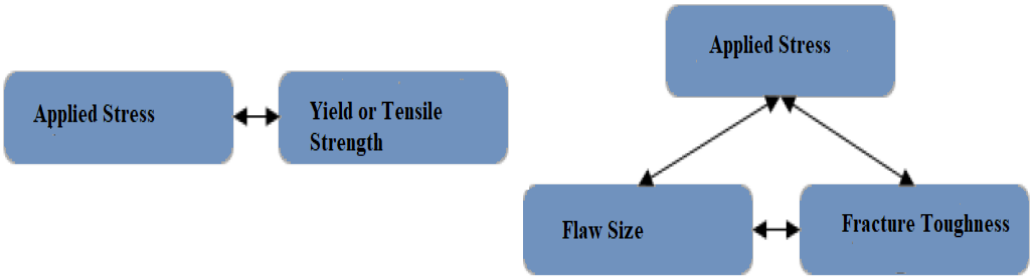

Figure 3-1: Relation of (a) Classical Failure (b) Fracture Mechanics

3.1.1 Stress Intensity Factor by The Raju and Newman Method

Longitudinal semi-elliptical surface cracks on are often present in pipelines, with geometry as in ***Figure 3.2*** [17]. According to Raju and Newman the stress intensity factor at the mid-point of a longitudinal semi-elliptical surface crack under internal pressure is:

$$K_I = \left(\frac{pR^2}{R_o^2 - R^2}\right)\sqrt{\frac{\pi a}{Q}}\left[2G_o + 2\left(\frac{a}{R_o}\right)G_1 + 3\left(\frac{a}{R_o}\right)^2 G_2 + 4\left(\frac{a}{R_o}\right)^3 G_3\right]$$

$$Q = 1 + 1.464\left(\frac{a}{c}\right)^{1.65} \qquad For \quad a/c \leq 1$$

Q is the shape factor [18], and other quantities are define in ***Figure 3-2***.

The corresponding coefficients Gj (j = 0, 1, 2, 3) was obtained from the appropriate finite element analysis results for the particular values of t/R, a/c, a/t, and $\emptyset$. The corresponding coefficients Gj (j = 0, 1, 2, 3) are determined by matching of the results with finite element analysis results in the case of a/c = 0.2, 0.4, 1.0; t/R= 0.1, 0.25, and a/t = 0.2, 0.5, 0.8. [19] .

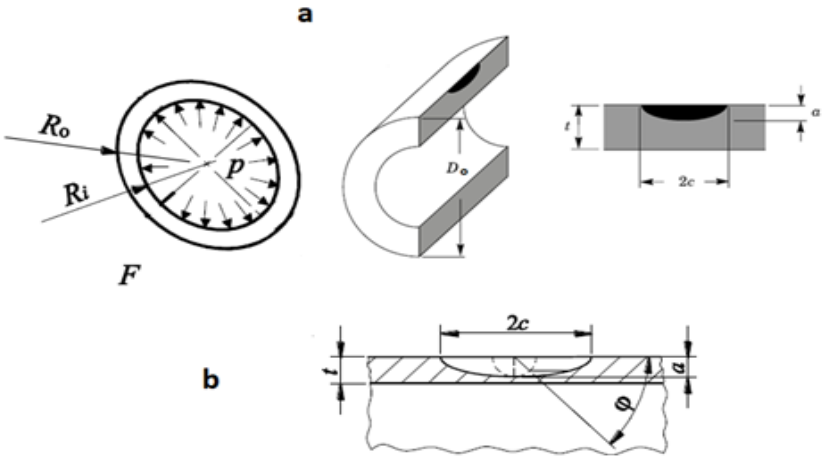

Figure 3-2: a) Schematic illustration of the pipe specimen with external surface crack, b) crack geometry. p - internal pressure, Ri - inner radius, Ro - outer radius, t - wall thickness, a – crack depth, c – crack half-length

3.2 Fatigue Crack

Cyclic loading may initiate microscopically small fatigue crack, which can be followed by crack grows to macroscopic size, and to failure, reducing thus the fatigue life. ***Figure 3.3*** presents this scenario graphically with the crack length a as a function of the number of cycles, N. Thereby, a_i is the initial crack length, a_d a detectable crack length, and a_c the critical crack length. The corresponding numbers of cycles are N_d, and Nc, so the extended life equals N_c-N_d, [20].

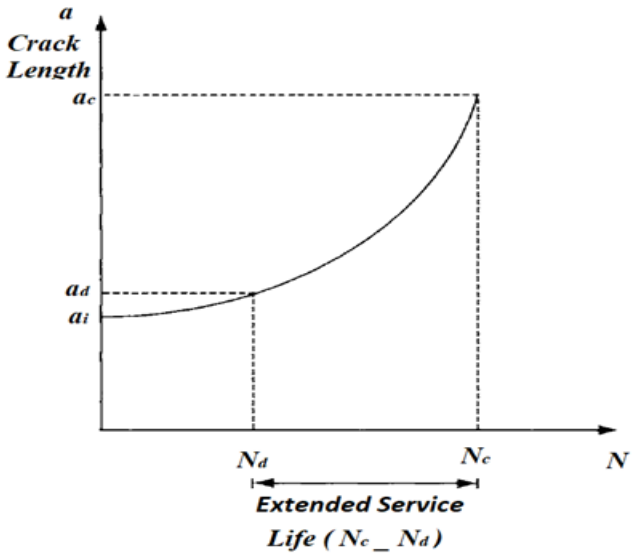

Figure 3-3: plotting the crack length a as a function of the number of cycles, N

3.3 Crack growth rate

If in one cycle fatigue crack grows by an increment Δa, its length becomes a+Δa, defining at the same time he fatigue crack growth rate, irrespective of the loading frequency. Therefore, if N denotes the number of cycles, the fatigue crack growth rate is defined as da/dN (mm/cycle), [21], ***Figures 3.4 and 3.5.***

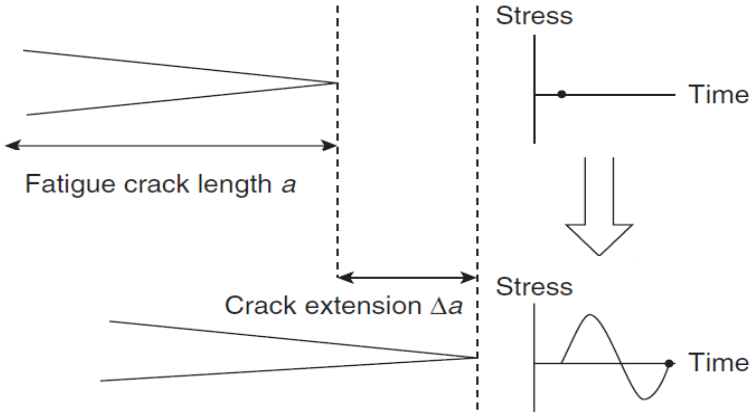

Figure 3-4: Fatigue crack extension over one stress cycle.

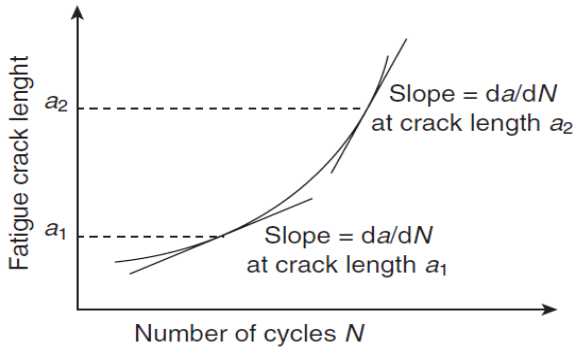

Figure 3-5: Fatigue crack length. The slope at any point gives the crack growth rate.

3.3.1 The Crack Growth Process

Because of microscopic plasticity which can occur below the yield stress, and damage accumulation with the number of cycles of loading, fatigue failure occurs. Four important stages of fatigue can be identified: 1. Crack initiation. This occurs mostly at surfaces or sometimes at internal interfaces. Crack initiation may represent within about 10% of the total life of the component. 2. Slip-band crack growth along planes of high shear stress, this an extension of the slip process which leads to crack formation (something like deepening of the crack formed). Crack growth: in this stage, the crack grows along with directions of maximum tensile stress, crack propagation is trans-granular. 4. Ductile failure: reduction in load-bearing area due to crack propagation leads to ultimate failure. When a specimen ***Figure3.6.a*** is subjected to uniform loading, dislocations moving on parallel slip planes

leave the free surface of crystal / grain, giving rise to slip lines on the surface of the specimen (***Figure 3.6b***). Due to the accumulation of slip, slip bands form which increases with the number of cycles, and further due to oscillatory loading, this can lead to extrusions ***Figure 3.6c*** and intrusions ***Figure 3.6d***. The intrusions can act like a notch, which is a stress concentrator and are a precursor to a full-blown crack, [22].

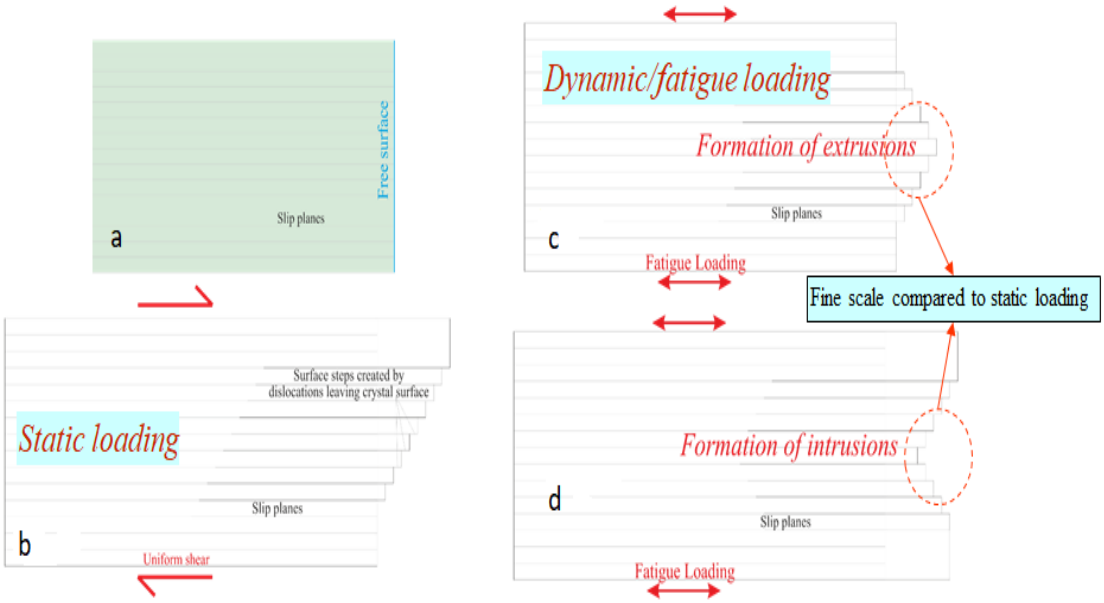

Figure 3-6: Crack growth process

4 Risk Assessment and Analysis

Due to accelerated technological development, a large amount of information that must be obtained and processed, understand, and evaluate has become essential for business, the large amount of information shows that enough empirical knowledge has already been gathered on how to understand and evaluate risk with the transformation of knowledge into concrete actions. The risk becomes the most important criterion for deciding in which direction to act when a situation is considered risky. One of the key factors and preconditions for long-term industrial competitiveness, making the industrial production safe, which contributes to successful and responsibly managed business, to enable a continuous business process. Safety in relation to industrial activities includes factors such as critical infrastructure safety; safety in the process and chemical industries; Safety in the production of oil and oil derivatives and their transport and distribution, transport systems related to industrial activities, energy supply, railway and road networks, domestic deliveries, airports, ports, etc. Prevention of major industrial accidents with off-site consequences for the environment, people, and society is a challenge that must be addressed through research that will later lead to innovations to promote safe processes and products. The study of safety does not take place within one scientific discipline but requires the cooperation of researchers from different fields: engineering to analyze risk and define boundaries for risk acceptance, sociology to understand risk aversion and ensure confidence that boundaries are set in accordance with perception and stakeholder expectations, as well as to propose appropriate communication and consultation mechanisms, accountability rules, etc. Investments in security refer not only to the reduction of financial losses caused by industrial accidents but also to represent an opportunity for development, which leads to industrial growth[23].

4.1 Structural Integrity

Structural integrity, a term used to describe objects or structures that are liable to breakage to describe an important problem in the event of a failure in service, that structural integrity can be considered at a global and at the local level. Global structural integrity refers to an object or structure as a whole. The loss of structural integrity at the global level means complete destruction of a structure that cannot be repaired, but also damage that can be repaired after important redesign and reconstruction. The loss of structural integrity at a local level indicates local deterioration or crack occurrence that requires small repair, and in some cases, after proper structural integrity assessment, the use of the structure can be permitted for specified. In many cases experienced failure of objects is not explicable at the time of occurrence, requiring detailed and extended investigation, research, and experimental analysis.

It became clear that the full answer to complex problems can be given only after a series of full-scale laboratory tests, the extended investigation was directed to cracks in a structure, to establish a new discipline, fracture mechanics. Fracture mechanics serves as the basis for structural integrity assessment. The term “structural integrity” is accepted to define the condition in which the structure can be used in service reliably, regarding function and safety, even in the case of existing defects.

Structural integrity assessment defines the significance of an existing crack (crack is considered as the most critical defect in a structure) in a structural component and all the actions that are to be taken to assure reliable operation. Structural integrity is considered an essential component of all structural engineering projects, structural engineering encompasses the parts of equipment of large structures, and structural integrity largely refers to the soundness of design and construction, including workability and safety. For that, it plays an important role in the safety of sometimes large populations of both humans and wildlife.

Two aspects of structural integrity require attention: the first is connected with the intended use and functionality, the second is the object size and its complexity. It is not possible to treat structural integrity in the same way for all. The difference in structural behavior can be characterized by many influencing factors. The first factor is design, depending on the intended function and use, in addition to, environment, loads, and material and manufacture of components. Structural integrity assessment is an approach to evaluate whether a structure is fit to withstand safely and reliably the loading and operating conditions, and integrity refers to the quality of the structure to be whole and complete, ready for the purpose, or in the unimpaired state.[24]

4.1.1 Pressure Equipment Structural Integrity

Pressure equipment considered an important part of modern life and production, basic components in pressure systems are pressure vessels and pipelines, exposed to the inner pressure. Pressurized components operating in severe conditions fail frequently, and thus structural integrity assessment is one of the basic requirements for their use. In spite of all measures undertaken, failures of pressurized equipment still occurred. The occurrence of an initial crack in the welded joints, fatigue crack growth under variable loading, continued stable crack growth in the ductile material, and final fracture of the reduced cross-section due to overloading, of the most predictable reasons for failures. [24]. The failure can be from negligible to till catastrophic consequences with human loss and great material damage and therefore welded joints are prone to crack occurrence, and for that, they are critical locations for safety and structural integrity. So, the cracks, as possible cause of fracture, present serious damage in welded structures, are not acceptable in welded structures according to standard

(EN ISO 5817), and quality assurance (QA) accepts only new products of certified quality, which means with defects and imperfections of acceptable size, according to relevant standards.

Inspection and maintenance in service are necessary to ensure structural integrity, and thus safe and reliable operation, redesign, reconstruction, and repair in service have to be performed frequently. And because welding is an important process in design and repairs. It is almost impossible to repair pressure equipment components without welding. Weld repairs should be performed in accordance with all previous decisions regarding the design of a considered structure, materials, standards processes, and procedures, hence, quality assurance and structural integrity in service have to be verified after the performed reconstruction or repair.

The defects are likely to appear in welded joints because of complex microstructure in different regions (Base Metal - BM , Weld Metal - WM, Heat Affected Zone - HAZ), being more or less sensitive to cracking, according to the Pressure Equipment Directive (PED 97/23/EC) .[25] Cracks are not acceptable defects in welded structures, according to standard (EN ISO 5817), therefore, disregarding their potentially disastrous effect is not an option .so if these defects are detected in so-called unaccepted form and size, according to standard (ISO 5817), careful consideration is definitely required and the decision to be made by top management, and knowledge structural integrity point of view and applied for pressure vessels based on fracture mechanics parameters, also introducing quality assurance, and risk-based approaches, as two specific , additional aspects[26]. Risk-based approach, in one of its simplest forms, uses the risk matrix ***Figure 4.1***with one axis representing probability and the other one, representing consequence.

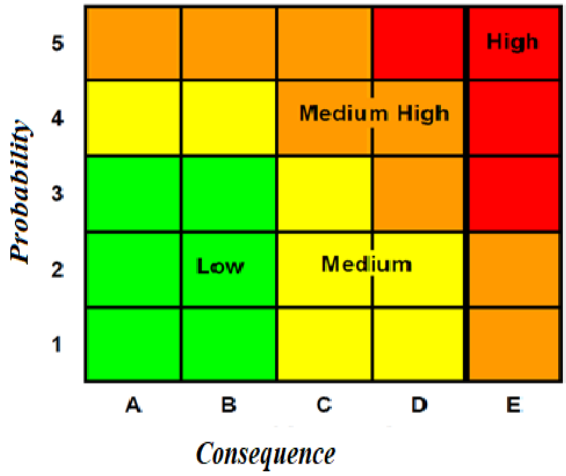

Figure 4-1: Risk matrix

4.2 Risk Analysis in Structural Integrity

Risk management within the business process is a challenge especially in industrial processes where certain risks can be at an extremely high level, and their consequences are great. New risk-based decision-making procedures are an effective operational tool if used properly. There are a number of applied risk-based concepts, such as Quantitative Risk Assessment (QRA), Risk-Based Control (RBI), Risk-Based Control and Maintenance (RBMI), Reliability-Based Maintenance (RCM), Risk-Based Lifecycle Management (RBLM), or simply, Risk -Based Management (RBM). These procedures are in an advanced stage of application in developed industrial countries, especially when it comes to operation, control, maintenance, and asset management, and form a well-established part of modern practice.

Due to the intention to increase the availability and efficiency of industrial plants, there is a great need to define the technical content and connection with local legislation and further integration of risk-based approaches. Risk-based control offers this concept, assessing risks that include determining the probability, while the consequences can be defined through the level of risk, and accordingly adjust the control intervals without compromising operational safety.

Equipment is exposed to deterioration and potential failures during its service life, where the consequences of losing the integrity of the equipment are such that its existence would be endangered (eg thermal and hydropower plants, oil companies, chemical, and petrochemical industries). A typical example of such equipment are pressure vessels, where the probability of loss of integrity is very small, but the possible consequence is so great that the risk of integrity must be placed at the center of the risk management process. The integrity of the equipment is ensured by good design, as well as its operation and maintenance, it is necessary to be sure of the current condition of the equipment in order to determine the date of the next inspection. Therefore, a risk-based approach (RBI) has been introduced that allows the assessment of the probability and potential consequences of equipment failure, which gives companies the opportunity to set control priorities. High-risk equipment components should be inspected frequently, while other components are inspected much less frequently, in proportion to their risk. In accordance with the contribution of the components to the overall risk of the equipment, it is possible to determine which components should be controlled according to the level of risk. Based on that, an appropriate control program can be established, which includes optimization of control methods, frequency and resources, [27].

4.3 Risk Assessment Based on Structural Integrity

According to API581 probability is defined as "the extent to which an event is likely to occur within the time frame under consideration. The mathematical definition of probability is a real number in the scale 0 to 1 attached to a random event. Probability can be related to a long-run relative frequency of occurrence or to a degree of belief that an event will occur. For a high degree of belief, the probability is near one. Frequency rather than probability may be used in describing risk. Degrees of belief about probability can be chosen as classes or ranks like, rare, unlikely, moderate, likely, almost certain, or incredible, improbable, remote, occasional, probable, frequent", [28]. Anyhow, API 581 procedure for risk assessment is complicated one, as is the case with its European competitor, [29], RIMAP. As defined in ISO 31010 standard, 3 approaches can be used to evaluate the probability:

a) The use of relevant historical data to identify relevant events or situations, with the aim to extrapolate the probability of their occurrence in the future.

b) Probability forecasts using predictive techniques such as fault tree analysis and event tree analysis. Simulation techniques may be required to estimate probability failures due to degradation processes, by calculating the effects of uncertainties.

c) Expert opinion, based on advanced knowledge, such as fracture mechanics and structural integrity. There are a number of different methods for eliciting expert judgement which provide an aid to the formulation of appropriate questions.

The first and second approach are not applicable here, since there is no data about previous history and it is based on survey or similar activities, respectively. The third one is actually used here, by applying the original methodology, based on risk matrix, ***Table 4.1***. Thus, the probability of failure is defined by the position of the point in ***Figure 4.2,*** **FAD**, corresponding to the given data on geometry, loading and material, including crack effects, keeping in mind the fact that point position close to zero indicates low probability, whereas position close to the limit curve indicates high probability. Obviously, any point in between indicates probability proportionally to its position. ***Figure 4.2*** also shows acceptable and unacceptable flows (defects) in accordance with their position at the FAD.

Table 4-2: Descriptive risk matrix [30][31]

	Potential consequences				Event Frequency				
	People	Property	Environment	Reputation	A	B	C	D	E
					Negligible	Low	Moderate	Medium	Large
1	Insignificant injuries	Loss up to 10 K€	Minor damage to environment	Insignificant consequences. Employees awareness.					
2	Minor injuries	Loss from 180 K€ to 540 K€	Minor consequence and damage to environment. Small costs..	Mild consequences. There is a concern at the local level.					
3	Serious injuries	Loss from540 K€ to 1,8 M€	Moderate consequence. Short-term damage to environment..	Minor consequences. There is a concern at the regional level					
4	Permanent incapability	Loss from 1,8 K€ to 50 M€	Major consequences. Big damage to environment. Large costs.	Moderate consequenes. There is a concern at the national level.					
5	Death	Loss over 50 M€	Dire consequences. Lomg-term and big damage. Huge costs.	Dire consequence..Concern and reaction at the international level.					

LOW RISK LEVEL

MODERATE RISK LEVEL

HIGH RISK LEVEL

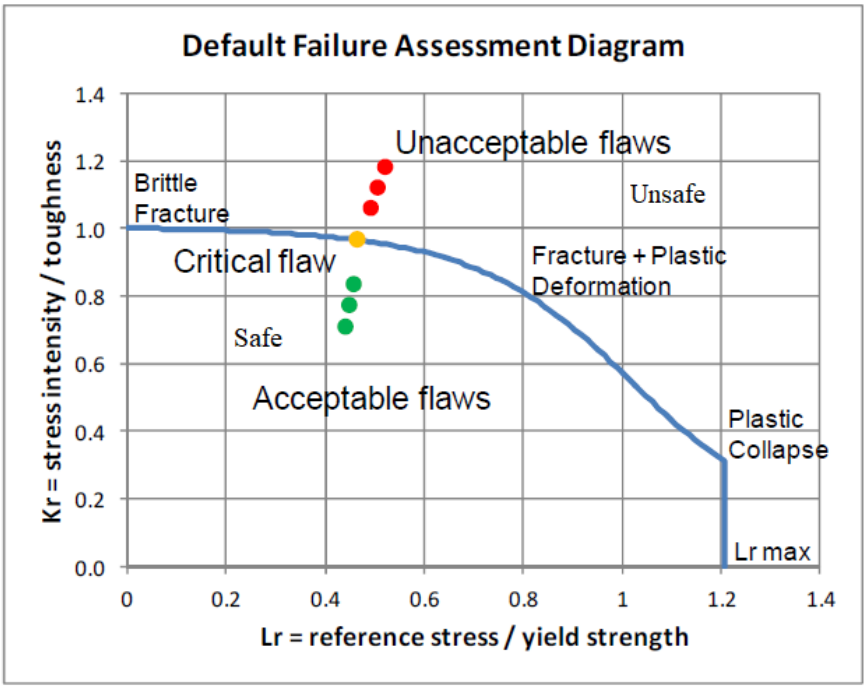

Figure 4-2: Failure Assessment Diagram

4.4 Fundamentals of Risk-Based Approaches

4.4.1 Risk Assessment

Risk assessment includes identification of event sources, estimating the risk as a function of the probability and consequence of the event, and evaluating the results. Risk in its simplest form is defined as the product of the probability and consequence: Risk = probability * consequence. Consequences are typically estimated according to four factors: - people, property, environmental and reputation, [32].

4.4.2 Risk Based Approach

Crack-like defects are the biggest risk in pressure vessels, these defects are likely to appear in welded joints because of complex microstructure in different regions (Base Metal - BM, Weld Metal - WM, Heat Affected Zone - HAZ), being more or less sensitive to cracking. Therefore, disregarding their potentially disastrous effect is not an option. So, if these defects are detected in so-called unaccepted form and size, according to ISO 5817 standard, careful consideration is definitely required and the decision to be made by top management. To overcome the gap between engineers and managers, there is a need to provide simple, e.g. risk-based structural integrity assessment of all cases involving crack-like defects[33].

Structural integrity point of view has been explained and applied for pressure vessels based on fracture mechanics parameters, but also introducing quality assurance, and risk-based approaches, as two specific, additional aspects. A risk-based approach, in one of its simplest forms, uses the risk matrix with one axis representing probability and the other one, representing consequence. In the risk matrix shown in ***Table 4.2***. Regarding consequence, they are categorized from lowest, almost negligible consequence, to fatal and serious consequences.

Regarding probability, new concept is used for crack-like defects, based on the linear elastic fracture mechanics, using the Failure Assessment Diagramme (FAD. The basic concept of FAD is to evaluate the ratio between the local stress and its critical value, i.e. Yield or Tensile Strength (X coordinate), which can be interpreted as the probability of plastic collapse, and the ratio between the stress intensity factor and its critical value, i.e. fracture toughness (Y coordinate), which can be interpreted as the probability of brittle fracture, and, ***Figure 4.3***. The point defined by these two coordinates can be in the safe or in the unsafe region, separated by the limit curve. Thus, the probability of failure can be estimated as the ratio of the distance from the point to zero points and the distance from the corresponding point at the limit curve and zero points.

Table 4-3: Risk matrix

Risk		Consequence category				
		VL	L	M	H	VH
Probability category	VH	Medium	Medium high	Medium high	High	Very high
	H	Medium Low	Medium	Medium high	High	High
	M	Low	Medium	Medium	Medium high	Medium High
	L	Low	Low	Medium	Medium	Medium high
	VL	Very low	Very low	Low	Medium	Medium

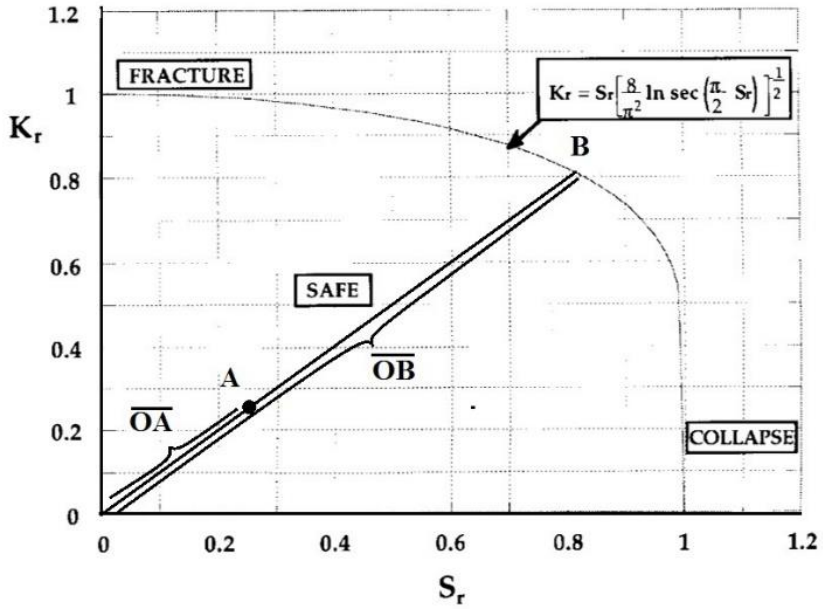

Figure 4-3: Failure Assessment Diagramme.

4.4.3 Approaches to Risk Analysis

Qualitative

Risks within a qualitative approach are usually presented within in a risk matrix as the qualitative approach of RBI[34] is intended for:

• screening of units within the location in order to select the level of the required analysis and determine the benefits of future analyzes

• ranking the degree of risk within the unit and assigning positions within the risk matrix, and identifying areas of potential interest in the plant.

This approach requires less detail and significantly more time. The results of this analysis are not accurate but this method provides a basis for prioritizing a risk-based control program.

Semi-quantitative

Semi-quantitative risk assessment is a combination of experience and operational and inspection data analysis for the mode of failure. This approach is popular among oil and gas companies because it takes into account the required engineering and scientific assessment and experience simultaneously.

The analysis of accident scenarios should generally be more numerically based and detailed than the qualitative approach, but may still contain a large element of engineering judgment[35].

Fully quantitative

A quantitative approach is more complex and software is increasingly necessary as it encourages standardization of assessment to improve efficiency. The approach uses engineering and scientific assessment to predict and calculate the mode and consequence of failure. Quantitative RBI requires more data input but should provide greater consistency between users and over time. The main disadvantage of this approach lacks the experience-based judgment to optimize the resultant risk.

Advantages and Benefits Of RBI

- Improve the efficiency of control and maintenance processes based on the analysis of all available data related to the equipment.
- Precise definition of the hazard zone during plant operation in accordance with standards, guidelines and / or rules that make plant safety issues transparent and competent authorities and the public.
- Reducing the level of potentially hazardous situations through more effective and timely control and maintenance, which would result in increased confidence in the operation of the plant.
- Provides a good basis for the implementation of a rational and cost-effective decision-making process which, at the same time, ensures the required level of safety, because:
- It is possible to identify the highest and least risky component of equipment.
- control, when it will be controlled and how the control will be performed.
- Basic requirements related to control methods can be determined.
- Saving 5-20% of maintenance costs based on control optimization programs and further cost savings.
- The control and maintenance system can be easily compared to similar plants [27].

5 Fatigue Life of The Structure

Cracks in the welded joint cannot be excluded but should be analyzed the influence of crack growth when considering construction safety, [36]**,**because the operation of a welded structure depends on its safety under the applied load. When a failure might endanger human lives the requirements regarding becoming security of the structure are very strict Nevertheless, catastrophic failures still occur in the exploitation of welded structures. In most, cases failure is caused by the existence of cracks of critical size. Structural safety and integrity analysis have to consider the influence of the fatigue crack and its threshold value, eventually followed by in-service propagation through parent metal (PM), weld metal (WM) and heat-affected-zone (HAZ) of the welded joint. To predict the service life of many structures, an understanding of the fatigue crack growth rate in structural material is essential[37]. For safe operation thus, the corresponding data have to be defined in the material specification when a detected crack initiates, and analyzed possible mechanisms of crack growth to a critical size and the condition of a fracture occurrence must be considered [38].

In operating conditions, basic requirements each welded structure has to satisfy are safety and reliability, for fulfilling this requirement requires experimental investigations and results in interpretation to obtained a detailed description of welded joint properties because they are of crucial importance. Surface cracks are the most frequent defects in welded structures resulting from imperfections in the welded joint, such as corrosion damages, cracks in the fusion region, welder's markings, inclusions. Crack existence in welded structures is a frequent problem that is the case with vessels pressure, in this case, tests become necessary to confirm whether welded joints are prone to crack initiation and growth is clear. For the known geometry of the structural component, the load, and the method of support it is necessary to describe the real behavior of the material as accurately as possible, that the most important characteristics for the service safety of welded joints are those describing crack initiation and growth caused by variable loading.

To understand better beahviour of a welded joint one should analyse how the heterogeneity of microstructure and mechanical properties of welded joints, primarily of WM and HAZ, [39].

Although with meeting stringent safety requirement when using mechanical structures, fractures occur, so it must be connected the principle of design based on the permissible stress, and not sufficiently relied on the degree of safety, especially if it applies to structures that include the welded structures with residual stress of unknown magnitude, low operating temperature or high load or variable (fatigue) load or aggressive environment.

Therefore, attention is being to studying the process of deformation development and fracture onset and development under different conditions. Some of the main causes of structural failure are:

• Inaccuracy in design and construction;
• Material errors;
• design defects;
• Inadequate and incomplete maintenance;
• Workload;

In the work requirements the impact of secondary loads has not been taken into account

• fatigue breakage;
• Environmental impact (temperature, humidity, corrosion, decarburization

Preparation process errors affect the material properties causing a decrease in strength and dynamic properties, which can lead to errors in the surface, inhomogeneity, anisotropy, adversely affect the life of the structure.

can be avoided side effects resulting from the Inadequate preparation process by careful preparation of the preparation errors in welded joints that can be classified into three large groups: design, welding, and metallurgical. where design errors include problems related to the details of the design and construction, representing the welding errors in namely: cracks, cavities, solid inclusions, unconnected places and imperfections, shape and dimension errors, and various imperfections.

5.1 Design Under Dynamic Load Condition

By determine the maximum stress that the material can withstand without fracture with an unlimited number of load changes - cycles, safe construction is obtained from the point of view of dynamic strength. This is a conservative approach to design, which gives heavier and more expensive constructions. In this way, even more, rational design is achieved, considered surface quality and condition, corrosion damage, load frequency, temperature, dimensions, and shape are quantities influential on strength at variable load, and for this, the behavior of the material under variable load is not easy to know. so that in many cases the calculation cannot be used to decide on the usability of a structure exposed to a variable load, but on the structure, or any more complex part of that structure, must be tested under conditions which are as similar as possible to those of the operation.

With continued load cycles, the crack grows to microscopic size and gradually becomes visible to the eyes. Fracture then occurs when a crack reaches to some critical size, [40].

5.1.1 Cyclic Stress

Parts of the structures and machinery are exposed to the most commonly uneven alternating load ***Figure. 5.1c***, although the load may also be periodically variable, as shown in ***Figure. 5.1a***. Cyclic stresses are characterized by maximum, minimum and mean stress, the range of stress, the stress amplitude, and the stress ratio. [41] [42].

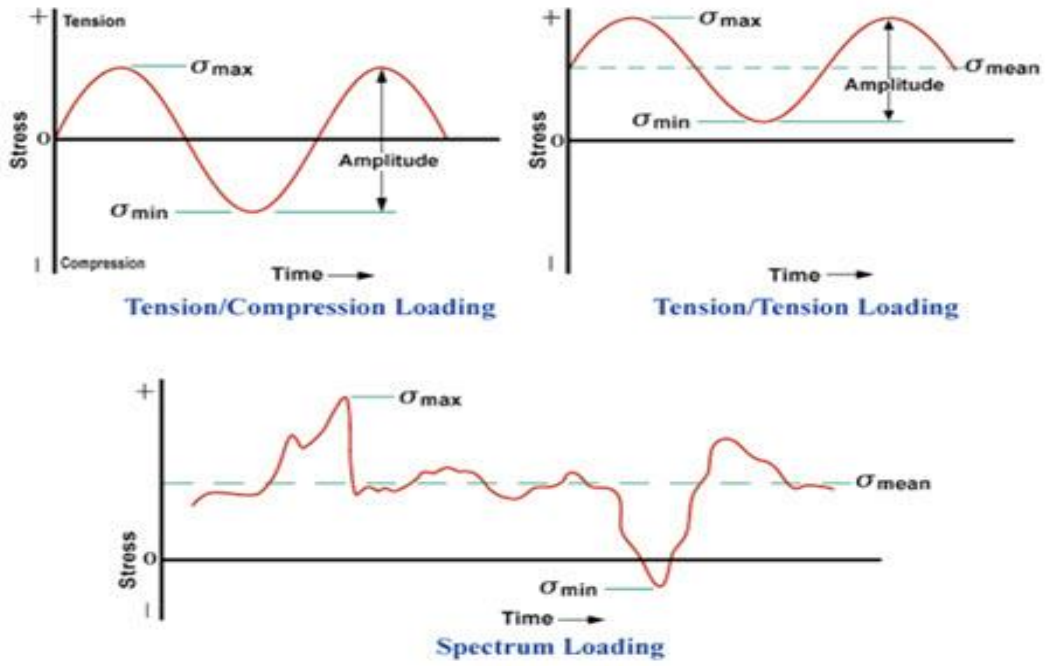

Figure 5-1: Typical fatigue stress cycles (a) Reversed stress (b) Repeated stress (c) Irregular or Random stress cycle.

As can be seen from ***Figure. 5-1b***, the range of stress is the difference between the maximum and minimum stress, [43].

$$\sigma_r = \sigma_{max} - \sigma_{min} \qquad 5\text{-}1$$

The amplitude stress, then, is one-half the range of stress.

$$\sigma_a = \frac{\sigma_r}{2} \qquad 5\text{-}2$$

The mean stress is the algebraic mean of the maximum and minimum stress.

$$\sigma_m = \frac{\sigma_{max} + \sigma_{min}}{2} \qquad 5\text{-}3$$

The stress ratio R is defined as

$$R = \frac{\sigma_{min}}{\sigma_{max}} \qquad 5\text{-}4$$

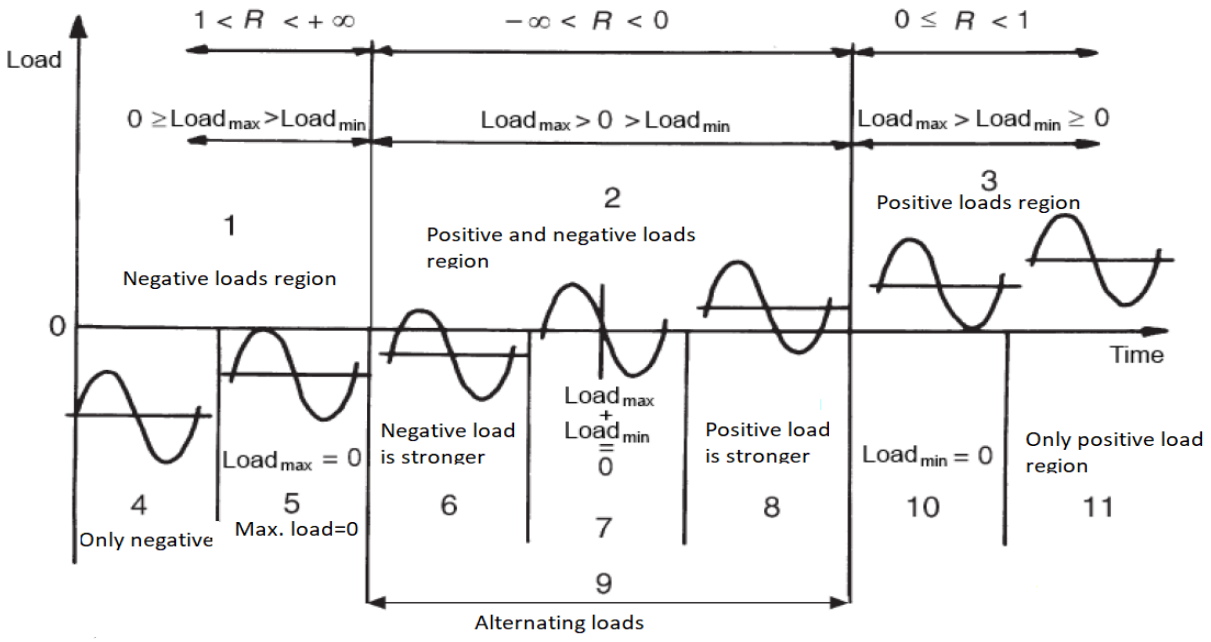

Figure 5-2: Load ratio R differences.[44]

5.1.2 Fatigue Life Curve

The total fatigue life is thus the sum of a crack initiation and a propagation phase, as shown in ***Figures 5.3-5.5***.

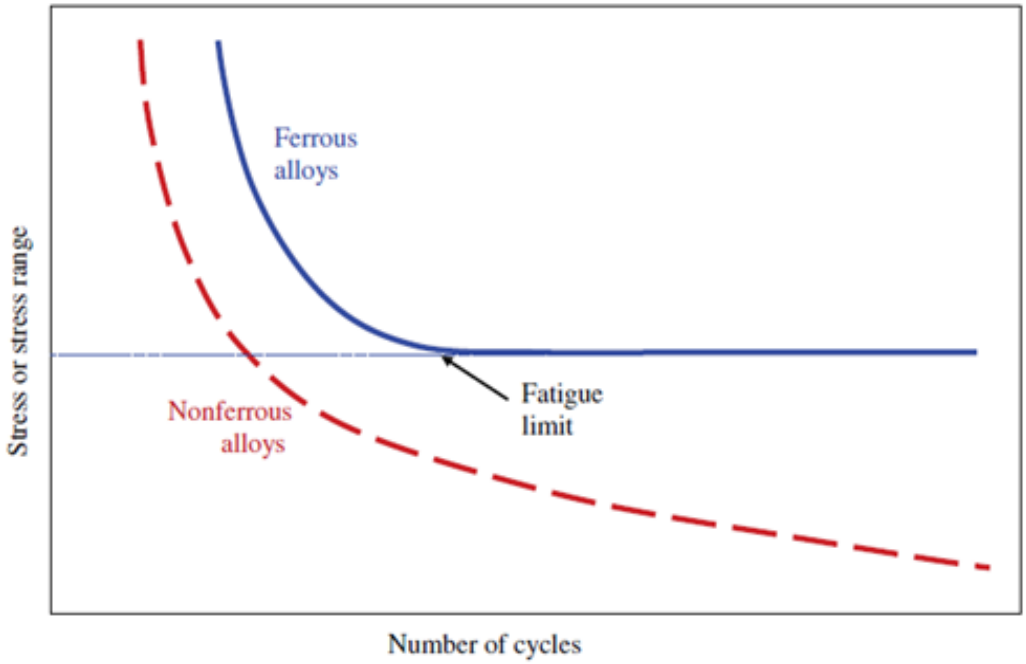

Figure 5-3: Typical S-N curves for ferrous and nonferrous alloys

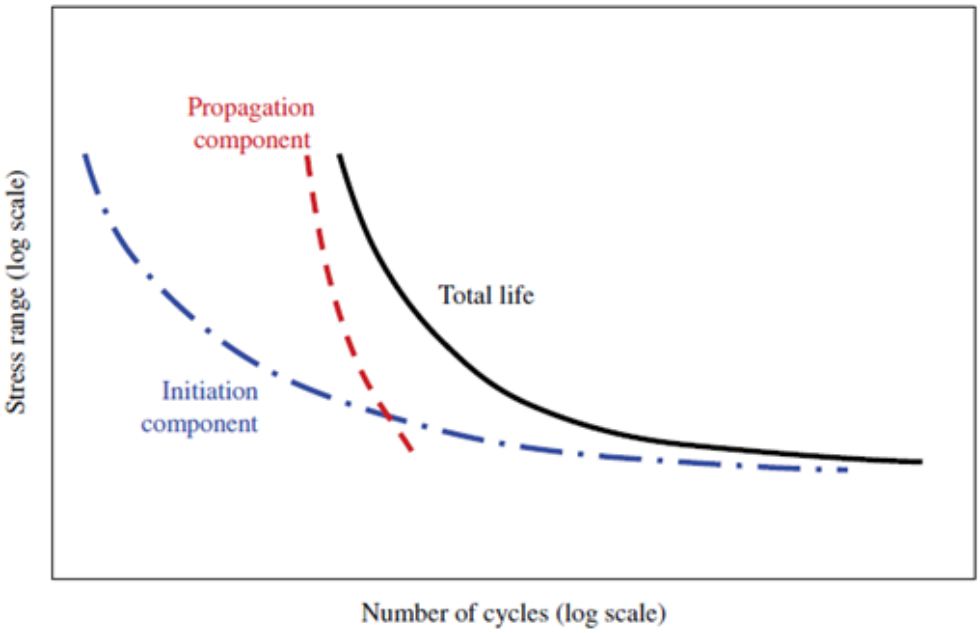

Figure 5-4: Initiation and propagation components total fatigue life

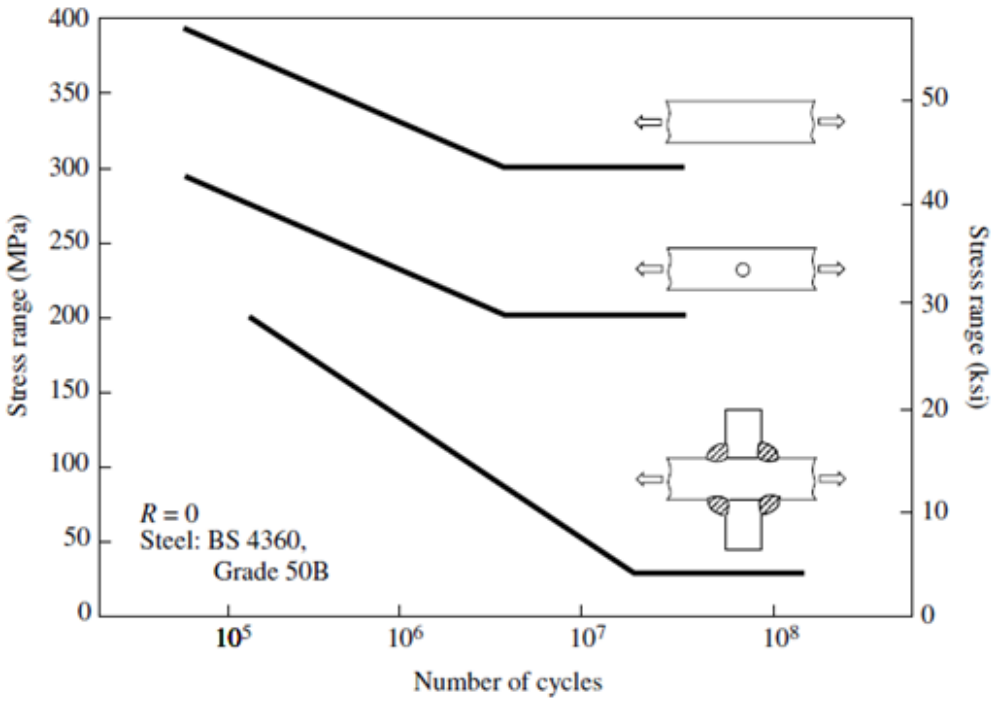

Figure 5-5: Effect of welded attachment on the fatigue behavior of a simple of beam loaded in tension

5.1.3 Fatigue Crack Growth Rate

Fatigue crack length vs. Number of cycles is shown in ***Figure 5.6***, with amplitude stress as the parameter. Three different regimes of crack growth can be recognized from the diagram in ***Figure 5.7***

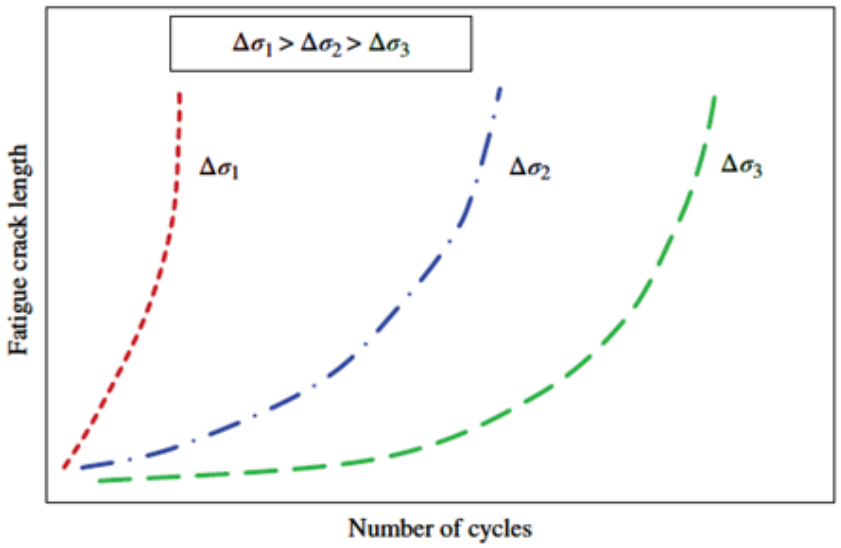

Figure 5-6: Effect of fluctuating stress (Δ σ)on fatigue crack propagation rate [45]

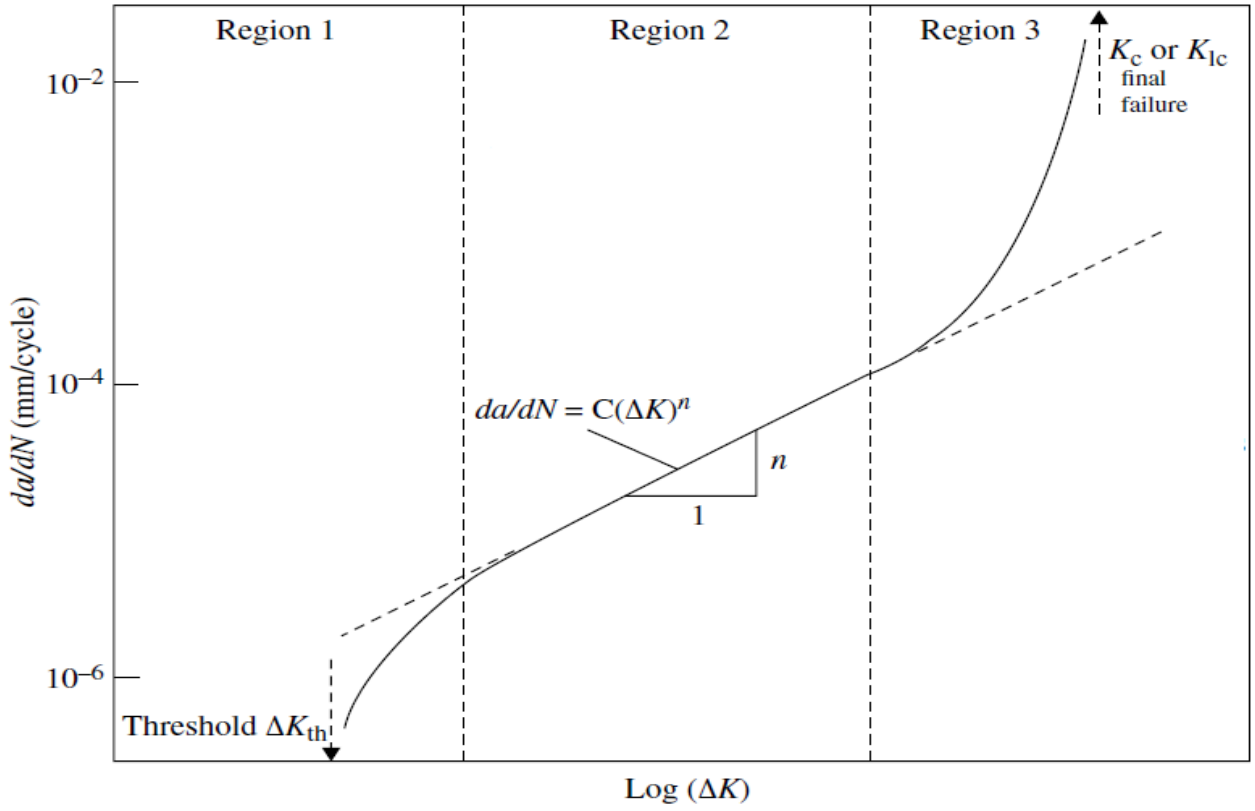

Figure 5-7: Fatigue crack growth rate (da / dN) as a function of stress intensity factor range (Δ K)[44][46]

5.2 Basic Concepts of Construction with Respect to Material Fatigue

Fracture occurrence of the structure may occur during production, assembly, transport, or operation, the fracture can be caused by static overload, or caused by the action of dynamic loading, where known as fatigue loading, also keep in mind the presence other parameters (temperature, humidity, corrosion) which, in combination with dynamic loading, can lead to fracture.

In order to ensure proper structural characteristics during operation, the structure has been designed for the following four types of damage, [47].

The design of the dynamic durability defines the resistance of the structure to crack formation and further expansion under the influence of dynamic (fatigue) loading. The damage tolerance of a structure is based on the damage accumulation until a crack occurs, and propagates until the complete failure of the structure, as shown in ***Figure. 5.8***

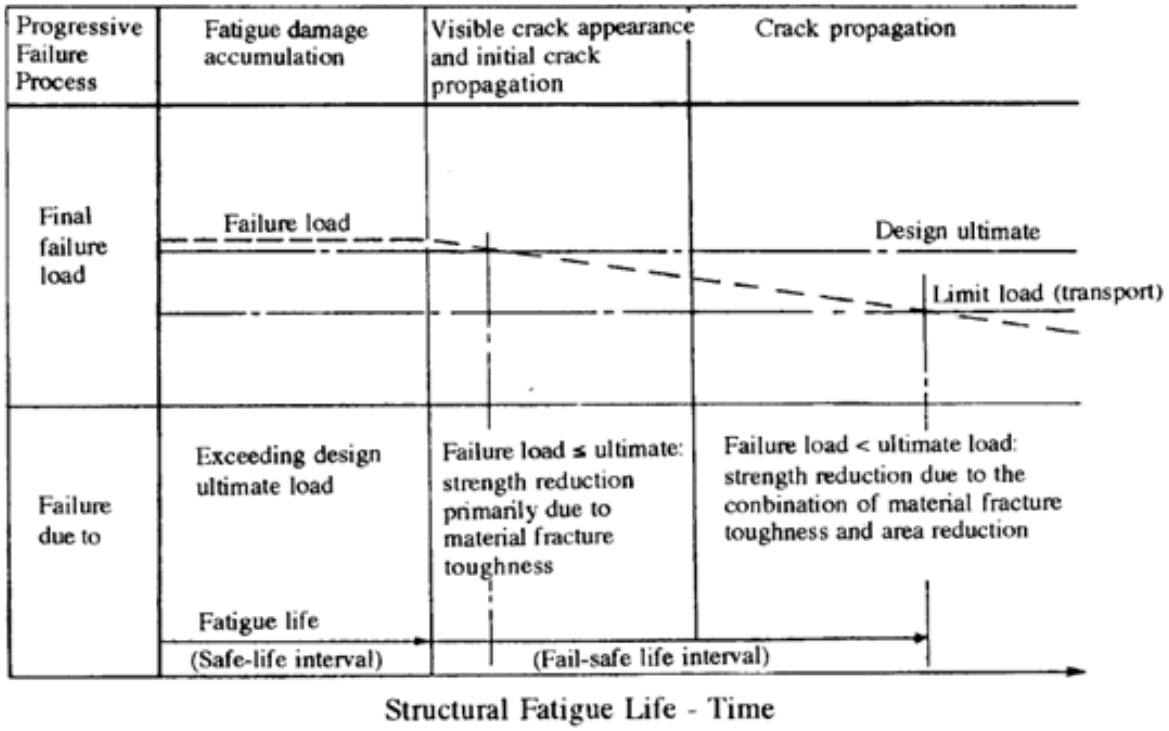

Figure 5-8: Progressive Failure of Structural Element

5.2.1 Safe Life Design

Safe life Design is based on laboratory testing of simple specimens that are cyclically-loaded to create test points in a S-N curve.

5.2.2 Fail-Safe

Basic concept of Fail-Safe approach is to use periodic inspection, under assumption that the damage detection techniques can identify flaws, thus enabling prompt repair or replacement. Some of techniques to enable fail-safe design include multiple load paths, load transfer between members ***Figure 5.10*** , crack arresters and inspection, [48].

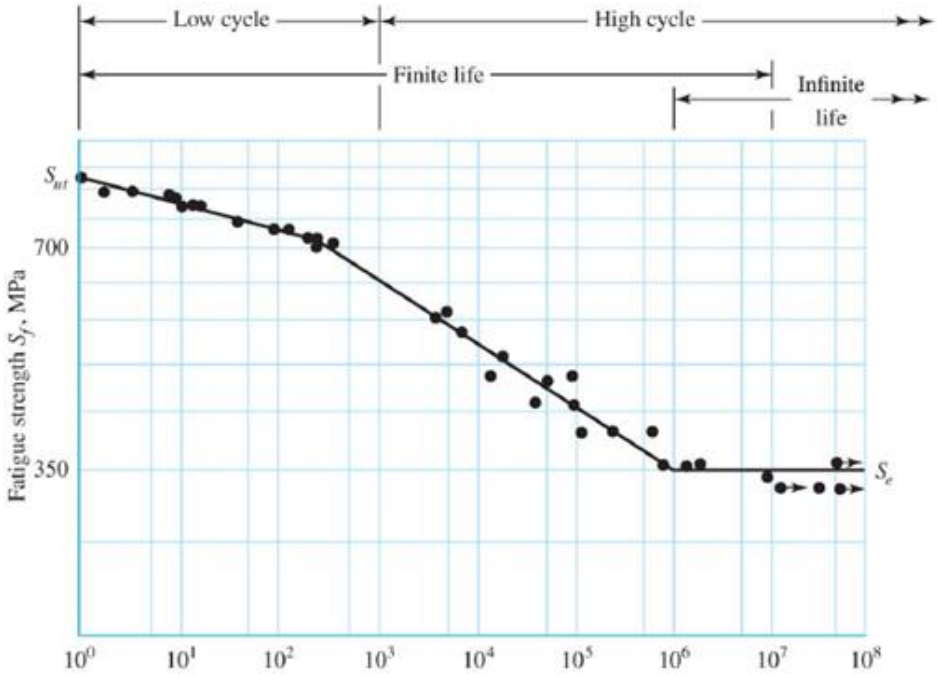

Figure 5-9: Number of stress cycles (log scale)

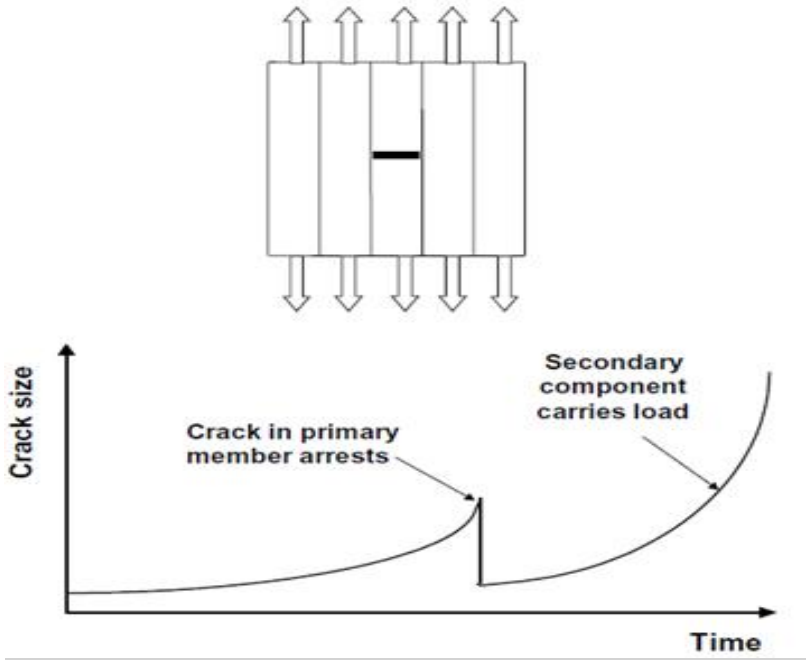

Figure 5-10: Multiple load paths, load transfer between members

Damage Tolerance Analysis

Damage tolerance analysis is another core tenet of fail-safe design (DTA), the foundation of damage tolerance is the concept of fracture mechanics, as shown in ***Figure 5-11***.

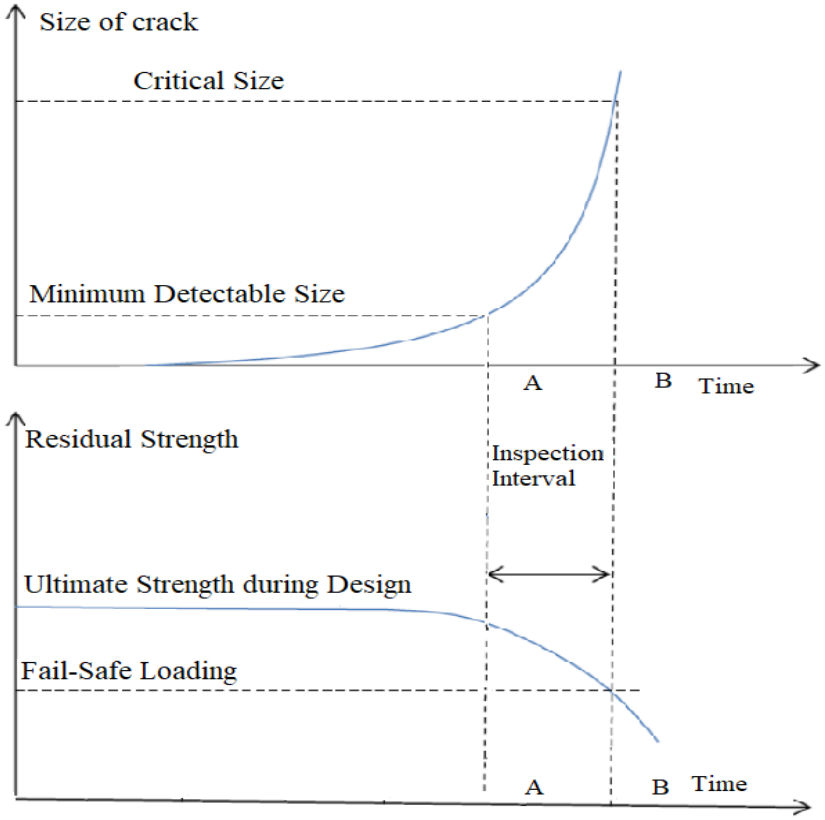

Figure 5-11: Damage Tolerance: Safety & Inspection

Fall-Safe Approach

Total life from first cycle to complete failure, can be divided into three stages :

I. Initial life interval span in which complete failure can only occur when the applied load exceeds the design ultimate strength K_{IC}, (time to initiate a crack which will tend to reduce the design ultimate strength capability)

This time interval is usually defined as the fatigue endurance period or the safe-life interval.

II. life interval, after safe-life interval, at which structural complete failure can occur even when the applied load is below the ultimate design load. Reduced durability due to the formation of a small crack.

III. The final interval of a lifetime in which complete failure can occur even when it is workload far below fracture toughness-K_{IC}. The structure is rather weakened, and the reduction in durability is a function of material toughness and reduction of the bearing surface due to crack growth.

Phases (II) and (III) together constitute a time interval called a "confidence interval"

The length of this interval is a function of: the residual strength reduction rate, crack propagation rate and the fail-safe design criteria which limits the residual strength to the limit load established.

The goal of good construction with respect to material fatigue is to achieve an interval safe use that would equal the design life of the structure. From a statistical point of view, the safe use interval can be defined as the initial interval lifetime, at which the probability of crack formation is an acceptable small size. At Destruction due to fatigue of the material during this interval only creates a crack, not complete fracture. Optimal design with respect to material fatigue provides a high probability of "safe-life" work to achieve operational readiness and economic justification as well as a reasonably long confidence interval ("Fail-safe"), and somewhat cost-effective system maintenance.

Fail-safe design principle, that is, adequate safety after some degree of damage, reduces fatigue problems from safety level to economical level. The following considerations are essential for the development of the concept of damage tolerance, Material selection. Dynamic strength, Crack growth tendency and Residual stress materials were originally considered because these characteristics actually determine the size of basic structures.

In summary, fatigue performance is a multivariate phenomenon. Hence, design criteria must be pointed towards controlling the many features of design and manufacturing affecting the realization of fatigue performance. design planning and execution, manufacturing quality control, analysis, test demonstration, inspection, and service monitoring and usage provide means to produce or maintain a high level of fatigue response requires appreciating dedication to the task as well as cultivation of detail analysis beyond the practice necessary for ultimate strength design

5.3 Estimation of Structural Life

5.3.1 The Fatigue Crack Growth Rate

The function (da/dN) vs. Log(ΔK) should be a straight line with a slope equal to Paris law coefficient n, which is the second of three regions, ***Figure 5.12.*** Region I is the slow growth (near the threshold K_{th}), Region II growth at a medium rate (Paris regime), and Region III growth at a high rate (near to fracture K_c), ***Figure 5.12.***

In the stage II, Paris law can be used to determine the number of cycles to failure, employing the amplitude stress intensity factor, ΔK, expressed in terms of $\Delta\sigma$:

$$\Delta K = K_{max} - K_{min} = (\sigma_{max} - \sigma_{min})Y\sqrt{\pi a} \qquad 5.5$$

where Y depends on the specific specimen geometry.

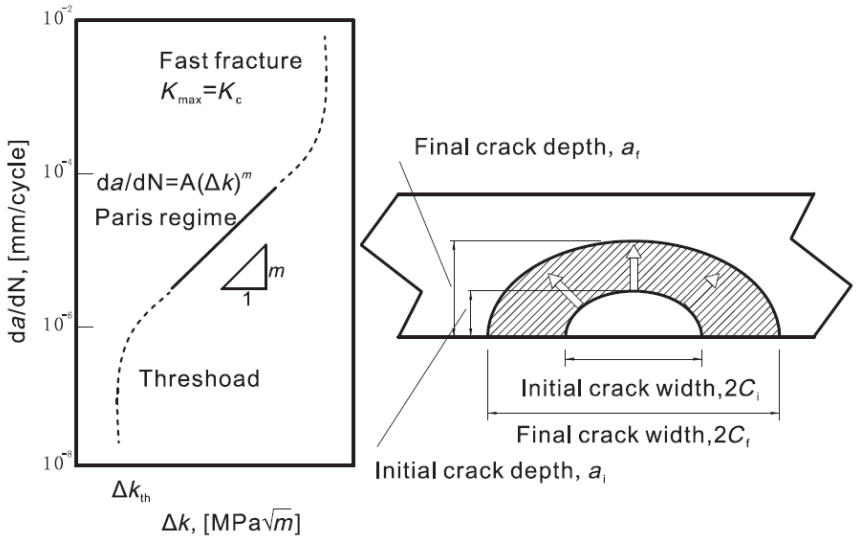

Figure 5-12: Fracture crack growth curve.[49]

Paris law can be written as follows:

$$\frac{da}{dN} = c\left(Y\Delta\sigma\sqrt{\pi a}\right)^n \qquad 5.6$$

where a is the crack length; N the number of load cycles; C the intercept of line along $\frac{da}{dN}$; and n is the slope of the line. As one can notice, Paris law is a differential equation in mathematical terms.

One of the main aims of fatigue analysis is to estimate the fatigue life. Toward this aim, the differential equation 5.6 can be solved for the crack size as a function of the number of cycles:

$$a_i = \left(CN_i\left(1-\frac{n}{2}\right)(Y\Delta\sigma)^n\pi^{n/2} + a_0^{1-n/2}\right)^{2/2-n} \qquad 5\text{-}7$$

where $a_0$is the initial crack size and $a_i$crack length at cycle N_i .

Eq. (5-7) can be used to calculate the crack size a_i after N_i cycles, starting from a crack with a_0 size, assuming that the parameters *C* and *m* are known and independent of the crack length.

Another important goal of this analysis is to calculate the number of cycles to failure, which corresponds to the critical crack size a_c, i.e. when the crack starts to grow in unstable manner:

$$dN = \frac{da}{C\left(Y\Delta\sigma\sqrt{\pi a}\right)^m} \qquad 5.8$$

$$N = \int_0^{N_f} dN = \int_{a_i}^{a_c} \frac{da}{C\left(Y\Delta\sigma\sqrt{\pi a}\right)^m} \qquad 5.9$$

$$N_f = \frac{1}{c(\pi)^{\frac{m}{2}}(Y\Delta\sigma)^m}\int_{a_i}^{a_c}\frac{da}{a^{m/2}} \qquad 5\text{-}10$$

$$N_f = \frac{{a_c}^{1-m/2} - {a_i}^{1-m/2}}{c\left(1-m/2\right)(Y\Delta\sigma)^m\pi^{m/2}} \qquad 5\text{-}11$$

Obviously, one has to know the initial crack length, a_i , and the final crack length, a_c, in order to calculate remaining number of cycles, N_f. Initial crack lengths can be detected using a number of nondestructive testing techniques. Even if crack is not detected, one can assumed that it exists and take its initial length as equal to the resolution of the detection equipment. For the final length, one should use the basic criterion of linear elastic fracture mechanics:

$$K_{max} = K_c = \left(Y\Delta\sigma\sqrt{\pi a_c}\right) \qquad 5.12$$

Solving for a_c *gives:* $$a_c = \frac{1}{\pi}\left(\frac{K_c}{Y\Delta\sigma_{max}}\right)^2 \qquad 5.13$$

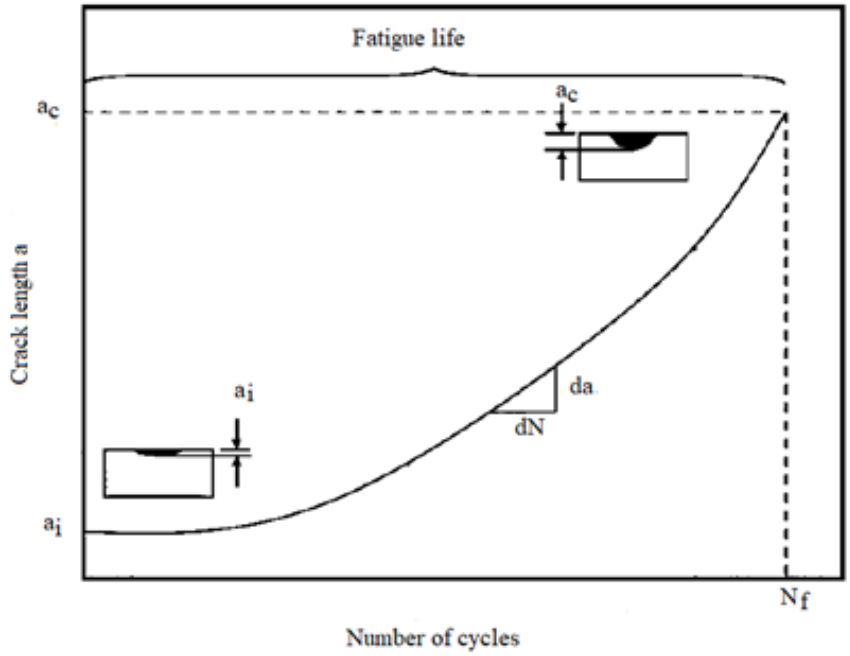

Figure 5-13: Crack length as a function of cycles

Foreman's Model

Because Paris law does not account for the load ratio R, Foreman introduced the modified law, [50]:

$$\frac{da}{dN} = \frac{c\left(Y\Delta\sigma\sqrt{\pi a}\right)^n}{(1-R)K_c - Y\Delta\sigma\sqrt{\pi a}} \qquad 5.14$$

Modified Walker's Model

Another modification of the Paris equation was made by Walker, also to account for the effect of stress ratio $= \frac{K_{min}}{K_{max}} = \frac{\sigma_{min}}{\sigma_{max}}$:

$$\frac{da}{dN} = C_0\left(\frac{Y\Delta\sigma\sqrt{\pi a}}{(1-R)^{(1-m)}}\right)^n \qquad 5.15$$

5.4 The Failure Assessment Diagram for Assessing Crack Stability

Failure Assessment Diagramme basically uses the limit curve to separate safe and unsafe regions as shown in ***Figure 5-14***, introducing also three different zones of material behavior:

Zone I: brittle fracture

Zone II: elastoplastic fracture

Zone III: plastic collapse, [51].

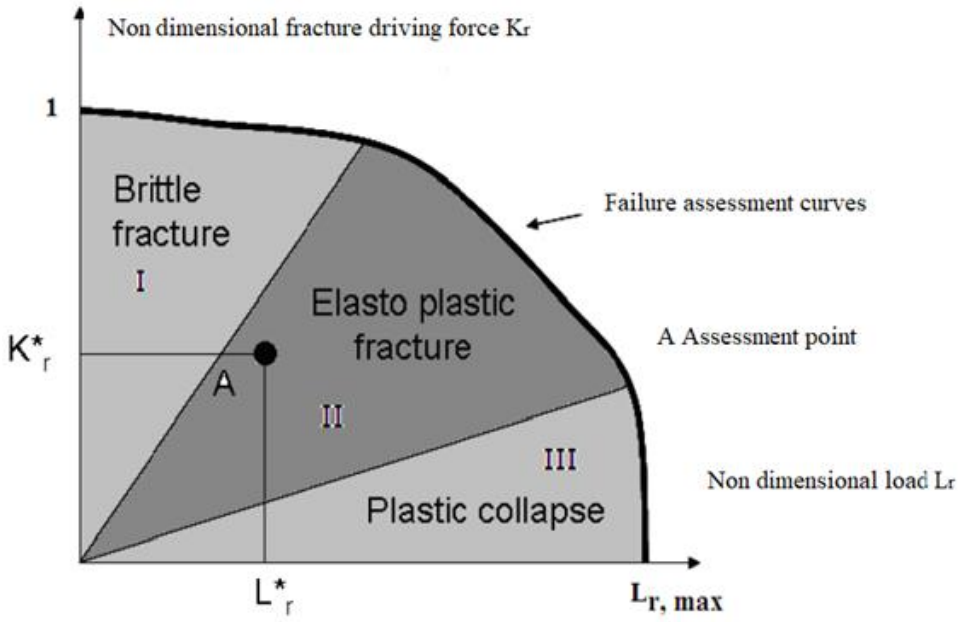

Figure 5-14: Failure assessment diagram indicating the domain of limit analysis

The axes are defined by the non-dimensional ratios, as follows: x-axis by L_r (plastic collapse ratio) and y-axis by $\mathrm{K_r}$ (brittle fracture ratio). The parameter L_r is defined as:

$$L_r = \frac{reference\ stress}{yield\ stress} = \frac{\sigma_{ref}}{\sigma_Y} \qquad 5\text{-}16$$

$\sigma_{ref} = \mathrm{f}\left(\frac{a}{w}, \frac{a}{c}, \frac{a}{t}, \sigma_i\right)$ is the reference stress at the given load, usually the design load or the operating load, and σ_Y is the yield strength, where (a, c) define the crack geometry, (t, w) the component geometry and σ_i the remote stress.

The second parameters $\mathrm{K_r}$, which is linked to the stress intensity factor criterion, is defined as:

$$K_r = \frac{applied\ stress\ intensity\ factor}{material's\ fracture\ toughness} = \frac{K_I}{K_{mat}} \qquad 5\text{-}17$$

where: $K_I = \mathrm{f}\left(\frac{a}{w}, \frac{a}{c}, \frac{a}{t}, \sigma_i\right)$ is stress intensity factor, $\mathrm{K_{mat}}$ is fracture toughness of the material [52].

6 Assessment of Retired Age Pipes and Determine Remaining Service Life

Research within this thesis aimed to investigate the fatigue behavior due to fatigue of protective welded tubes made of J55 steel. This material was chosen because it has the highest tolerance for chemical composition and heat treatment capability, and meets all the requirements of the API standard. However, carbon and low alloy steels, including J55, are subject to general and point corrosion, ie stress corrosion, which makes them particularly sensitive to the formation and growth of fatigue cracks, and therefore require detailed studies of their fatigue resistance and integrity assessment in the stated operating catches. Pressure welded pipes can be very sensitive to cracks and their stable or unstable growth and these are the most common reasons that lead to pipeline failure. These failures are also important when it comes to the environmental aspect, because the substances they transport, if they spill, affect the quality of the environment. Methods for the assessment of pressure pipe damage are very important for maintaining the safety and stability of pipelines in plants [53][54][55][56][57][58] as well as defining reliable criteria for evaluating the remaining life of pressure pipes with cracks in the base material and welded joints . The essence of pipe integrity analysis is the efficient and accurate estimation of the maximum allowable pressure, as well as the determination of fracture mechanics parameters, such as the stress intensity factor K_{IC} and J integral of damaged pipes. In the previous period, a large number of studies related to the outer or inner circumferential and axial semi-elliptical surface cracks in cylindrical vessels. Very few studies are concerned with determining these parameters under external surface axial crack conditions [59] In recent decades, many studies have been conducted to develop a model for estimating the remaining life at highly cyclic fatigue, as it takes time and enormous effort to construct (S-N) diagrams. Previous models for life expectancy estimation in high-cycle fatigue have primarily been based on continuum mechanics. Many papers are devoted to the development of different models for predicting the lifetime of highly cyclic fatigue using the concept of a small crack, but only a few models have included microstructural parameters [60].[61] More recently, models have been developed to estimate the lifetime of low-cycle fatigue [62]. It is important to note that the working environment can significantly reduce the safety of the structure [63]. Low-alloy steels are widely used in pipeline design due to their mechanical properties and good weldability[64] . However, the problem of pipe breakage for oil and gas pipelines is still an ongoing issue. Several methods have been proposed to estimate the remaining pipeline life[65] .For these reasons, this chapter analyzes the integrity using a FAD diagram and estimates the remaining life of welded tubes made of API J55 steel, based on experimental data obtained under the project "Research and Development of Methods for Assessing the Integrity and Reliability of Welded pipes in the oil industry " [13]. Within the framework of this project, the influence of the exploitation conditions on

the properties of J55 steel was tested by experiments on a new one and a pipe that had been in operation for 70,000 hours (8 years) . Based on these data, an estimate of the remaining century will be made by analytical method, on the geometry of the tube type with external axial damage, for different values of crack depths. Also, some of the experimental data from this chapter will be used in the next section to verify the use of XFEM in the 3D analysis of crack growth simulation on tube-type geometry with an initial axial surface crack.

6.1 Test For Resistance to Crack Initiation and Propagation of The Base Metal and The Welded Pipe Joint of API J55

Testing the modified CT test pieces was carried out at room temperature on a machine-SCHENCK TREBEL RM 100 to determine the resistance of base metal and the welded pipe joint of API J55 to crack initiation and propagation. Thickness modified CT tube, d = 6.98 mm (equal to the thickness of the pipe wall) ***Figure 6.6.*** Indirectly through critical J-integral values JIC,(standard ASTM E813, ASTM 1820-99) are determined the critical value of stress intensity factor, K_{Ic}, on the basis of expressions (6.1) to be the base material (BM), the heat-affected zone (HAZ) and weld metal (WM) are given in ***Table 6.1,6.2*** for the new pipe and the tube from service.

$$K_{Ic} = \sqrt{\frac{J_{Ic} \cdot E}{1-\nu^2}} \qquad 6.1$$

Critical values of the crack length ac in BM-in, the HAZ-in and the WM-in is calculated using the expression:

$$K_{Ic} = Y(a/W)\,\sigma_{max}\sqrt{\pi \cdot a_c} \qquad 6.2$$

where σ_{max} is the applid stress (failure), which implies for a_c:

$$a_c = \frac{1}{\pi}\left(\frac{K_{Ic}}{Y(a/W)\,\sigma_{max}}\right)^2 \qquad 6.3$$

Based on the obtained K_{Ic} and a_c values for the base material, the heat-affected zone, and the welded joint, the base material has the least resistance to crack formation and growth[66].

Table 6-1: K_{IC} and J_{IC} values - exploited material

Specimen	Temperature / °C	J_{Ic}, kN/m	K_{Ic}, MPa·m$^{1/2}$	a_c, mm
BM-NR-E	20	35,8	91,4	14,4
HAZ-NW-E		48,5	106,4	19,6
WM-NW-E		45,7	103,3	18,5

Table 6-2: K_{IC} and J_{IC} values - new material

Specimen	Temperature / °C	J_{Ic}, kN/m	K_{Ic}, MPa·m$^{1/2}$	a_c, mm
BM-NR-N	20	63,1	121,4	25,5
HAZ-NW-N		68,4	126,4	27,5
WM-NW-N		64,1	122,3	25,9

6.2 Experimental Determination of Fatigue Crack Growth Parameters

Since the crack propagation under variable loading of the machine parts and structure has a most important effect on the life span and from the place of stress concentration under conditions of variable loading, after a certain number of cycles, crack formation and growth will occur if the fatigue threshold ΔK_{th} is exceeded and also because a cracked structure will not be compromised until the crack reaches a critical value, so the exploitation of such a structure may be permitted so it is important information when deciding on exploitation is knowledge of the growth rate of the crack and its dependence on the workload. The standard ASTM E647, prescribes the measurement of the fatigue crack growth rate da/dN and the calculation of the range of stress intensity factors, ΔK.

The test was carried out at room temperature to determine that da/ dN and ΔK_{th}. Standard Charpy specimens ***Figure 6.1*** made of the base material by the three-point bending method were tested. The tests were made on specimens from the crack tip in the base material (BM) because the results of experimental tests on the modified CT specimens showed that the minimum critical crack length in this zone. Based on the tests of pipes extracted from the basic material (BM) at room temperature, the dependences of crack lengths and the number of loading N of cycles were obtained for the new material and material from service. The resulting dependence is shown in the diagrams, ***Figure 6.3*** and ***Figure 6.4***

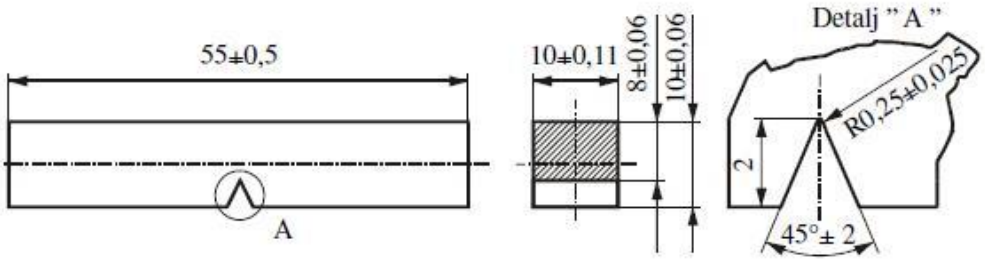

Figure 6-1: Shape and dimensions of a standard Sharpie impact test specimens

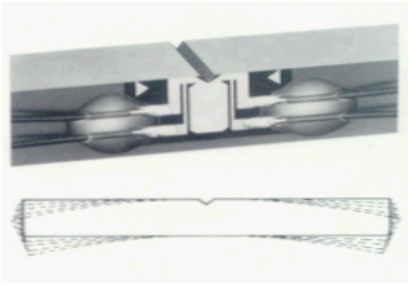

Figure 6-2: specimens sharps equipped with RUMUL RMF A-5 foil for continuous crack length monitoring

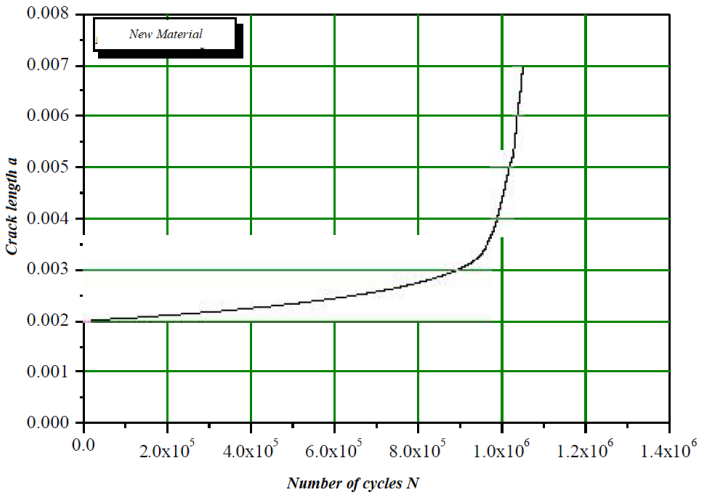

Figure 6-3: Diagram a - N for a new pipe

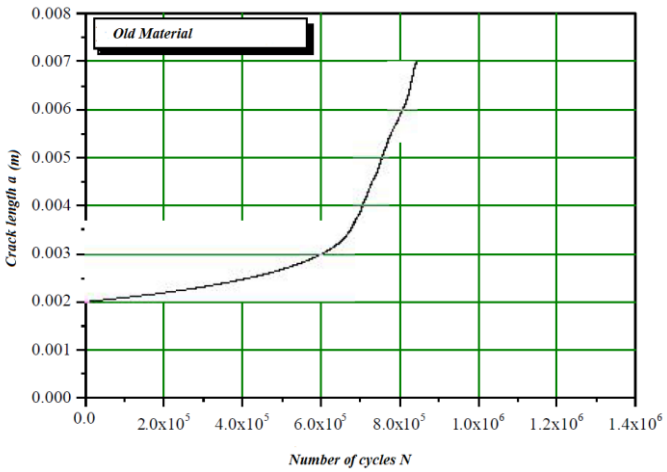

Figure 6-4: Diagram a - N for the pipe from service

Depending on the variable load, ΔK, the fatigue crack growth rates da / dN were calculated and the log curves were drawn, log(da/dN) – log(ΔK), ***Figure 6.5.*** The obtained values of the parameters of the Paris equation for new and exploited material are shown in ***Table 6.3.*** values of fatigue crack growth pare for test tubes made of new pipes and, for test tubes made of pipes from exploitation. Note the fatigue crack growth rate da / dN increases with time and operating conditions, ie resistance decreaseson crack propagation, which does not apply to fatigue threshold values ΔKth.

Table 6-3: Parameters of the fatigue crack growth

	Fatigue threshold ΔK_{th} [$MPa\sqrt{m}$]	Coefficient C [m/cyc· $MPa\sqrt{m}$m]	Exponent m [-]	da/dN [m/cyc] for ΔK=15 $MPa\sqrt{m}$
New material	9,5	$1{,}23 \cdot 10^{-13}$	3,931	$5{,}17 \cdot 10^{-9}$
Old material	9,2	$2{,}11 \cdot 10^{-15}$	6,166	$3{,}75 \cdot 10^{-8}$

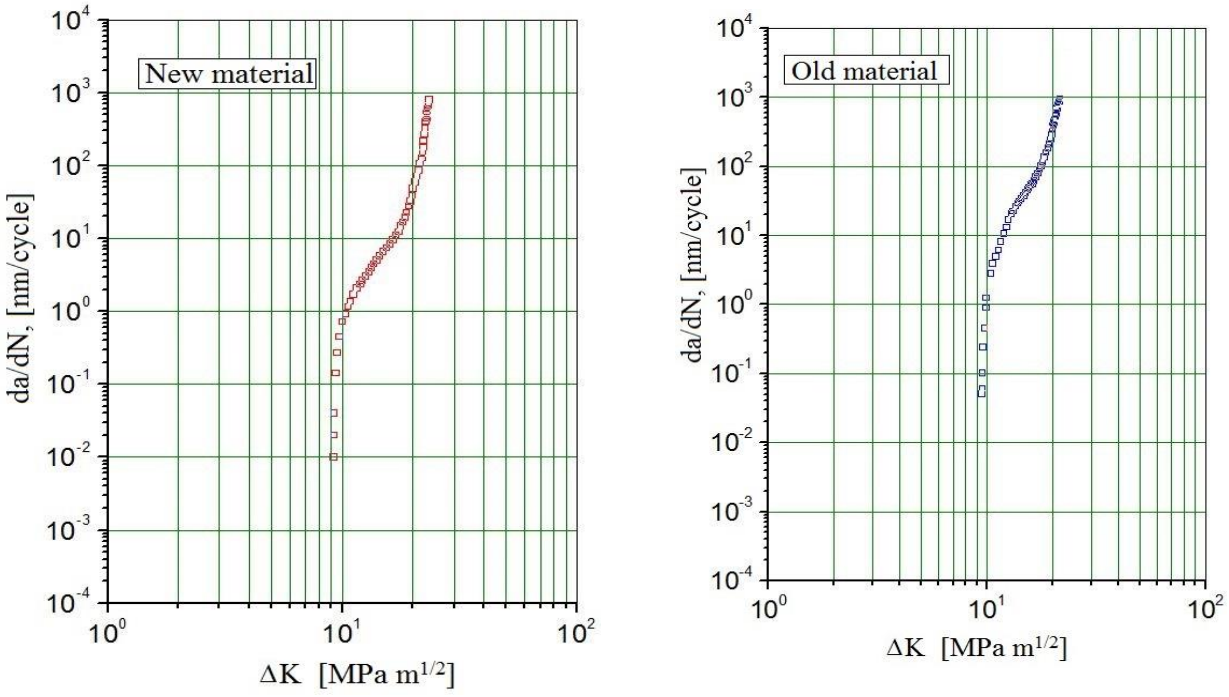

a) *b)*

Figure 6-5: FCG vs. ΔK for (a) new material, $\Delta Kth = 9.2\ MPa\sqrt{m}$: (b) old material,$\Delta Kth = 9.5\ MPa\sqrt{m}$

6.3 Estimation of the Remaining Life of Pipes with Axial Surface Crack

6.3.1 Analytically Using Paris law

Schematic presentation of the cracked pipe is shown in Fig.6.6, whereas tensile properties of API J55 steel are given in ***Tables 6.1, 6.2***.

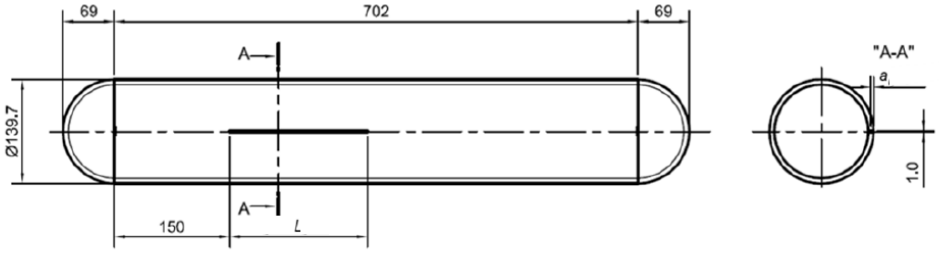

Figure 6-6: Dimensions of the pipe and crack, [31, 62, 64, 67]

Basic data for HF welded pipe, with an axial crack, made of API J55 steel, ***Figure. 6.6***, is as follows:

• Diameter 139.7 mm, thickness 6.98 mm, length 702 mm

• maximum pressure = 10 [MPa]

• number of strokes of pump rod: n_{PR} = 9.6 [min^{-1}]

Axial surface crack was made on the outer surface with length 2c=200 mm and depth a=3.5 mm. It was located in BM, i.e. in the region with the lowest values of the fracture toughness, [31, 67]. Results for standard testing of K_{IC} (via J_{IC}) for base material (BM), heat affected zone (HAZ) and weld metal (WM), are presented in Table 6.1 and 6.2 for pipes taken from service and for the new one. Now one can use Paris law

$$\frac{da}{dN} = C(\Delta K)^m = C\left(Y(\frac{a}{W})\Delta\sigma\sqrt{\pi \cdot a}\right)^m \qquad 6.4$$

where *Y(a/W)* is the geometry factor depending on crack length and geometry (component width), ΔK stress intensity factor range corresponding to stress amplitude $\Delta\sigma$=21.2 MPa, to calculate the fatigue crack growth, first into depth, and then along pipe length, [31, 67]. For the first phase of crack growth, i.e. its growth into depth, the initial length (depth) was 3.5 mm, with the final length 6.98 mm, to be used in directly integrated value of number of cycles:

$$N = \frac{2}{(m-2)\cdot C\cdot(Y(a/W)\cdot\Delta\sigma)^m\cdot\pi^{\frac{m}{2}}}\left(\frac{1}{a_0^{\frac{m-2}{2}}} - \frac{1}{a_{cr}^{\frac{m-2}{2}}}\right) \qquad 6.5$$

where C and m denotes real data obtained by testing: C=2.11E-15, m=6.166 for used material and C=1.23E-13, m=3.931 for new one. Geometry coefficient Y(a/W) was taken to be 3.791 for surface crack (length 200 mm, depth 3.5 mm), without changing its value during crack growth. For the stress amplitude, Δσ=21.2 MPa, the calculated number of cycles is shown in table 6.4 for all three zones in welded joint.

Table 6-4 Number of cycles for crack growth into length

Specimen	$2c_c$ [mm] old / new	a(mm) old/new	N_{total} (cycles) old / new
BM	227.2 / 226	4.88/6.26	578,731.7 / 2,172,429.5
HAZ	251.2/ 245	5.57/6.26	716,619.07 / 2,375,948.45
WM	236.8 / 229.44	5.57/6.26	699,662.3 / 2,210,869.79

The number of cycles for a crack to penetrate through the thickness in one year of operation can be calculated as follows: Ny=60·Ty·n= 60·8760·9.6 = 5.046·10^6 cycles, where Ty is number of working hours per year, $n = \frac{N}{N_y}$,

where C and m denotes real data obtained by testing of new material: C=1.23E-13, m=3.931. Geometry coefficient Y(a/W) was taken to be 2.34169 for surface crack (length 200 mm, depth 3.5 mm), kept as the constant value to the final value of crack depth. For the stress amplitude, $\Delta\sigma$=21.2 MPa, the number of cycles was 21,482,122.18 to a_c =6.9

6.3.2 Comparison Between Numerical Simulation and Analytical Method, [67]

Extended method of finite elements (XFEM). This method allows the simulation of crack growth and determining the stress intensity factor without creating a new network after each step propagation, thanks to "improved" finite elements. This significantly simplifies the work of the simulation, because once defined, the network of nodes remains so until the end. The extended finite element method is a relatively new method, and in order to gain affirmation and begin to be more widely applied in practice, the results obtained by this method must be supported by the results from the experiment. Proving the reliability of the extended finite element method for estimation fatigue age should indicate the possibility that numerical simulations can very effectively replace extensive, time-consuming and expensive experimental trials. Extended FEM (XFEM) was applied to evaluate the number of cycles under fatigue loading and to check the accuracy of the direct integration of Paris law. This method is relatively new and successfully applied to solve different problems. Two FE models were used, one with coarse mesh (129,989 nodes) and the other with a fine mesh (414,537 nodes) ***Figure 6-7***, proving the sensitivity of XFEM results on mesh refinement. As a relevant result, 15,968,030 cycles were accepted, obtained with the refined mesh. Comparing this to the result obtained directly by applying Paris law one can see that the agreement with refined mesh is good, but one should notice that the geometry coefficient constant Y (a/W) was used in direct integration of Paris law, where C and m denotes real data obtained by testing of exploited material: C = 2.11E-15, m = 6.166, Geometry coefficient Y (a / W) was taken 2.29 for surface crack (length 200 mm, depth 3.5 mm), kept as the constant value to the final value of crack depth. For the stress amplitude, $\Delta\sigma$ = 21.2 MPa, the number of cycles was 17,446,707 for crack depth 4.88 mm and 26,428,206.3 for final crack depth ac = 6.9. [67].

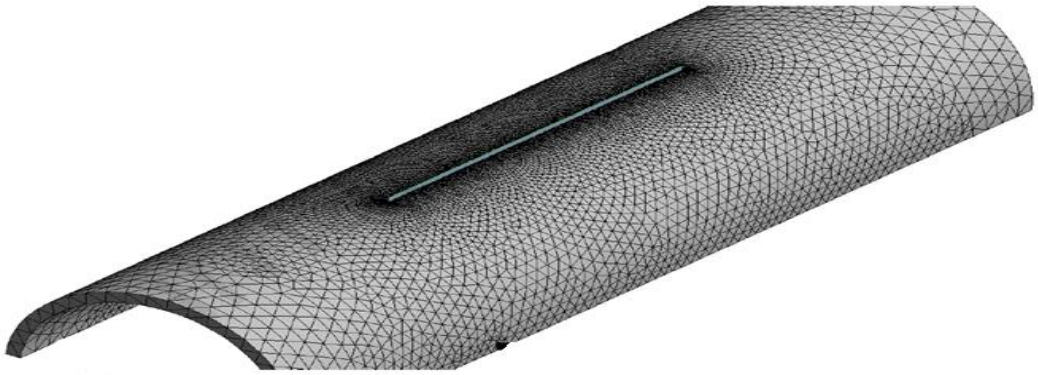

Figure 6-7:Fine FE mesh with 414537 nodes

If experimental or numerical analysis is at disposal, it can enable more precise estimation of probability and risk, but if it is not, then simple engineering analysis can provide fast and conservative estimation.

6.4 Verification of the Analytical Method Using Experimental and Numerical Results Obtained on Standard Specimen

The analytical method of crack growth using standard was done on the model of a standard Charpy test tube made of API J55 steel (***Figure 6.1***). will be used to compare with the results obtained by 3D simulation and experimental. The results from ***Table 6.5*** shown in the graph in ***Figure 6.8. Figures 6.9-6.12*** show the number of load cycles as a function of crack length, where it can be notice when the crack reaches a length of some 5.5 mm its further growth is extremely fast.

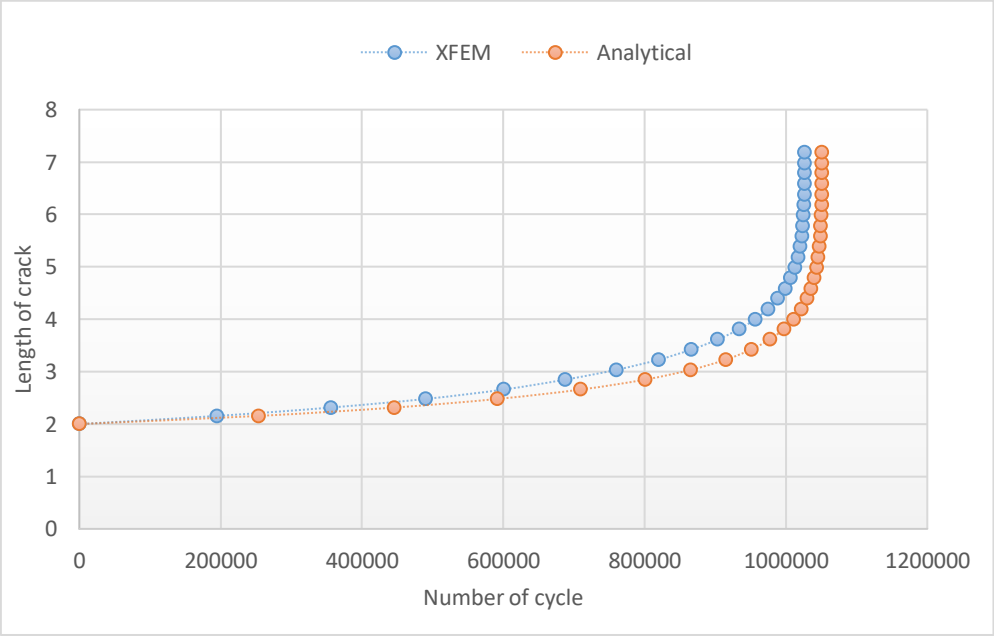

Figure 6-8: Number of cycle obtained from XFEM and Analytical method

Table 6-5: show number of cycles obtained from XFEM and analytical methods

a	N (XFEM)	N(Analytical)
2	0	0
2.155	194821	2.53E+05
2.315	355437	4.46E+05
2.479	489954	5.92E+05
2.658	599916	7.09E+05
2.848	687566.9	8.00E+05
3.034	759748.8	8.65E+05
3.227	819398.4	9.14E+05
3.421	865916.8	9.51E+05
3.611	903164.4	9.77E+05
3.808	933272.8	9.97E+05
3.996	956237.6	1.01E+06
4.197	974105.8	1.02E+06
4.394	988175.5	1.03E+06
4.585	998609.7	1.04E+06
4.787	1006434.7	1.04E+06
4.989	1012397.39	1.04E+06
5.181	1016651.61	1.05E+06
5.384	1019694.92	1.05E+06
5.588	1021907.65	1.05E+06
5.78	1023393.67	1.05E+06
5.984	1024387.43	1.05E+06
6.187	1025062.8	1.05E+06
6.379	1025481.65	1.05E+06
6.584	1025738.81	1.05E+06
6.788	1025899.32	1.05E+06
6.98	1025987.61	1.05E+06
7.183	1026034.29	1.05E+06

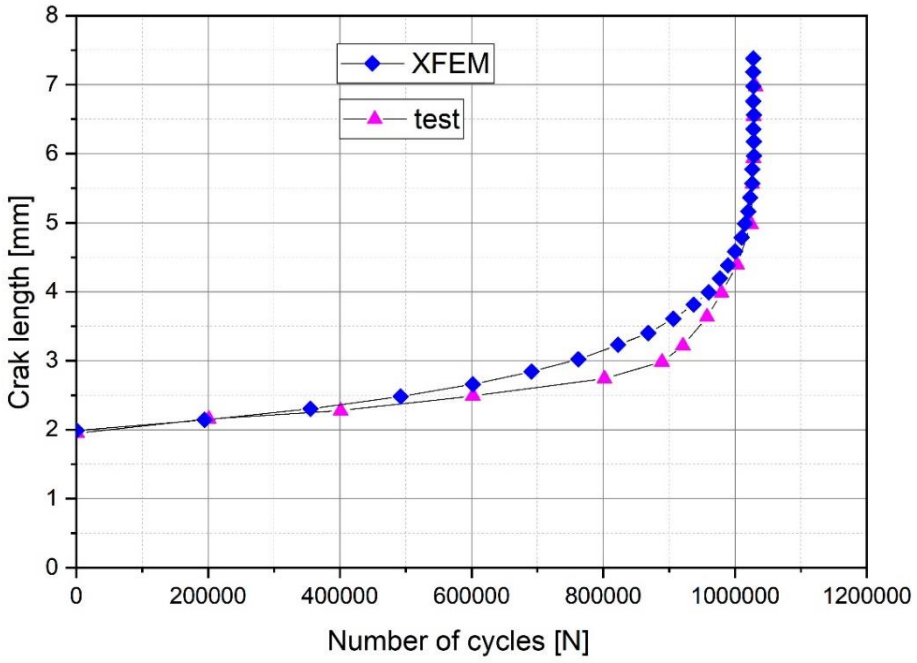

Figure 6-9: Number of cycles obtained from XFEM and Test results

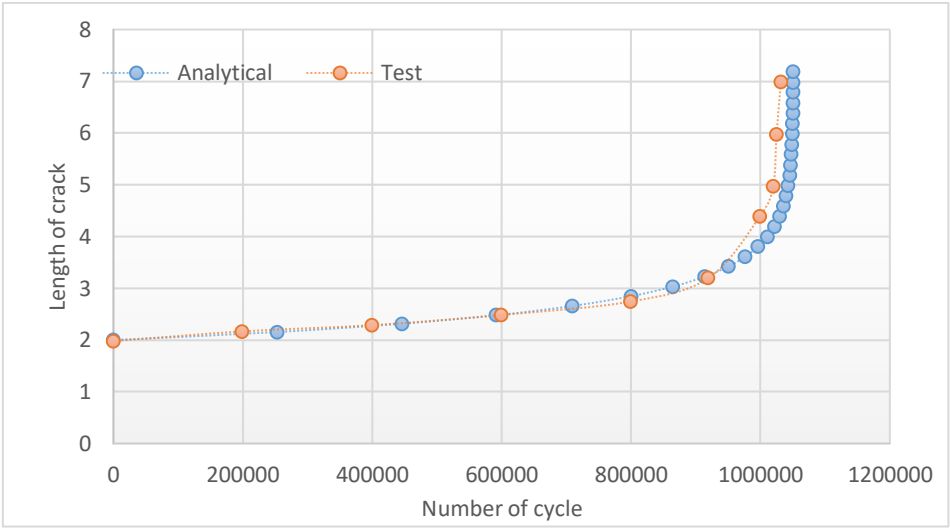

Figure 6-10: Number of cycles obtained from Experimental and Analytical method

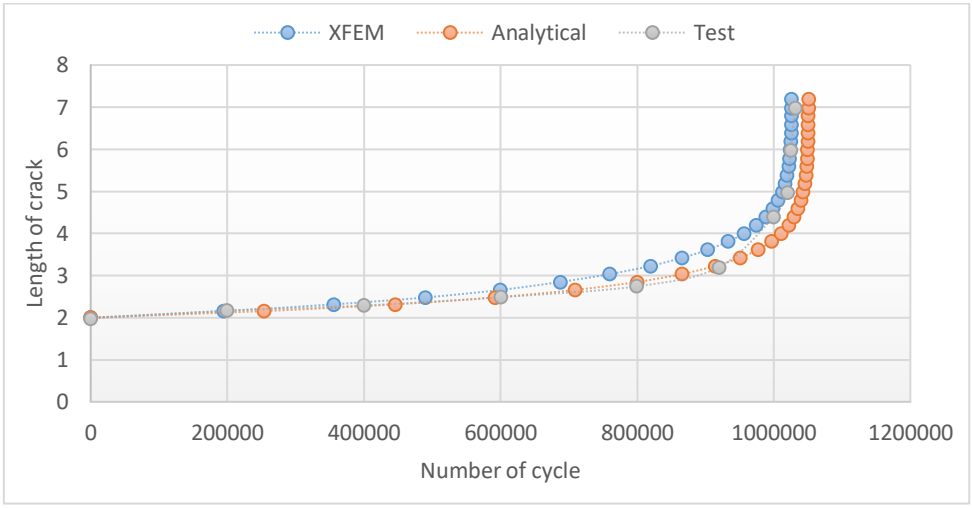

Figure 6-11: Comparison Number of cycles between XFEM, Experimental and Analytical method

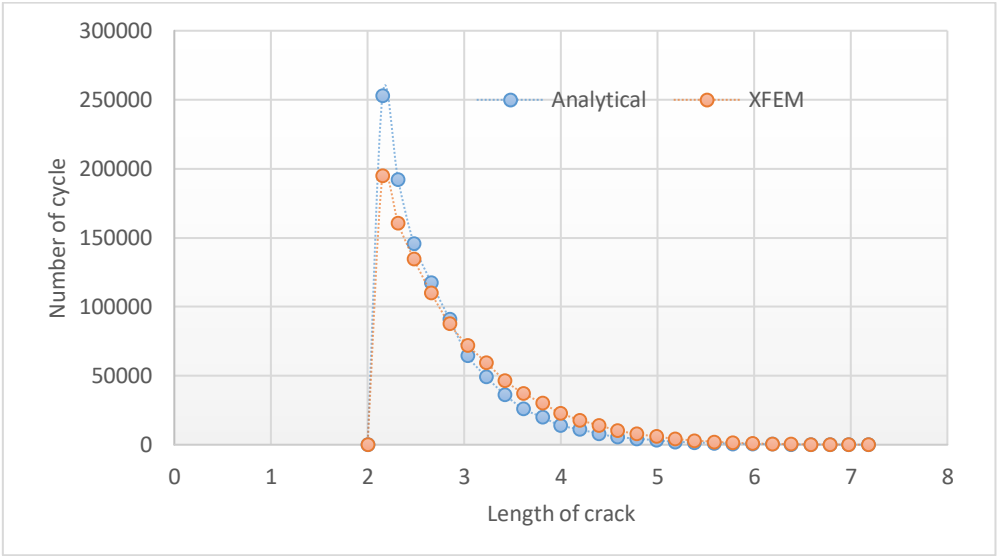

Figure 6-12: Required number of cycles for crack propagation

Comparing this the result obtained directly by applying Paris law one can see that the agreement with XFEM and experimental method is good, we note that the results of the analysis are very close to the results obtained by experiment, but one should notice that the geometry coefficient constant Y (a / W) was used in direct integration of Paris law, where C and m denotes real data obtained by testing it has an impact on the results, I expect the difference that has occurred was due to the difference in Δa which leads to difference in geometry coefficient constant Y (a/W).

6.5 Assessment of The Integrity of Pipes with Axial Surface Crack Based on K_{IC} And L_{IC}

6.5.1 Using The *M* Factors (Newman and Raju's) To Find K_I

Calaculation of the $\boldsymbol{M}$ factors is made in accordance with [68], starting from:

$$K_I = \sqrt{\frac{\pi a}{Q}} F\left(\frac{a}{t}, \frac{a}{c}, \varphi\right) \qquad 6.7$$

where

$$\boldsymbol{F = \left[M_1 + M_2\left(\frac{a}{t}\right)^2 + M_3\left(\frac{a}{t}\right)^4\right] f_\varphi g f_w} \qquad 6.8$$

$$\boldsymbol{M_1 = \left[1.13 - 0.09\left(\frac{a}{c}\right)\right]} \qquad 6.9$$

$$\boldsymbol{M_1 = -0.54 + \frac{0.89}{0.2 + (a/c)}}\ , \qquad 6.10$$

$$\boldsymbol{M_3 = -0.5 - \frac{1}{0.65 + \frac{a}{c}} + 14\left(1 - \frac{a}{c}\right)^{24}} \qquad 6.11$$

$$\boldsymbol{g = 1 + 0.35\left(\frac{a}{t}\right)^2 (1 - sin\varphi)^3} \qquad 6.12$$

$$\boldsymbol{f_\varphi = \left[\left(\frac{c}{a}\right)^2 sin^2\varphi + cos^2\varphi\right]^{1/4}}, \qquad 6.13$$

$$\left[\left(1 + \frac{R_i^2}{R_0^2} \Big/ 1 - \frac{R_i^2}{R_0^2}\right) + 1 - 0.5\sqrt{\frac{a}{t}}\right]\frac{t}{R} \qquad 6.14$$

and the constant Q is calculated on the basis of:

$$Q = 1 + 1.464\left(\frac{a}{c}\right)^{1.65} \qquad 6.15$$

For the crack with the initial depth of a = 3.5 mm and length 2c = 200 mm, one gets:

$K_I = 26.14\ MPa\sqrt{m}$, $K_I = 57.5\ MPa\sqrt{m}$ so it is:

where $K_{Ic} = 91.4$, P=10 and P=22

$K_r = 0.286\ and\ 0.629$

Stress in the net cross-section is σ_n = 2 pR/t, where factor 2 is applied because the net cross-section for the crack length of 3.5 mm to a thickness of 6.98 mm i 50%, so one gets $\sigma = \frac{PR}{t} 100\ MPa$, $\sigma_n = \frac{\sigma}{0.5} = 200\ MPa$. Thereby, for $\sigma_c = 471\ MPa$, Lr=0.424 and 0.934 is obtained for p=10 and 22 MPa, respectively. Taking into account corresposnding values for y coordinate, 2 points are presented in ***Figure 6.13,*** one for p=10 MPa, the other one for p=22 MPa.

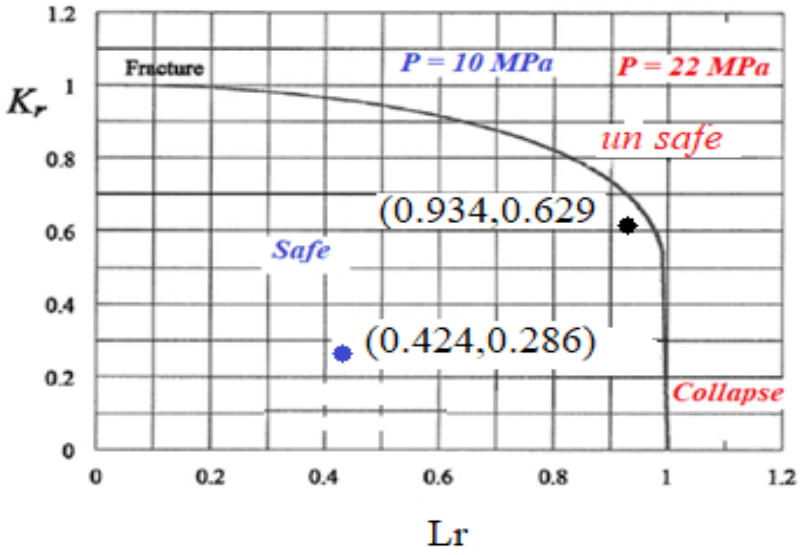

Figure 6-13: (FAD) Failure Assessment Diagram. Different values load

Having in mind the conservatism of FAD analysis in all its aspects, it can be concluded that welded pipes are safe not only from brittle fracture, but also from plastic collapse. It is important to note that FAD allows a simple integrity analysis that can reliably determine whether a welded pipe is safe from breakage, provided that the geometry and load are presented in a conservative manner. On the other hand, if integrity cannot be proven, that additional, more complicated analyzes are needed.

6.5.2 Risk Assessment

Table 6.4 presents the risk matrix for fatigue failure of an oil drilling rig pipe, with consequence taken as the medium, and between high and very high dependence on Kr and Lr probabilities for p = 10 MPa and point coordinates (0.424,0.286), the probability is 0.34, being in the low risk level, for p = 22 MPa, and point coordinates (0.935, 0.629), probability is 0.95, being is the high risk level, ***Table 6.6.***

Table 6-6: presents the risk matrix for fatigue failure of an oil drilling rig pipe

Probability **category**	Consequence category					
	1 – very low	2 - low	3 - medium	4 - high	5 - very high	**Risk legend**
≤0.2 very low						**Very low**
0.2-0.4 low			**P=10 FAD**			**Low**
0.4-0.6 medium						**Medium**
0.6-0.8 high						**High**
0.8-1.0 very high					**P=22 FAD**	**Very High**

6.6 Theoretical Analysis of Axial Cracks in Pipes

Various methods are used for analyying the proplem of semi-ellipticall surface cracks in the outer wall of cylindricalshells or pipe ***Figure 6.6.***Finite method and the method of boundary integral equation ,or various alternative methods (e.g the weight functtion method)[69][70] are used to estimate the stress intensity factor.

Scott and Thorpe therefore tested the sccuracy of the solutions presented by various authors by measuring changein the shape of a crack throughout its fatigue growth. They concluded that the best engineering estimation of the stress intensity factor for a part through crack in a plat and adjust form for a thin walled shell was provided by Newman solution.

SIF Calculation In this manuscript SIF calculation is performed using three different methods. First is analytically using the formula given[71] ,second is using the formula given[72] and third is FEM.

6.6.1 Various Methods For Analyzing The Proplem of Semi-Ellipticall Surface Cracks

API 579

The Mode I Stress Intensity Factor for cylinder – surface crack, longitudinal direction – semi-elliptical shape, internal pressure

$$K_1 = G_O \sigma \sqrt{\frac{\pi a}{\emptyset}} \qquad 6.18$$

$$K_1 = G_1 \sigma \sqrt{\frac{\pi a}{\emptyset}} \qquad 6.19$$

The values of G_o and G_1 at the deepest point and the surface point.

The influence coefficients G_o and G_1 for inside and outside surface cracks can be determined using the following equations:

Deepest point $G_o = a_0 + a_1\left(\frac{a}{t}\right)^{0.5} + a_2\left(\frac{a}{t}\right) + a_3\left(\frac{a}{t}\right)^3$ *6.20*

Surface point $G_1 = c_0 + c_1\left(\frac{a}{t}\right) + c_2\left(\frac{a}{t}\right)^2 + c_3\left(\frac{a}{t}\right)^4$ *6.21*

Where can fined values of a_0, a_1, a_2, a_3 and c_0, c_1, c_2, c_3 from [73][74][75][76]

$\emptyset = 1.0 + 1.464\left(\frac{a}{c}\right)^{1.65}$ *6.22*

$\sigma_{ref} = \sqrt{9(M_s * \sigma)^2}/3$ *6.23*

$M_s = \Big/ 1 - \frac{a}{t} + \left({}^{a}/_{t}\Big/_{M_t}\right)$ *6.24*

Newman solution

Adjust form by Newman solution for a thin walled shell is given by

$K_1 = \left[M_F + \left(E_K\sqrt{\frac{C}{a}} - M_F\right)\left(\frac{a}{t}\right)^s\right]\frac{\sigma\sqrt{\pi a}}{E_K}M_{TM}$ *6.25*

Where M_F is the function depending on the geometry (on the ratio $\frac{a}{c}$)

$M_F = 1.13 - 0.1\left(\frac{a}{c}\right)$ *6.26*

$E_K = 1.0 + 1.464\left(\frac{a}{c}\right)^{1.65}$ *6.27*

$S = 2 + 8\left(\frac{a}{c}\right)^3 \qquad 0.02 \le \left(\frac{a}{c}\right) \le 1$ *6.28*

$M_{TM} = \frac{1 - C\frac{({}^{a}/_{t})}{M_T}}{1 - C({}^{a}/_{t})} \qquad C = 0.85$ *6.29*

M_{TM} is the correction factor [77][78].

BS-7910 Solution

As per BS7910, SIF can be simply expressed as a function of crack size and loading conditions using a closed form solution for the stress intensity factor:

$K_1 = \sigma_o Y\sqrt{\pi a}$ 6.30

Since Y depends on the geometry, it is a complex function of the crack size [71]. The geometric function for the calculation of SIF is given in Annex M of BS-7910 and is stated as: $Y =$

$Mf_w M_m$where M is the bulging factor. The detailed calculation for evaluating Y is given in [69], [79]**.** Once the value of Y has been calculated next step involves the calculation of K_1.[80]**.**

6.6.2 Newman Solution for a Thin-Walled Cylindrical shells

Various method is used for analyzing the problem of semi-elliptical surface crack in the wall of cylindrical shells a very good estimate of the stress intensity factor for such a crack is given

$$K_1 = \left[M_F + \left(E_K\sqrt{\frac{c}{a}} - M_F\right)\left(\frac{a}{t}\right)^S\right]\frac{\sigma\sqrt{\pi a}}{E_K}M_{TM} \qquad 6.31$$

This is an adjusted form of the Newman solution for a thin-walled cylindrical shells where M_F function depending on the crack geometry (a/c ratio),s function depending on the crack geometry (a/c ratio)and on the relative crack depth (a/t ratio),$M_{TM}(M_S)$ surface correction factor for a surface crack . FunctionM_F and s differ in form for the lowest point of crack (point A depth crack) and for surface crack (point B on the surface) ***Figure 6.14***. M_T is the Folias correction factor, several relation have been reported for determining the Folias correction factor, this factor function of ʎ. The value of parameter (s) determines how the stress intensity factor varies with the fractional crack depth a/t and a/c[81]. The parameter s to fit Raju and Newman results for the deepest point θ=π/2 is given by

$$S = 1.6 + 3(a/c)^3\_8(a/c)(a/t)^5 + 0.008(a/c) \qquad 6.32$$

For the surface θ=0 is given by

$$S = 0.3 + 1.15\left(\frac{c}{a}\right)^{1.3(a/t)(a/c)^{0.2}} + 0.8\left(\frac{a}{c}\right)^3 \qquad 6.33$$

When the surface crack 2c=14 mm, the previous method do not give the acceptable result (the geometric factor values decrease with increasing values of a). Methods to calculate the stress intensity factor was used depending on the influence coefficients G_j used as the input only G_0 andG_1 in table was used as input influence coefficients G_2 and G_3 were calculated as a function of G_0 and G_1 for the deepest point and surface point of the crack [82], where F is the boundary correction factor for a surface crack, given by:

$$F = \frac{t}{R}(R^2/(R_o^2 - R^2)(2G_o - 2\left(\frac{a}{R}\right)G_1 + 3\left(\frac{a}{R}\right)^2 G_2 - 4\left(\frac{a}{R}\right)^3 G_3) \qquad 6.34$$

$$K = \sigma\sqrt{\frac{\pi a}{\varphi}}\,F(\frac{a}{c}, \frac{a}{t}, \frac{R}{t}) \qquad 6.35$$

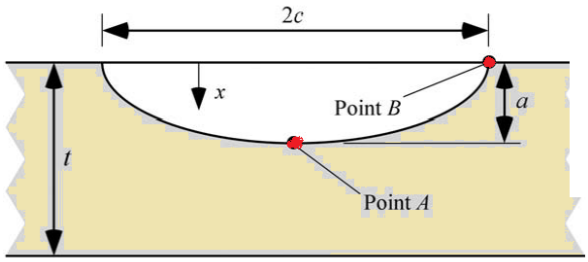

Figure 6-14: Crack geometry and dimensions surface crack

Table 6.7shows the comparison of the values of K1 between the three methods and results obtained from XFEM. We note through the comparison that the Newman method is closest.

Table 6-7: the comparison of the values of K1 between the three methods and results obtained from XFEM

a	K1 (BS7910	K1(API579)	K1(Newman)	K1 XFEM
3.5	930.08	824.8761	1257.26	1896.5
4.19	1546.83	1075.919	1531.13	2198.7
4.88	2139.50	1381.219	1861.18	2432.9
5.57	2913.05	1747.162	2316.03	2745.8
6.26	4035.3	2179.635	3099.41	2984.54
6.9	10655.2	2645.023	4762.55	3647.01

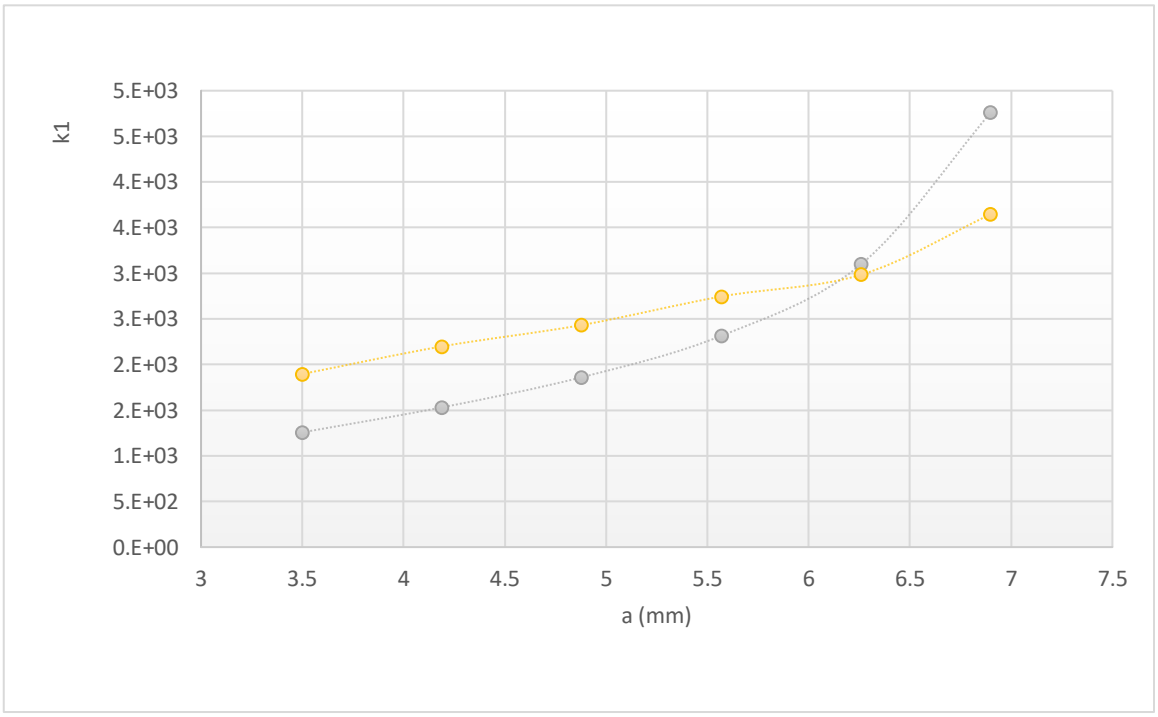

Figure 6-15: Show of relation between K1 and crack depth for Newman solution and XFEM

Table 6-8: show the comparison (Lr,Kr) between three approaches

	BS 7910			API 579			Newman solution		
a/2c=200	Lr	Kr old	Kr	Lr	Kr old	Kr new	Lr	Kr old	Kr new
3.5	0.260315	0.32179	0.242271	0.420464	0.285393	0.214867	0.43145	0.434991	0.327498
4.19	0.263046	0.535177	0.402926	0.519429	0.372249	0.28026	0.43815	0.529746	0.398837
4.88	0.267572	0.74023	0.557307	0.678393	0.477878	0.359786	0.4500	0.643934	0.484807
5.57	0.276527	1.007866	0.758806	0.975673	0.604488	0.455109	0.4713	0.801305	0.603289
6.26	0.302648	1.396142	1.051132	1.730875	0.754116	0.567761	0.51266	1.072342	0.807348
6.9	0.729662	3.68652	2.77552	6.072698	0.915132	0.688988	0.596549	1.647758	1.24057

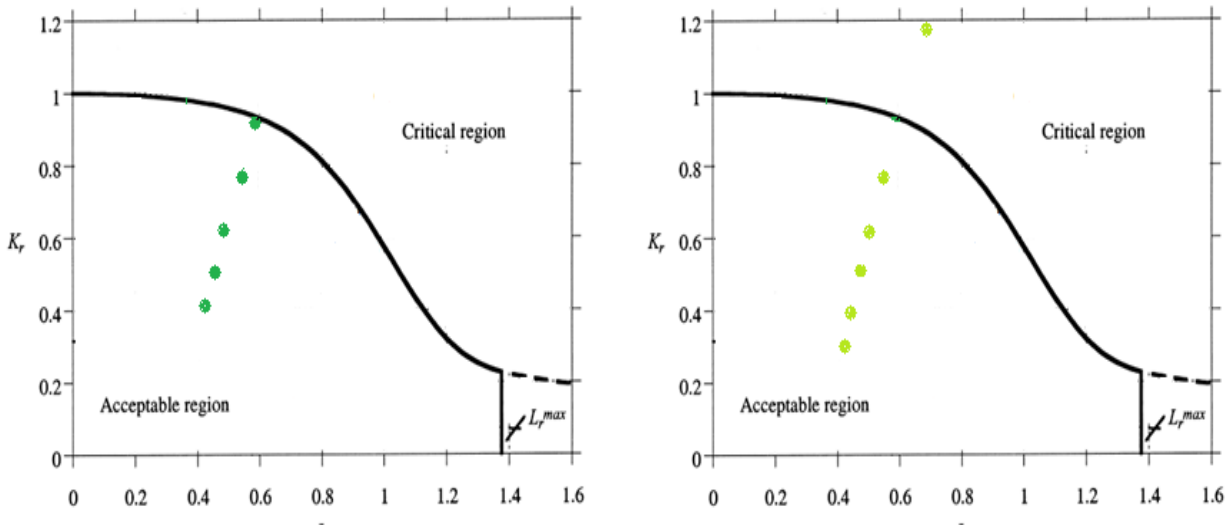

Figure 6-16: FAD (Newman solution Kr old and Kr new material)

For the initial external damage, length 2c = 200mm and depth a = 3.5mm, calculation was done for new and material from exploitation, as well as for two values of stress ratio R = 0.8 and R = 0.7. The results of crack growth as a function of the number of cycles N for new material and for stress coefficients R = 0.8 and R = 0.7 shown in the ***Figure 6.18, 6.19.*** a much shorter life (almost 5 times) is obvious for the stress ratio R = 0.7 in relation to R = 0.8. When it comes to material from exploitation, this influence is even more pronounced ,where the number of cycles to crack penetration is 12 times smaller ***Table 6.9, 6.10***.

Table 6-9: number of cycles to crack penetration is 12 times smaller

Old material				
R=0.8	R=0.7	R0.8/R0.7	n(R=0.8)	n(R=0.7)
464212.47	38101.15	12.18373	0.097414	0.007995

For crack growth from initial crack length until final length of 227.3 mm, 130941 cycles are necessary,where it requires the crack to through-wall to 103601.4 from a=4.19 to a=4.88 mm after

360611 cycles from initial crack a=3.5 mm, to be the finl number of the cycle from the initial crack to critical crack at ac = 4.88 mm equal 464212 cycles, and 595154 cycles to failure.

In the case R=0.7 from initial crack length until final length of 227.3 mm required to 10747.29 cycle, and the crack to through-wall to 8503 cycle from a=4.19 to a=4.88 after 29597.87 cycle from initial crack, so that is the final number of cycle 38101.15, and 48848.4 cycle to failure, [83], ***Figure 6.19.***

Table 6-10 : The final number of cycles to failure

New material				
R=0.8	R=0.7	R0.8/R0.7	n(R=0.8)	n(R=0.7)
2433641.3	494358.3	5	0.456	0.092707

As for the new material at R=0.8 it requires (428741.6)cycle until final length 226.06 mm (surface crack),and 130745.5 cycle to the crack through-wall (depth crack) from a=5.57 to final ac=6.26 mm after 2302895.8 from initial crack , to be the finl number of the cycle from the initial crack to critical crack at ac =6.26mm equal (2433641.3),and 2862382.9 cycle to failure. At R=0.7 from initial crack length until final length of 226.06mm required to (87092.5)cycle and 26559 required to penetrate the wall at ac=6.26 from a=5.57 after (467799.3) number of cycle from initial crack a=3.5mm , to become 494358.3 cycle was the finial number of cycle to critical crack at 6.26 mm,and 581450.83 cycle to failure.***Figure 6.18***

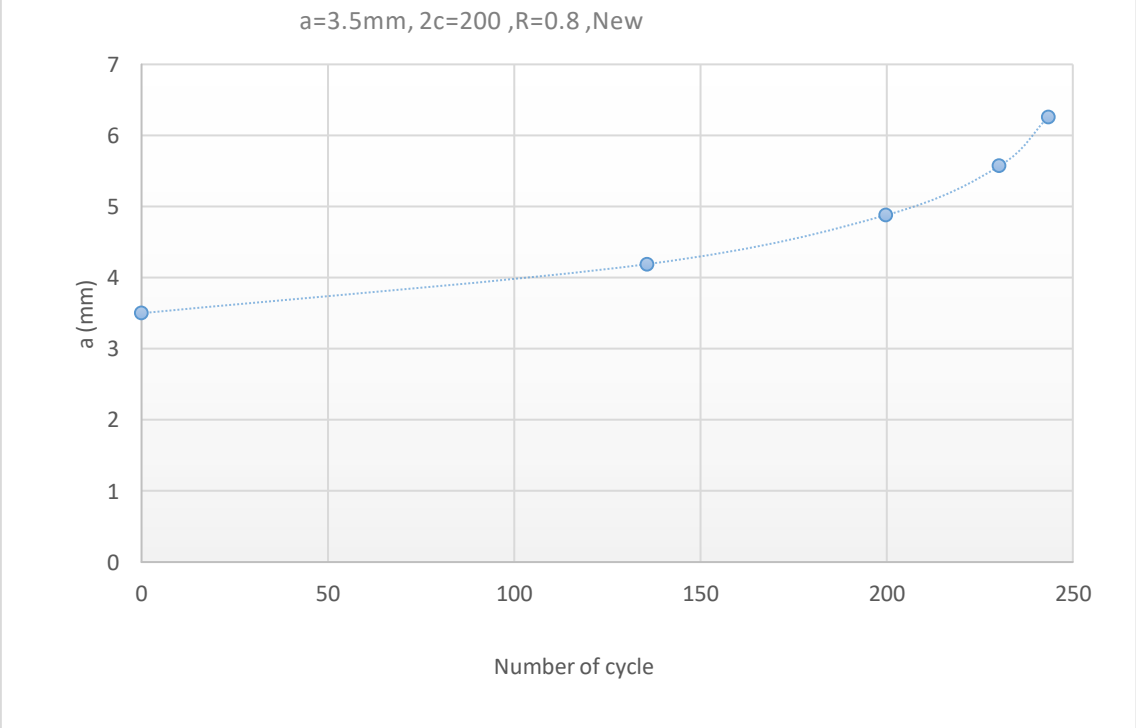

Figure 6-17: Number of cycle Propagation of a crack into the depth of the pipe wall

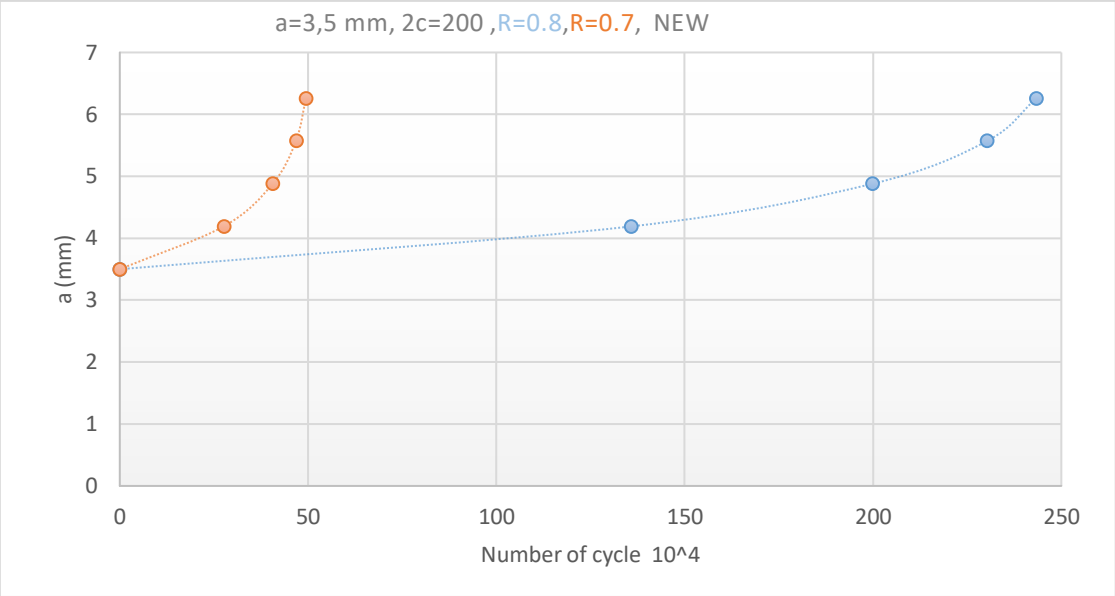

Figure 6-18: Influence of stress ratio on service life; (depth crack) new material

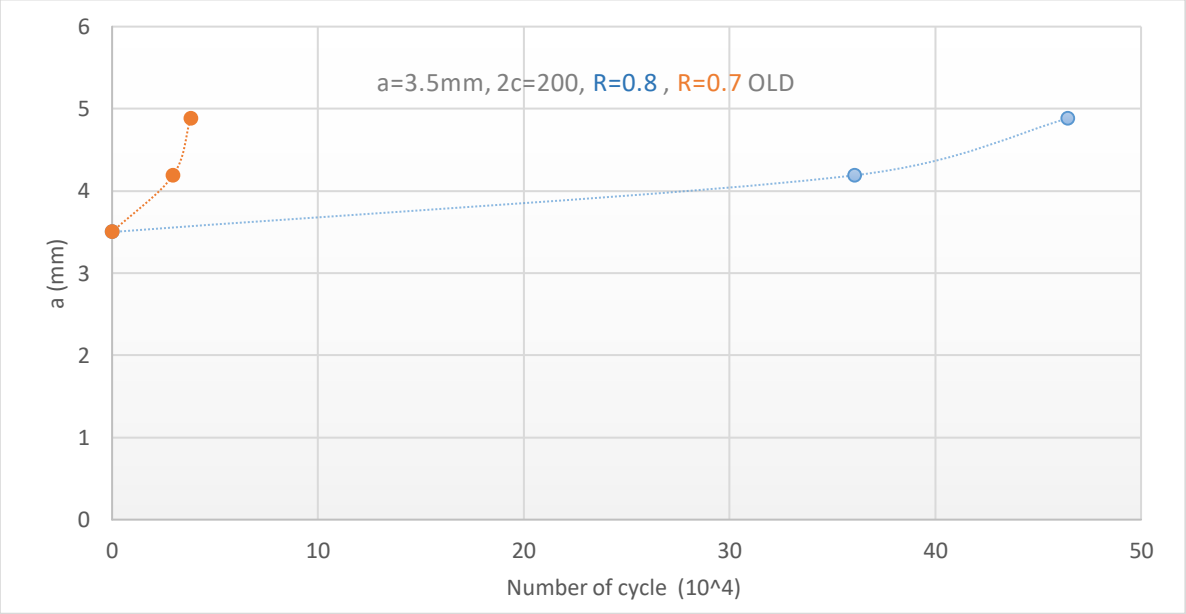

Figure 6-19: Influence of stress ratio on service life; (depth crack and surface crack) old material

Generally, when the crack penetrates the pipe wall, the number of cycles required for crack growth becomes significantly smaller crack continues to grow in the axial direction. For example, the number of cycles for the crack to grow from an initial length of 200 mm and a depth of 3.5 mm to a final length of **226**mm was **286** cycles, the propagation of the crack into the depth of the pipe wall it consumes the largest part, **243** cycles. After that the crack growth is Somewhat slower, up to a length of **226** mm (only about **43** cycles are required. Obviously, the largest number of cycles is required for the crack until it penetrates the pipe wall ***Figure 6.20***

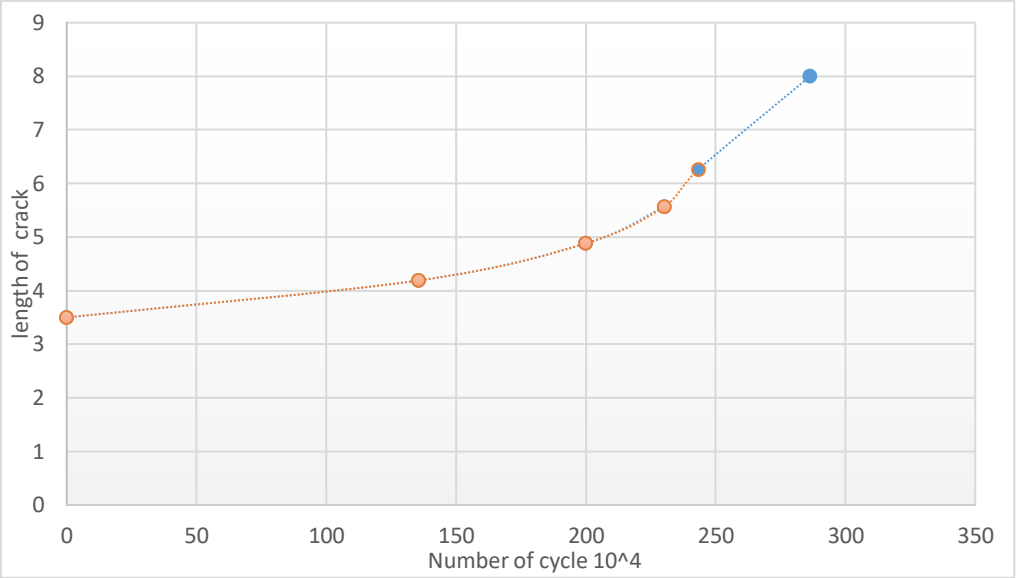

Figure 6-20: cycles from penetrates the pipe wall to failure

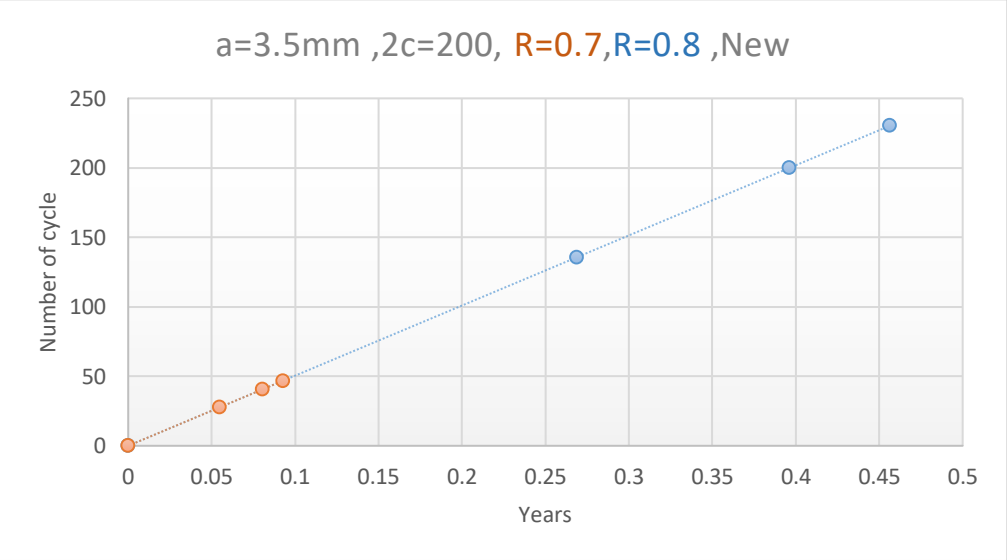

Figure 6-21: show years Vs Number of cycles (depth crack) at R=0.8, R=0.7

For an initial crack depth of a = 2mm and ,2c = 200mm, the predicted fatigue life is 4673530cycles until crack penetration, this is equal 9.4 times when was the initial depth of a = 3.5mm (new material in the same stress ratio R = 0.7), and 99065.5 cycle required to until final length 2c=229.2 mm, that is, the final life of fatigue is about 4772595.6 cycle. ***Figure 6.22***.

At R = 0.8 the predicted fatigue life was 23006988 cycles until crack penetration, and 487682 cycles until final length 2c=229.2 mm, that is, the full life of fatigue equal 23494671 cycle around 4.656 years, failure occurs at a_c=3.2 mm which indicating the extent of the effect of surface crack length for fatigue life. ***Figure 6.23.***

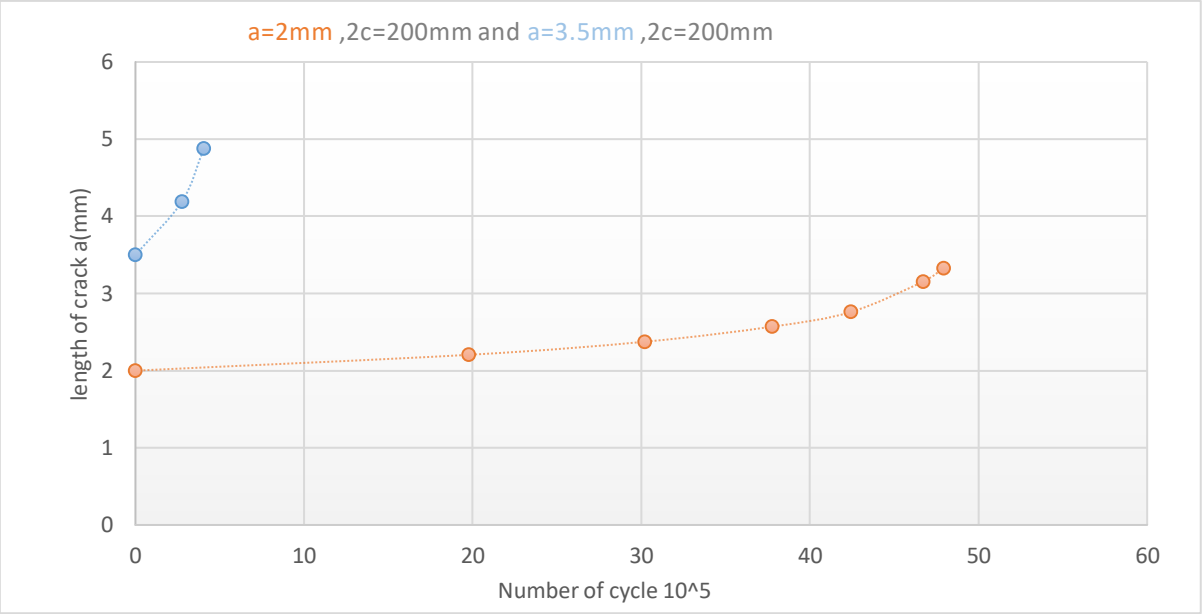

Figure 6-22; Number of cycles Vs. length of crack a(mm) at R=0.7 whereas ac=4.88 when initial crack a=3.5mm, and ac = 3.2mm when initial crack a=2mm.

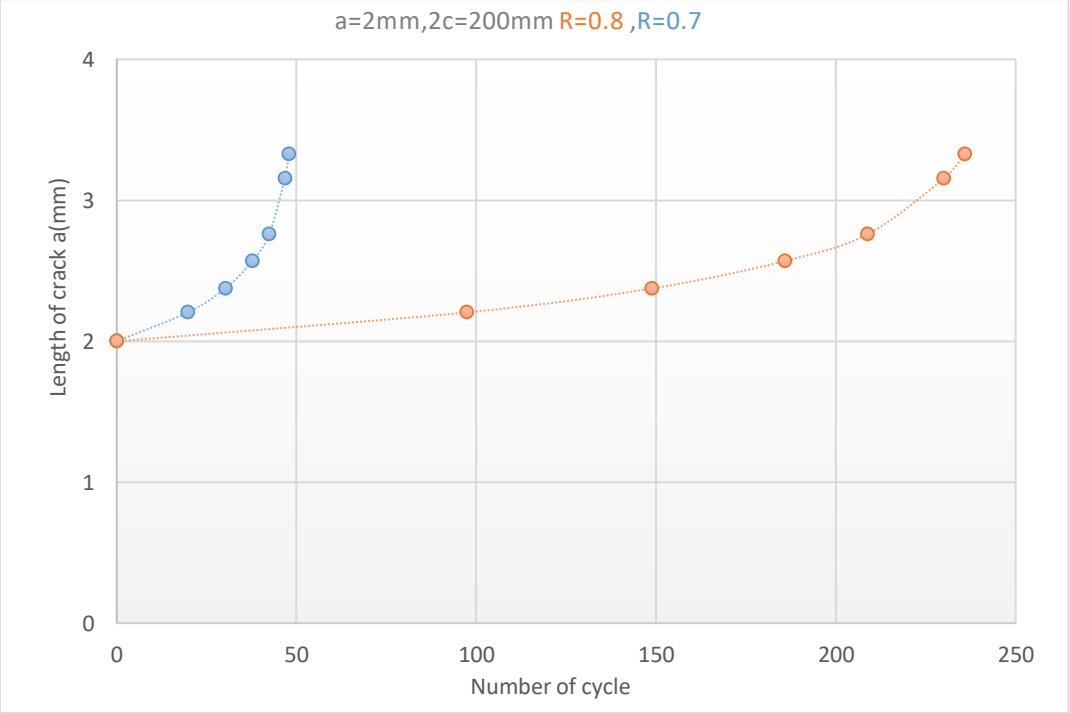

Figure 6-23: Number of cycles Vs. length of crack a(mm) when initial crack a=2mm, and ac = 3.2mm.

When comparing the previous case with taken initial crack length 2c = 14mm, depth a = 2mm is found that the fatigue life increasing at R = 0.8 from 4.65 years to 27.8 years ***Figure 6.24***, ***6.25***.***Figures 6.28, 6.30*** show the effect of each crack length and stress ratio on the life of fatigue.

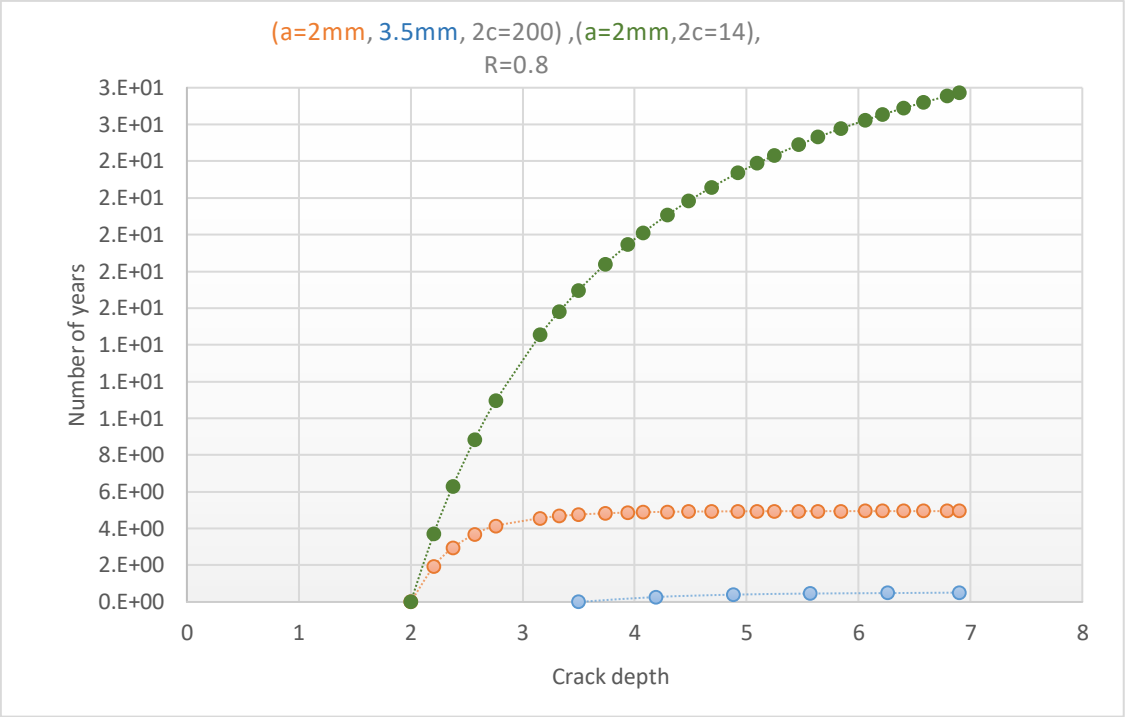

Figure 6-24: Number of years vs. crack depth

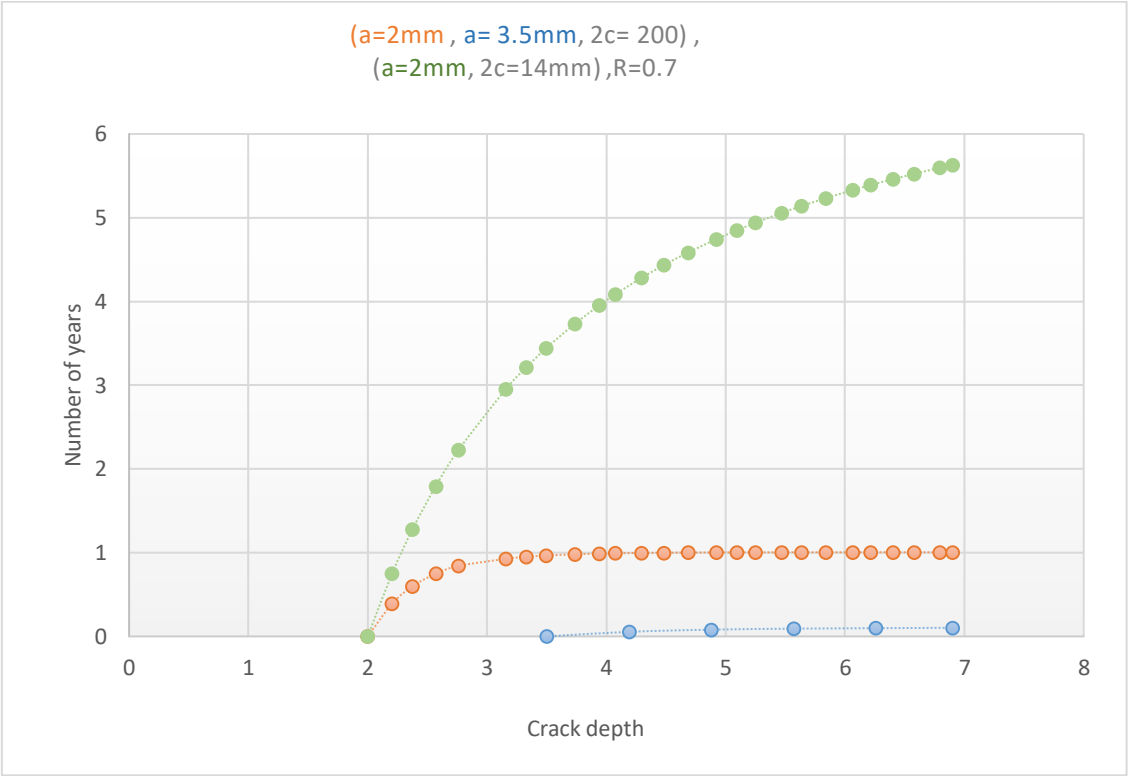

Figure 6-25: Number of years vs. crack depth

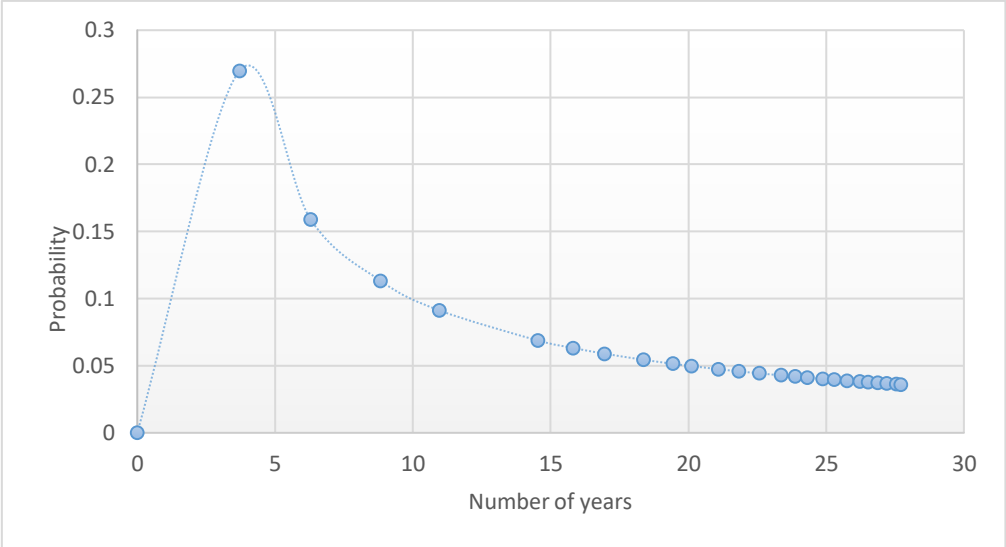

Figure 6-26: Number of cycles vs. Probability (a=2mm,2c=14mm, R=0.8)

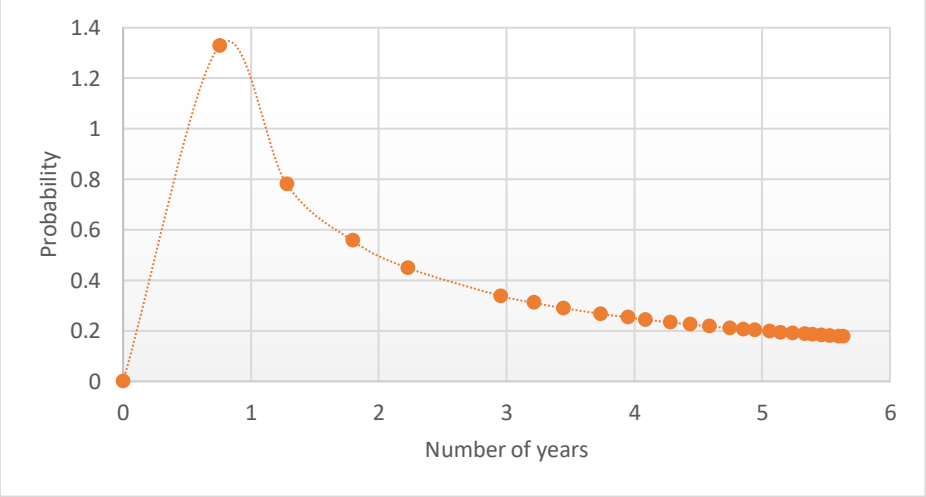

Figure 6-27: Number of cycles vs. Probability (a=2mm,2c=14mm, R=0.7)

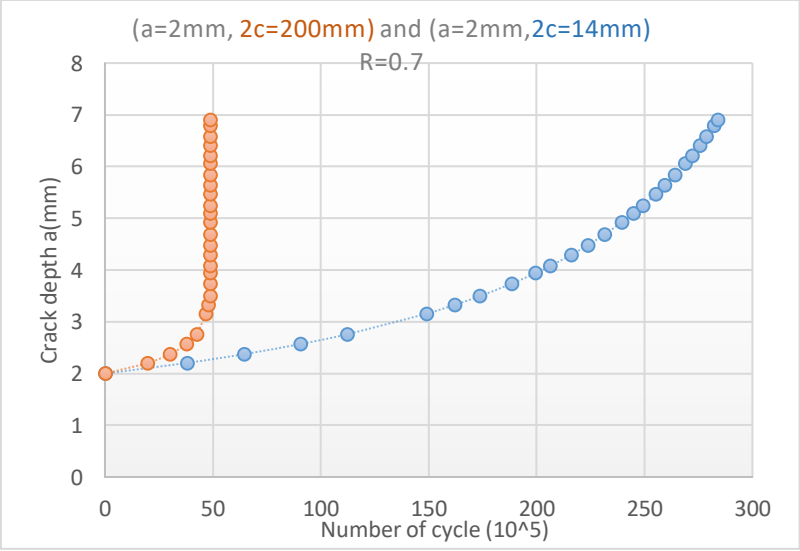

Figure 6-28: Influence of initial crack length (surface crack) on fatigue life; new material

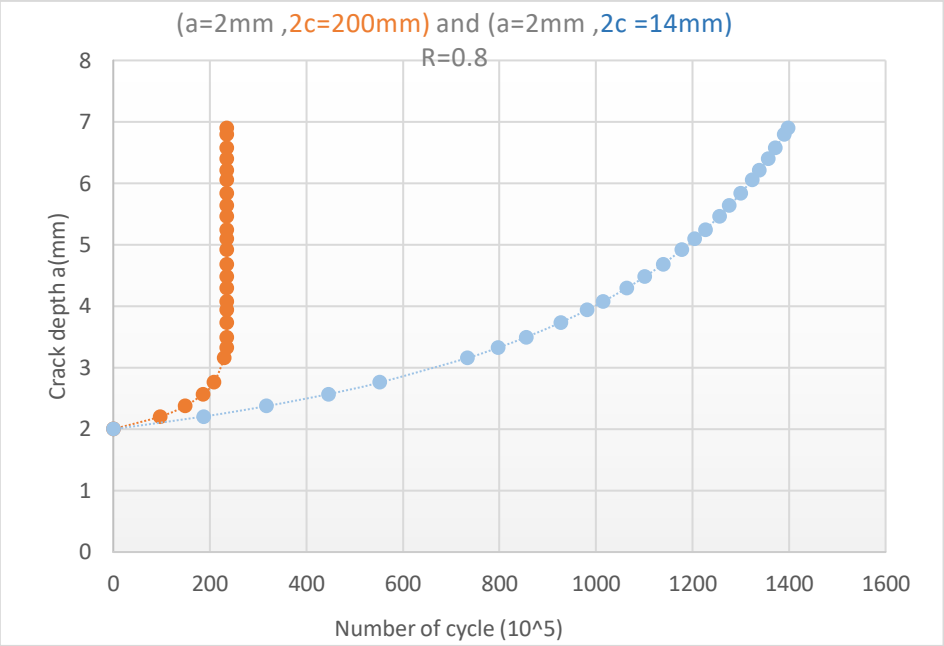

Figure 6-29: Influence of initial crack length on fatigue life; new material, the fatigue life increase from 4.656 years to 27.87 years, failure occurs at ac=3.2 where 2c=200mm.

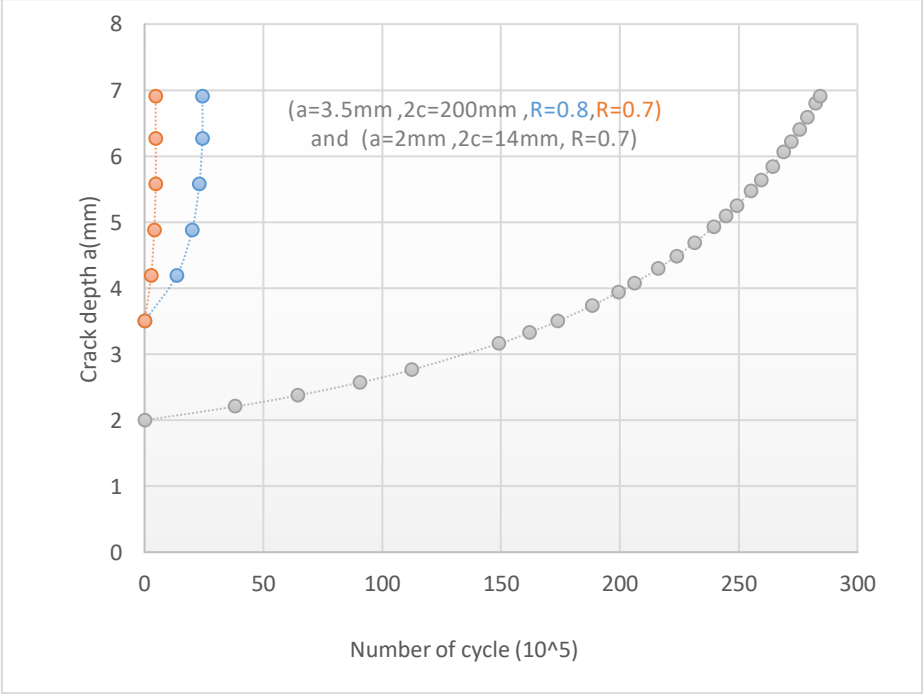

Figure 6-30:Comparison show influence of initial crack length and stress ratio on fatigue life; new material

Risk assessment

Risk based analysis is useful method to bridge the gap between engineers and managers and provide common solution in the case when decision about further treatment of cracked components should be made.

Table 6.12 presents the risk matrix for fatigue failure of an oil drilling rig pipe, from data given in ***Table 6.11*** with consequences taken between the low, high, and very high, and probabilities as given in ***Table 6.11*** one should notice the extent of the effect crack length and stress ratio to change from low to high and very high. Anyhow, this is a conservative estimation, since one can expect slower or faster fatigue crack growth in the case analyzed here.

Table 6-11: Consequences taken between the low, high, and very high

	R=0.7		R=0.8	
2c/a	2mm	3,5mm	2mm	3.5mm
14mm	28573712.07	6525391.024	140663494.8	32123383.36
n(year)	5.662646069	1.29318094	27.87623	6.366108473
probability	0.176595886	0.773286993	0.036092159	0.157081835
200mm	4772595.6	581450.83	23494671.57	2862382.944
n(year)	0.94581	0.1152	4.656098211	0.567625
probability	1.042882868	8.680	0.214772102	1.761

Table 6-12: Risk matrix for fatigue failure of an oil drilling rig pip

Probability **category**	Consequence category					
	1 – very low	2 - low	3 - medium	4 - high	5 - very high	**Risk legend**
≤0.2 very low	a=2mm,2c=14mm R=0.8, R=0.7 a=3.5mm,2c=14mm R=0.8					**Very low**
0.2-0.4 low		2mm,2c=200, R=0.8				**Low**
0.4-0.6 medium						**Medium**
0.6-0.8 high				a=3.5mm,2c=14mm R=0.7		**High**
0.8-1.0 very high				a=2mm,2c=200 R=0.7	a=3.5mm,2c =200mm, R=0.8,R=0.7	**Very High**

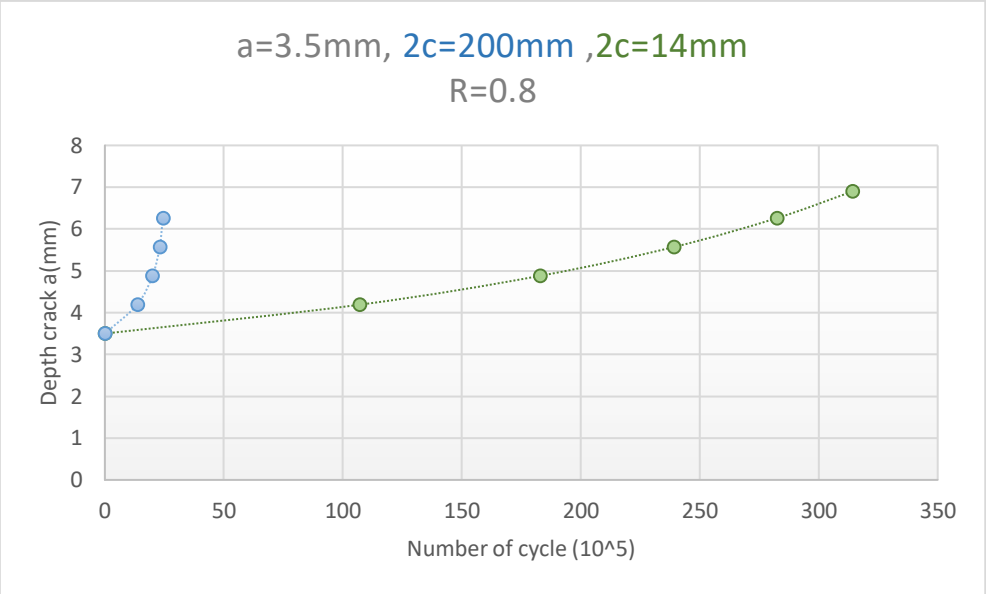

Figure 6-31: Influence of crack length in axial direction at initial crack depth of a = 3.5mm and for two values of crack length in the axial direction: 2c = 14mm and 2c = 200mm.

Ratio R = 0.8, fatigue life increase from 0.567 years to 6.366 years

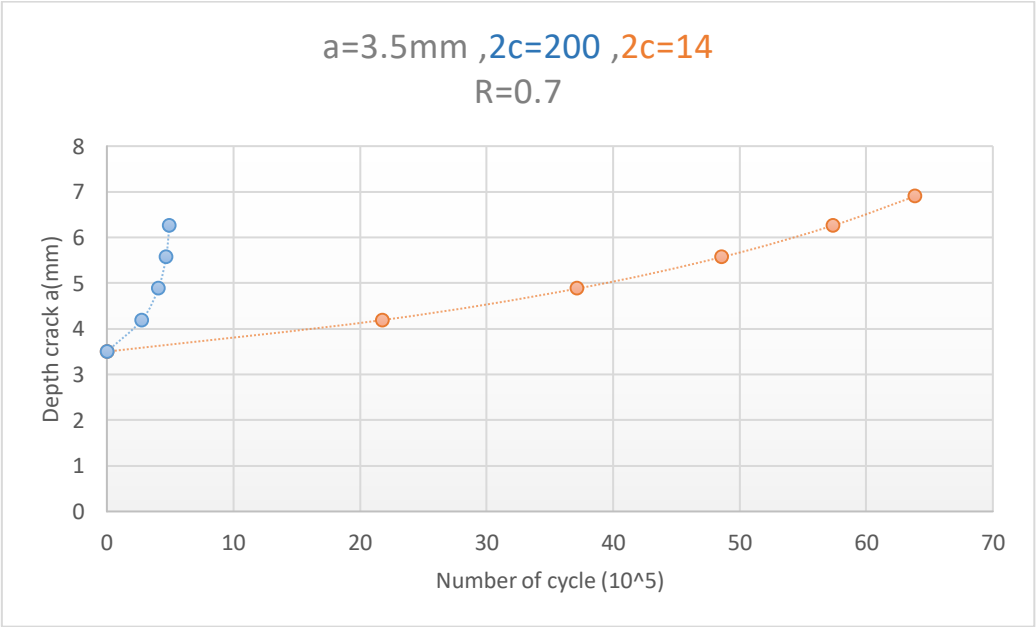

Figure 6-32: Influence of crack length in axial direction at initial crack depth of a = 3.5mm and for two values of crack length in the axial direction: 2c = 14mm and 2c = 200mm.

Ratio R = 0.7.

6.6.3 Comparison of Different Lengths of Surface Cracks at The Same Deep Crack

Table 6.13,6.14 Includes number of cycles for different lengths of surface crack (2c) at the same initial depth crack a = 2mm, which is can show the effect of longitudinal cracks (surface crack) on fatigue life, this explains the decrease in the expected fatigue life for pipes welded pipes made of API

J55 steel from 30 years to 8 years. Whenever the longitudinal cracks are small, the longer fatigue life will be. Note in the case 2c = 14mm, the fatigue life is 27 years until the wall breaks through, the fatigue life may continue longer than that until collapse occurs when the longitudinal cracks reach the critical length. This confirms that the expectation that the fatigue life of the pipe will be 30 is correct and maybe more in the case of the initial cracks very small.

Table 6-13: show different of longitudinal crack (surface crack) at a=2mm (depth crack) and R=0.8

2c	N	n(year)	probability	ac
200	23494671.57	4.656	0.21477663	3.2
100	43924620.39	8.704	0.11520737	4.92
60	80507656.1	15.954	0.06269592	6.06
14	140663494.8	27.876	0.03584229	6.98

Table 6-14: show different of longitudinal crack (surface crack) at a=2mm (depth crack) and R=0.7

2c	N	n(year)	probability
200	4772595.5	0.945817	1.05728631
100	8922638.08	1.7682	0.56552781
60	16353941.63	3.2409	0.30854947
14	28573712.07	5.66262	0.17763489

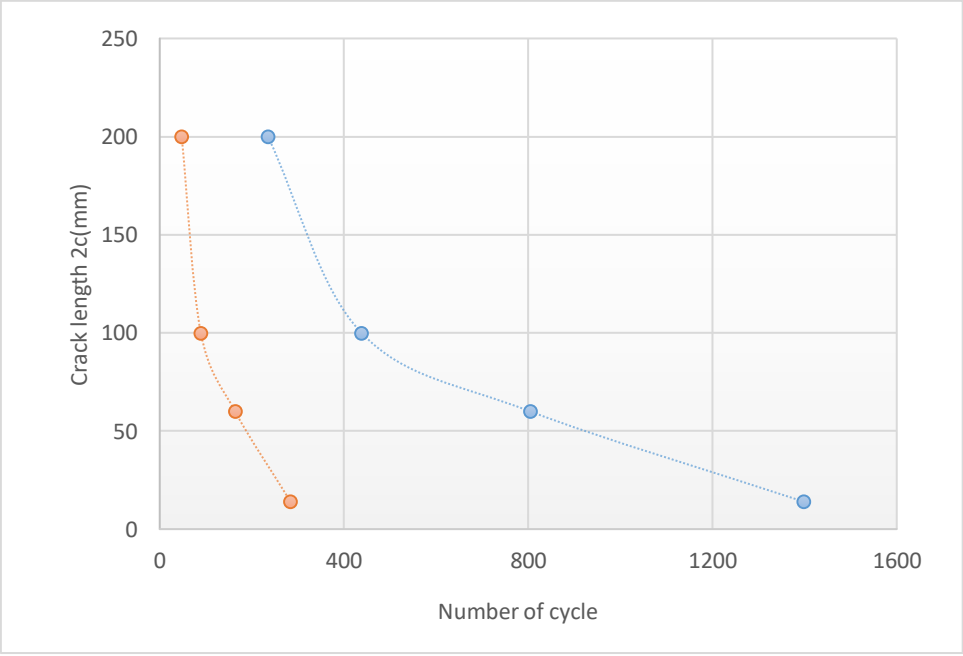

Figure 6-33: Clarifies changed number of cycles with changed length of surface cracks

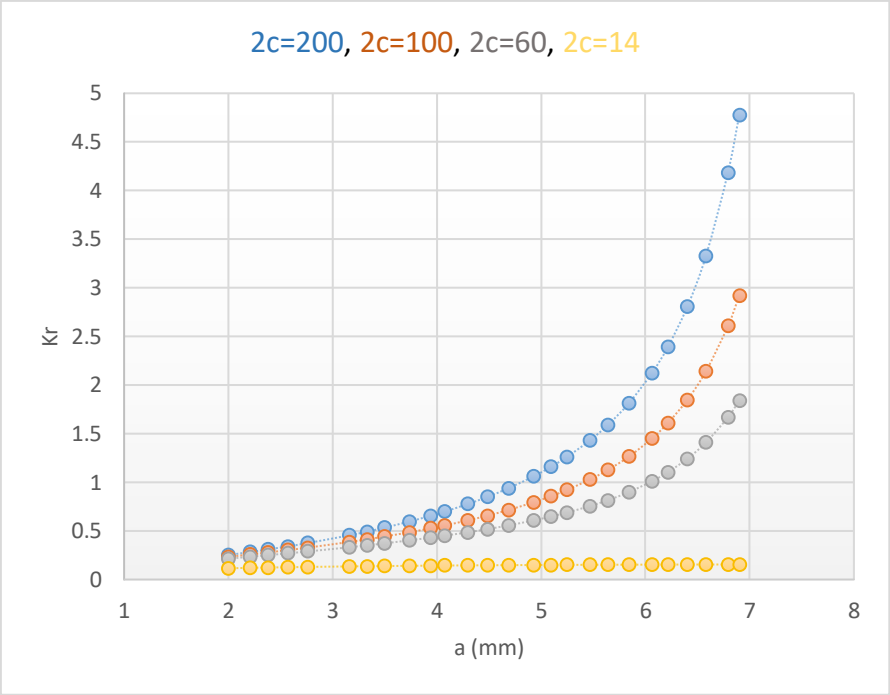

Figure 6-34: Kr at different surface crack 2c at depth crack a=2mm

We notice from the shape of the curve at value of 2c =14 that the fatigue life may continue even after penetrating the wall and that the pipe continues to serve for a long period.

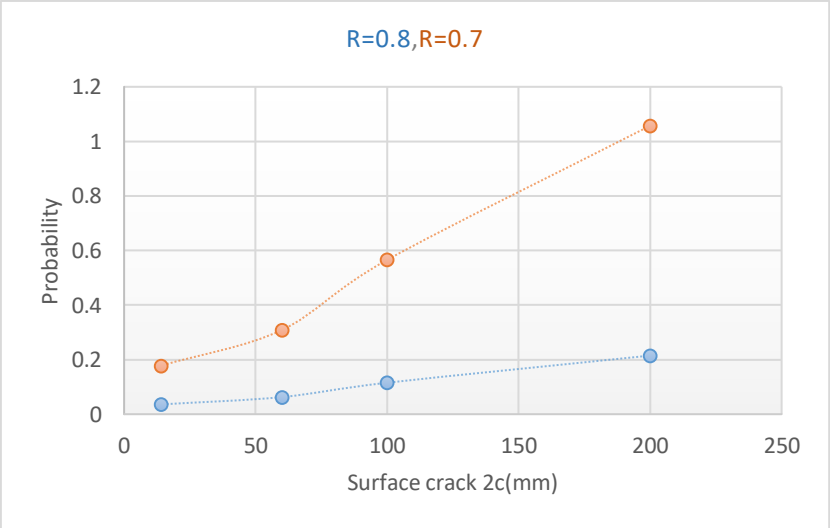

Figure 6-35: Surface crack (2c mm) Vs. probability at a=2mm

More precise methods like FEM and experiment are more expensive, especially the later one, but often inevitable in the case of critical component. Probably the best approach would be to adopt two-phase decision-making process, with the first one based on simple engineering approach, based on analytical tools, and then, if needed, more sophisticated numerical and/or experimental analysis, in the second phase.

6.5.3.1 Risk Assessment

Table 6.15 presents the risk matrix for different lengths of surface crack 2c at depth crack a = 2mm, as given in ***Table 6.13, 6.14***consequences taken between the very low, low, medium, high, very high, Anyhow, this is a conservative estimation, since one can expect slower or faster fatigue crack growth in the cases analyzed here.

Table 6-15: risk matrix for different lengths of surface crack 2c at depth crack a = 2mm

Probability **category**	Consequence category					
	1 – very low	2 - low	3 - medium	4 - high	5 - very high	**Risk legend**
≤0.2 very low	a=2mm,2c=100mm a=2mm,2c=60mm R=0.8 a=2mm,2c=100mm R=0.8,R=0.7					**Very low**
0.2-0.4 low		2mm,2c=200, R=0.8 2mm,2c=60 R=0.7				**Low**
0.4-0.6 medium			a=2mm,2c=100 R=0.7			**Medium**
0.6-0.8 high						**High**
0.8-1.0 very high					a=2mm,2c =200mm, R=0.7	**Very High**

The existence of a database of data obtained from experiments, realistic events and numerical results and arranging them in matrices that help in calculating the life expectancy by analytical methods without the need to conduct costly experiments especially if the geometric shape is uncomplicated and by knowing the percentage of error between the analytical methods, experimental methods and numerical methods that are inferred comparison with the database, the results will be more accurate.

6.7 Discussion

Crack depth on a structural element subjected to variable load has a significant impact on the life of that element. However, by analyzing it is evident that the remaining fatigue life also is more sensitive to changes in the stress range and the length of surface crack in addition to the reference values of the external damage depth. If, for example, at a fixed value Crack depth a = 3.5 mm and 2c = 200mm change the stress range from R = 0.8 to R = 0.7 shortens the fatigue life by 79%. On the other hand, when the crack depth a = 2 mm and surface crack 2c = 200 mm, at the same stress range R = 0.8, the fatigue life increasing 9.6 times than when a = 3.5mm in the same case when R = 0.7. In the case of the depth of the initial crack a = 2 mm and 2c = 14 mm (change from 2c = 200mm to 2c = 14mm) at

the same stress range R = 0.8, it increasing the fatigue life from 4.656 years to 27.876 years. The different between values R = 0.8 and R = 0.7 when a = 2mm and 2c = 14mm 4.92 times.

The influence dominant from the stress range and surface crack is very important in addition to the depth of damage, with this in mind, it can be concluded that it is for this species problems, in cases where there is a crack of a certain depth in the structural element, it is more important to monitor the load range and surface crack in addition to the depth.

However, the results obtained must be taken into consideration. Given the anticipated operating conditions (elevated pressures and temperatures, as well as the chemically aggressive working environment). The prediction of crack growth rate and strength of pipe demands accurate calculation of stress intensity factors (SIFs), which determine the appropriate crack growth increment for the crack. Based on the presented results, one can conclude that experimental and numerical, and theoretical results well, with some differences which require further investigation. Therefore, the presence of the database of experimental and realistic results with the obtained stress factor histories helps to predict fatigue crack growth rates by using numerical and theoretical results.

We can use analytical methods when having uncomplicated geometric shapes instead of expensive experiments or by applying XFEM, where it is necessary to model a test tube, generate a network, and then define the load, boundary conditions, to be obtained results in short time.

6.8 Extended finite element method (XFEM) in 3D crack growth simulation on a standard Charpy specimen

The simulation of crack growth using XFEM will be done first on the model of a standard Charpy test tube made of API J55 steel ***Figure 6.36***. will be used to compare with the results obtained from an experiment with a Charpy test tube. The Charpy test tube model is defined in the Abaqus software as well as the characteristics of the material (steel, whose Young's modulus is 2.1 105 MPa and Poisson's coefficient 0.33), bending stress value 7 MPa and corresponding boundary conditions, [83].

In Abaqus, a finite element network of the hexahedral type is defined ***Figure 6.36a***. The notch on the test tube, 2 mm deep, is treated as the initial crack length. The figure shows that in the area where the crack growth is expected, a much denser network is generated, with a larger number of nodes, in order to increase the accuracy of the obtained values. This tetrahedral network consists of 72692 nodes and 67254 elements. ***Figure 6.36b*** shows the initial crack (notch) on a standard Charpy specimen and the mesh around it, [83].

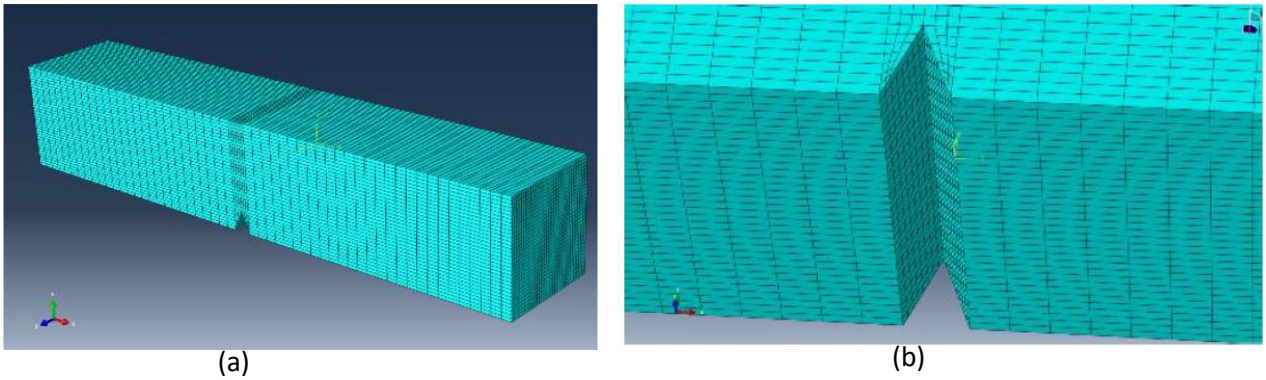

Figure 6-36: (a) Finite element network of the Charpy specimen model (b) Initial crack (notch) in a standard Charpy specimen

The first step in 3D crack growth analysis using XFEM is to "open" the crack. Here, the stresses in the test tube were calculated and based on them, the stress intensity factors at the crack tip and the deflection angle in relation to the initial expected growth direction were determined. To calculate stress factors of forms I, II and III use a plug-in called Morfeo / Crack for Abaqus. This software add-on uses a solution from Abaqus because it does not own solver for finite elements. Morfeo / Crack for Abaqus, calculates all stress intensity factor (K) modes in crack front nodes and prepares a value file required for the next crack growth step in Abaqus. Abaqus keeps in special files the obtained values of stress and strain for each step of the calculation. Shown in ***Figure 6.37*** are von Mises stress that occur on the test tube in the first step of the simulation.

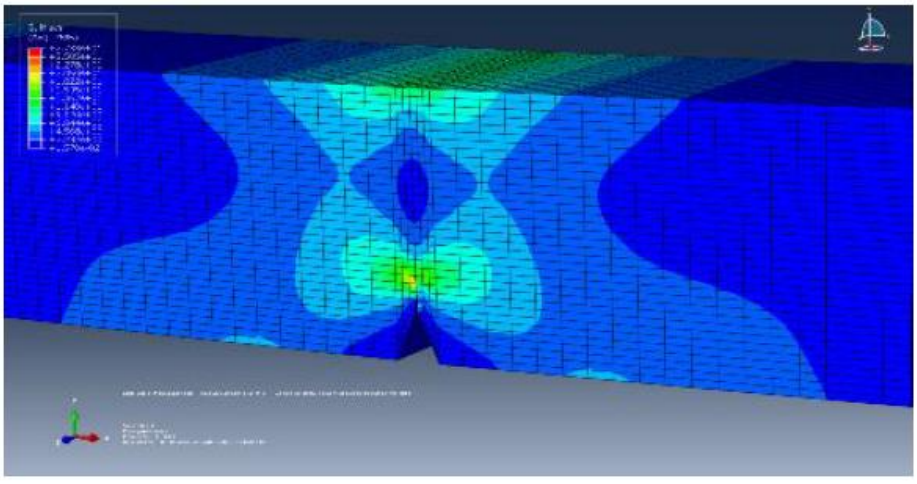

Figure 6-37: Stress state (von mises) on the test tube in the first step of the simulation

Morfeo / Crack for Abacus provides two crack growth options: forced crack growth in the plane (force in-plain propagation), which is controlled by the user and free crack growth, which the software automatically performs. Here, the option of free expansion of the crack with a step of 0.3

mm was chosen and its growth was monitored during 28 steps. The crack grew through an unchanged network of elements in the vertical plane (y direction in the figure), almost exactly between two rows of hexahedra, (***Figures 6.38-6.40***), slight deviation from that direction to the right (in the first few steps, by 0.006 mm, and from the tenth steps all the way to the end, to some 0.03 mm) and continued to grow through the hexahedra. The stress states around the crack tip after the eighth, fourteenth, and twenty-seventh propagation steps are shown in ***Figures 6.41-6.44.***

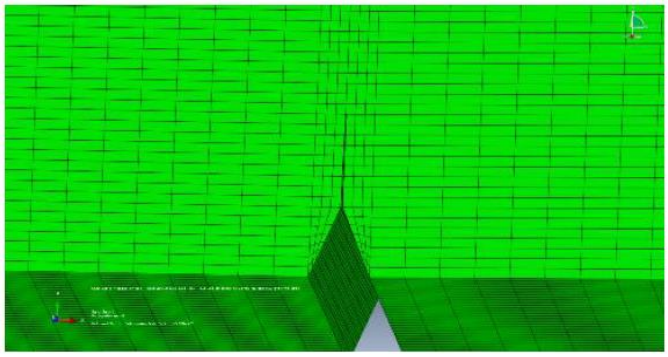

Figure 6-38: The appearance of the crack on the test tube after the eighth growth step

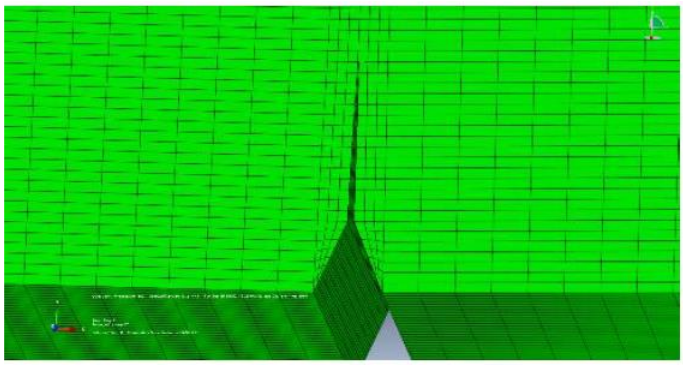

Figure 6-39: Appearance of the crack on the specimen after the seventeenth growth step

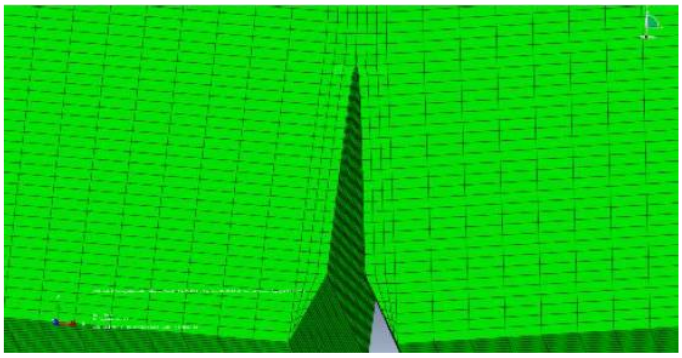

Figure 6-40: Appearance of the crack on the specimen after the twenty-seventh step of growth step

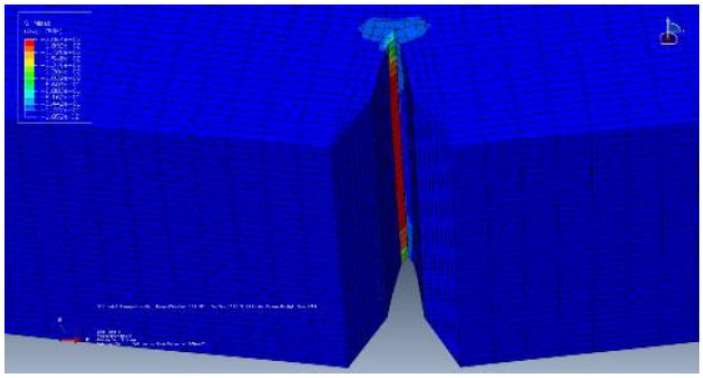

Figure 6-41: Von Moses stresses at the crack tip after 8 growth steps.

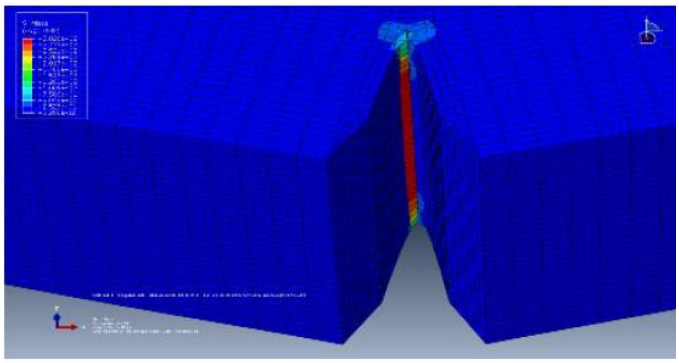

Figure 6-42: Stress state (von mises) after 14 crack growth steps

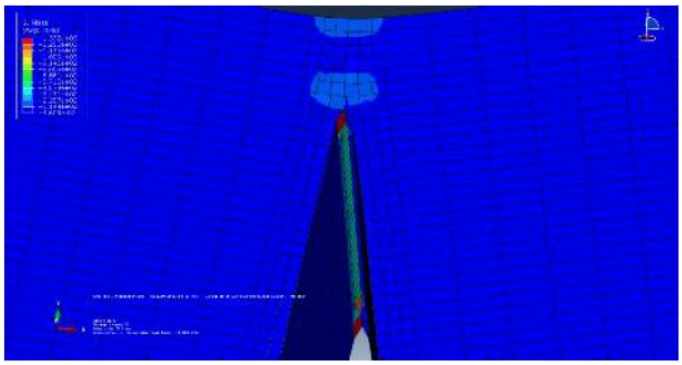

Figure 6-43: Stress state (von mises) after 27 crack growth steps

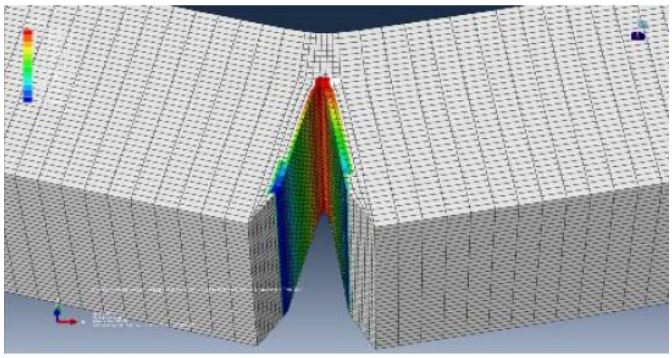

Figure 6-44: Distribution of stress around the crack for the twenty-third step of crack propagations

Here it is important to point out that the values of the stress intensity factor obtained by 3D simulation are calculated at several points along the crack front, which expands spatially. This is quite different from 2D simulations, in which the value of the stress intensity factor is calculated only at one point, the crack tip. This possibility of spatial crack development and stress intensity factor (SIF) calculation at all points of the crack front provides SIF values for all three forms of crack propagation, KI, KII and KIII. In addition to these values, the software gives the value of the equivalent stress intensity factor K_{eq}, which is the resultant of these three mentioned factors. use of K_{eq}, is the most suitable because it has sublimated the SIF values for all three forms. ***Table 6.16***, it is obvious that the values for KI are significantly higher, and therefore more influential, than the values for KII and KIII, so it would not be a big mistake to consider values for KI only. The values obtained in Abaqus using XFEM are shown in ***Table 6.16***, which shows that Morfeo / Crack for Abaqus during each propagation step calculates the curvilinear coordinate of each point along the crack front, the coordinates of the points in the global xyz system, values for stress intensity factors of forms I, II and III, as well as the value of the equivalent voltage intensity factor. The number of output values in each propagation step depends on the number of points on the front, i.e. the density of the finite network elements, and is quite large.

Table 6-16: Display the values that the software provides for each crack growth step

curvilinear abscissa along the crack front	*The coordinate of the front point*			K_{eq}	K_I	K_{II}	K_{III}
	X	*Y*	*Z*				
0	0.033	0.781	0.035	67.41	67.31	-0.080	0.760
0.152	0.030	0.791	0.187	67.43	67.33	-0.098	0.710
0.294	0.028	0.801	0.328	67.46	67.36	-0.115	0.657
0.446	0.025	0.816	0.479	67.48	67.39	-0.134	0.594
0.585	0.023	0.828	0.618	67.49	67.41	-0.150	0.531
0.716	0.021	0.841	0.749	67.50	67.43	-0.164	0.470
0.855	0.0182	0.854	0.887	67.51	67.44	-0.178	0.403

The number of crack front points is the same in each crack propagation step (from 66 to 68), which means that the crack spreads through an equal number of network elements. As can be seen from ***Table 6.17***, the crack growth per step was smaller than that initially given, 0.3 mm. This given step

of 0.3 mm is the maximum value that the crack growth per step should reach, but Morfeo / Crack for Abaqus "chose" the growth that is appropriate for him (of course, within the given limits). ***Figure 6.45*** shows this crack growth per step, where it is seen that the dependence is almost linear.

Table 6-17: The values for equivalent stress intensity factor, K_{eq} and stress intensity factor mode I, K_I for crack propagation in 28 steps

			Equivalent SIF, K_{eq} $[MPa\sqrt{mm}]$			SIF style I, K_I $[MPa\sqrt{mm}]$		
step	Crack length (a) [mm]	The number of front points cracks	max	min	Middle value	max	min	Middle value
1	2	66	28.0933	26.3349	27.60046	28.0999	26.3488	27.60795
2	2.155	68	29.622	27.9383	29.08235	29.6379	27.9303	29.08584
3	2.315	66	31.1018	29.5332	30.68409	30.9711	29.5076	30.60972
4	2.479	68	32.3888	31.4986	32.14672	32.4476	31.4603	32.1652
5	2.658	68	34.3203	33.8014	34.03595	34.3492	33.8197	34.04157
6	2.848	66	36.4714	35.8266	36.25288	36.425	35.8257	36.22021
7	3.034	68	37.7957	37.3897	37.6594	37.846	37.3914	37.68904
8	3.227	68	40.1995	39.7751	40.00304	40.2244	39.7717	39.99278
9	3.421	66	43.0343	42.6685	42.87502	42.9754	42.6236	42.82151
10	3.611	68	44.9149	44.5703	44.8051	44.9382	44.5832	44.83156
11	3.808	68	47.9569	47.572	47.7665	47.9998	47.4984	47.75301
12	3.996	66	51.6597	51.2891	51.52489	51.6232	51.1947	51.46525
13	4.197	68	54.3792	54.1382	54.26672	54.4012	54.1578	54.30418
14	4.394	68	58.3509	58.0395	58.18973	58.4343	57.9133	58.17982
15	4.585	66	63.4721	63.1964	63.32829	63.4361	63.0737	63.25105
16	4.787	68	67.5058	67.0816	67.27562	67.4519	67.1949	67.33336
17	4.989	68	73.1073	72.5755	72.80161	73.0249	72.5907	72.80897
18	5.181	66	80.4388	79.9463	80.21043	80.3042	79.8409	80.10434
19	5.384	68	86.3236	85.7624	86.04558	86.2694	85.914	86.11601
20	5.588	68	95.1008	93.9812	94.39053	94.7788	94.0989	94.40396
21	5.78	66	106.233	105.287	105.7143	106.006	105.167	105.5827
22	5.984	68	116.029	114.749	115.3681	115.783	115.079	115.4853
23	6.187	66	130.002	128.015	128.6781	129.665	128.219	128.726
24	6.379	66	148.738	146.775	147.7052	148.406	146.73	147.5672
25	6.584	68	165.457	163.29	164.1606	165.096	164.017	164.3781
26	6.788	68	190.811	187.023	188.1383	190.236	187.304	188.2178
27	6.98	66	226.315	223.023	224.0823	225.715	222.788	223.7425
28	7.183	68	261.416	257.561	258.9905	261.119	257.682	258.9038

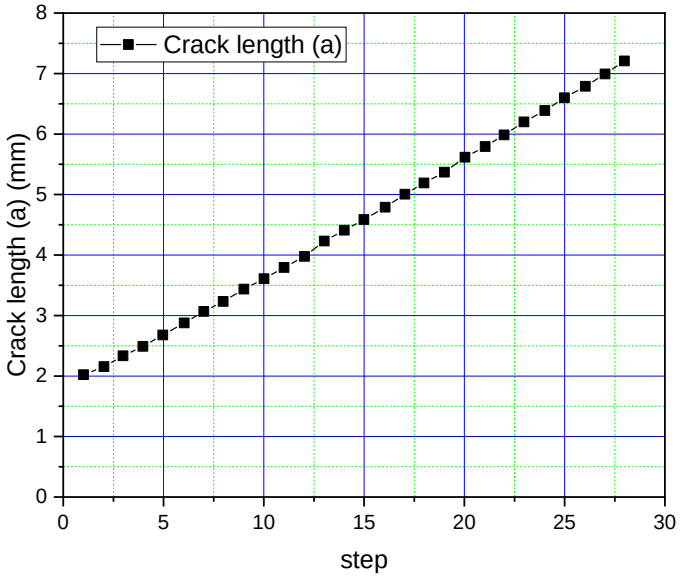

Figure 6-45: crack growth per step

Table 6.17 shows the minimum and maximum values of the stress intensity factors K_I and K_{eq} during the 28 crack propagation steps. The values for K_{II} and K_{III} are negligibly small in relation to the value of KI (because the crack is formed by splitting), so that they are not specifically considered, but their influence is certainly taken into account through the value of the equivalent stress intensity factor K_{eq}. ***Figure 6-46*** shows the obtained dependence of the equivalent stress intensity factor K_{eq}, and crack length a.

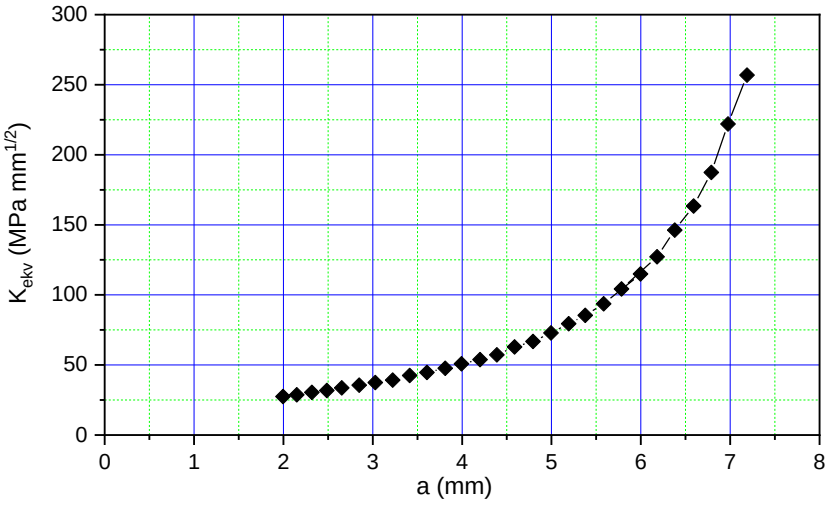

Figure 6-46: Graph of change of mean value Keq, as a function of crack length a, obtained by 3D simulation (XFEM)

In ***Table 6.18*** the results obtained by 3D simulation show the dependence of the current crack length ac and the required number of N cycles for its growth in that step, as well as the total number of N cycles.

Table 6-18: Data for crack lengths a and the required number of cycles N obtained by 3D simulation

Crack propagation step, *k* (*k=1,2,...28)*	The number of cycles required for crack growth in the current step N_k	The total number of cycles N to the *k-tog* step *(∑N_k=N)*	Crack length *a* [mm]
1.00	0.00	0.00	2
2.00	194821.00	194821.00	2.155
3.00	160616.00	355437.00	2.315
4.00	134517.00	489954.00	2.479
5.00	109962.00	599916.00	2.658
6.00	87650.90	687566.90	2.848
7.00	72181.90	759748.80	3.034
8.00	59649.60	819398.40	3.227
9.00	46518.40	865916.80	3.421
10.00	37247.60	903164.40	3.611
11.00	30108.40	933272.80	3.808
12.00	22964.80	956237.60	3.996
13.00	17868.20	974105.80	4.197
14.00	14069.70	988175.50	4.394
15.00	10434.20	998609.70	4.585
16.00	7825.00	1006434.70	4.787
17.00	5962.69	1012397.39	4.989
18.00	4254.22	1016651.61	5.181
19.00	3043.31	1019694.92	5.384
20.00	2212.73	1021907.65	5.588
21.00	1486.02	1023393.67	5.78
22.00	993.76	1024387.43	5.984
23.00	675.37	1025062.80	6.187
24.00	418.85	1025481.65	6.379
25.00	257.17	1025738.81	6.584
26.00	160.51	1025899.32	6.788
27.00	88.30	1025987.61	6.98
28.00	46.67	1026034.29	7.183

The results from ***Table 6.18*** shown in the graph in ***Figure 6.47***show the number of load cycles as a function of steps, where it can be seen that already somewhere from the twentieth step is required an extremely small number of cycles per step for crack growth. As seen in the diagram in ***Figure 6.48***, when the crack reaches a length of some 5.5 mm (in the twentieth step), its further growth is extremely fast.

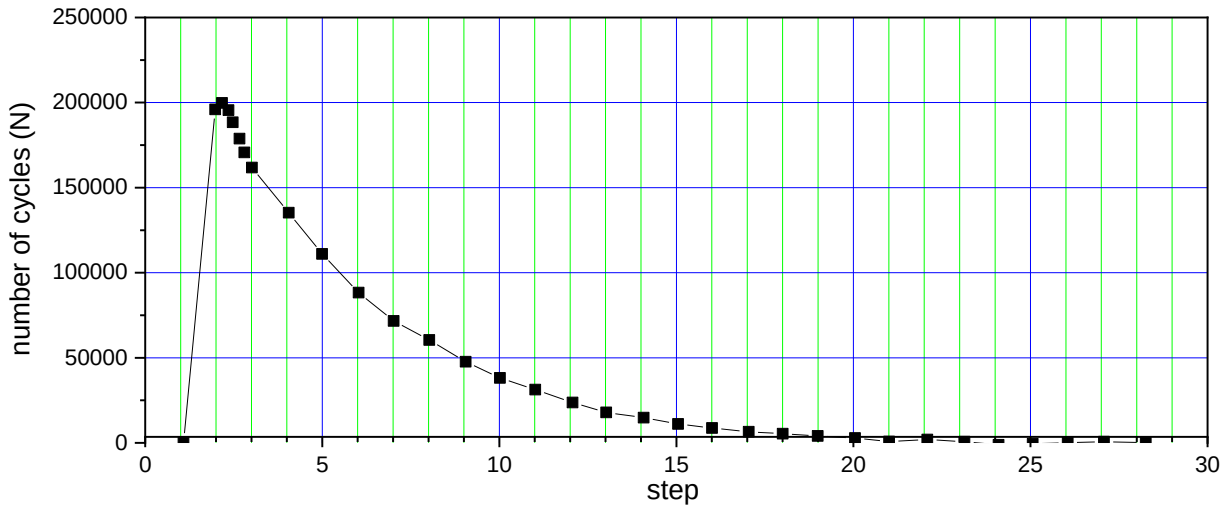

Figure 6-47: Required number of cycles for crack propagation per step (3D simulation)

Diagram in ***Figure 6.48*** shows the results of the experiment and 3D simulation (XFEM) for a standard Charpy specimen.

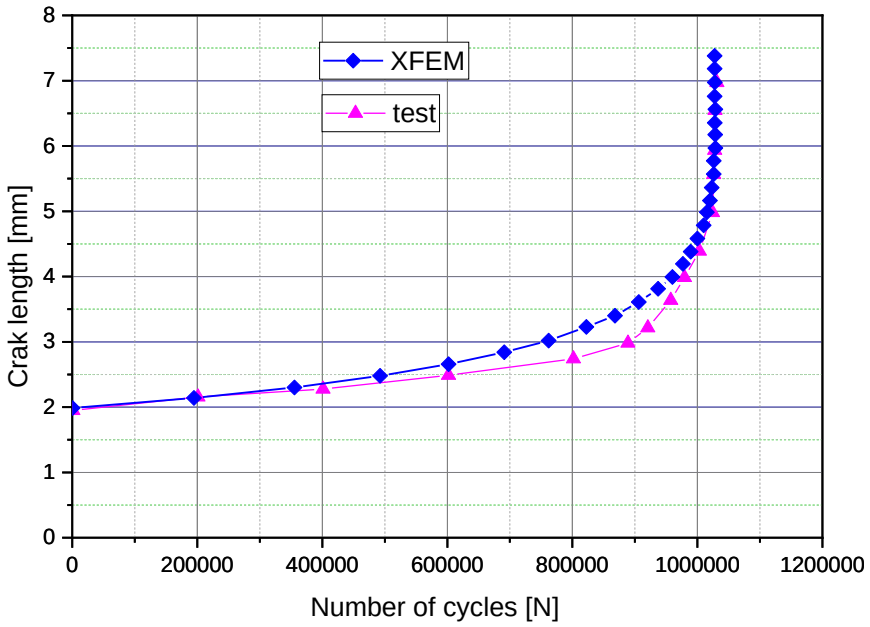

Figure 6-48: Comparative display of results from experiment and 3D simulation (XFEM) for

By comparing the results obtained by 3D simulation and the results obtained by performance experiment on a Charpy test tube, a very good match can be observed, especially from the moment when the crack increased over a value of 4mm. Before this crack length exists a certain deviation in the values, which could be attributed to the fact that the simulation was done for an ideally homogeneous material, and the values from the experiment were obtained for real. For crack length values above 4 mm up to fracture, experiment and 3D match. The simulation is excellent, which is of great importance because the fracture of the test tube occurred at the same time experiment and in

prediction through simulation. On the other hand, the deviation of the crack growth rate in the part of the diagram cannot be considered a disadvantage. It just goes into a contribution to the prediction of the life to failure by XFEM, ie the reliability of this method, because it can be seen that the crack grows slower in real conditions than according to the 3D simulation. This means that the results of the prediction of the lifetime to fracture of the specimen obtained by XFEM from this material could certainly be taken as relevant and sufficiently reliable because they represent stricter conditions than are realistic. As already mentioned, the extended finite element method is a relatively new method, and in order to gain affirmation and begin to be more widely applied in practice, the results obtained by this method must be supported by practical results. The aim of this comparison of experimental data and data obtained by 3D simulation, was precisely the verification of this new method, so that with some certainty. Otherwise, as for the use of the extended finite element method on simple geometries as is the case with this test tube, in order to obtain the relevant fatigue parameters, it does not make any excessive sense, because can obtain these values in a significantly shorter time than by applying XFEM, by using an analytical method.

6.9 Extended Finite Element Method (XFEM) In Estimating The Fatigue Life of A Pipe With An Axial Surface Crack

Extended finite element method (***XFEM***) in the estimation of the fatigue life of a pipe with an axial surface crack a 3D simulation of fatigue fracture was performed using extended finite element methods (***XFEM***) on a standard Charpy test tube made of material API J55. The pipe whose resistance to fatigue fracture will be tested by 3D simulation of axial surface crack growth at this point is also made of the same material. By comparing the test results from the 3D simulation with that from the experiment, a fairly good match was obtained values, so that the design life of the test tube is the same as the life obtained by the 3D simulation.

The geometry used in the simulation is a pipe of dimensions as in ***Figure 6.6***, closed at both ends to create the effect of a pressure vessel. On the outside of the pipe (vessel) there is an initial crack in the base material (OM), length 2 c = 200 and depth a= 3.5 mm. The wall thickness of the pipe is t = 6.98 mm.

A pipe model with an external axial crack is defined in the Abaqus software, where the material characteristics are also defined: API J55 steel, whose Young module $2{,}1 \cdot 10_5$ MPa and a Poisson's ratio of 0.33, and the corresponding boundary conditions (***Figure 6.49***) . A pressure of p = 10 MPa was taken as the load, which is the maximum value of the working pressure 2.1×10^5 MPa.

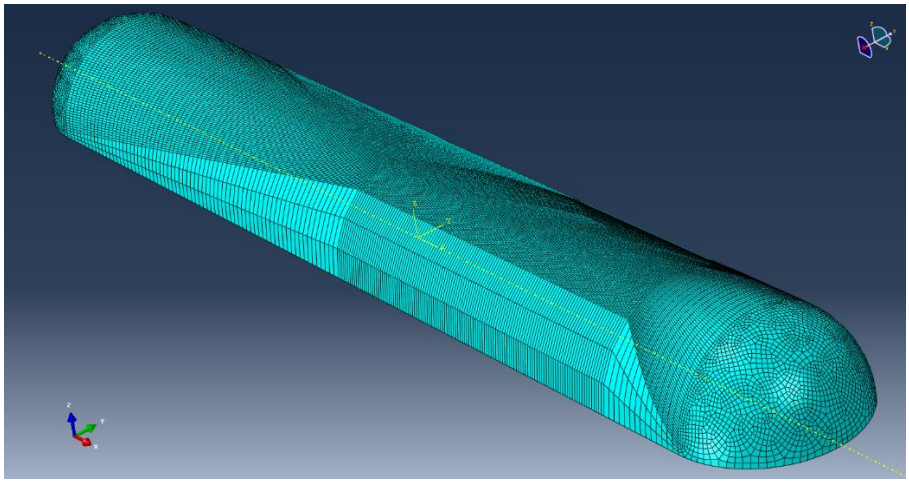

Figure 6-49:Pipe model with initial axial surface crack

Abaqus, where a finite element network of the hexahedral type is defined in ***Figure 6***-50, consisting of 286033 nodes and 257560 elements. The initial crack is in axial direction of length 2c = 200 mm and depth a = 3.5 mm. With this initial crack, the wall was weakened so that its thickness was practically halved, it was reduced to only 3.48 mm, and in the area where the crack is expected to increase generated a much denser network, with a larger number of nodes, so as to increase accuracy obtained values. ***Figure 6***-51 shows the initial crack on the pipe and the mesh in its immediate vicinity. the growth simulation was 0.2 mm, in the free crack propagation option. However, it is a crack propagated by the step that Morfeo / Crack for Abaqus chose himself, based on the calculated ones the values of the stress intensity factor in the current step, so that the crack growth per step is very different. In the first 6 steps they are 0.69 mm per step, while from the seventh step further increments of a few millimeters.

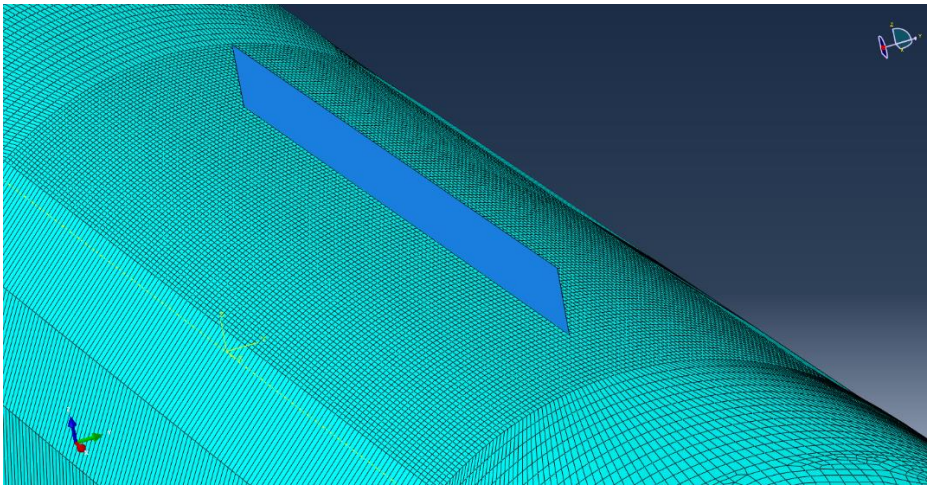

Figure 6-50: Finite element network of a pipe model with an initial axial surface crack (extracted is shown in the figure) in the immediate vicinity of the crack

Three-dimensional crack growth simulation was done for a total of 100 steps so that the final crack length was 209,417 mm. The crack growth option used was free crack growth. The first step in the analysis of crack growth using XFEM is "opening" crack (no growth) and the stresses in the pipe are calculated and based on the stress intensity factors at the top of the crack and the angle of deflection in relation to the initial direction of the crack is determined. ***Figure 6***-51 shows the network in the first step, the so-called “Opening” the crack, and in ***Figure*** 6-52 stress at the top of the crack for the first step. ***Figure 6***-53 shows the crack at the second growth step.

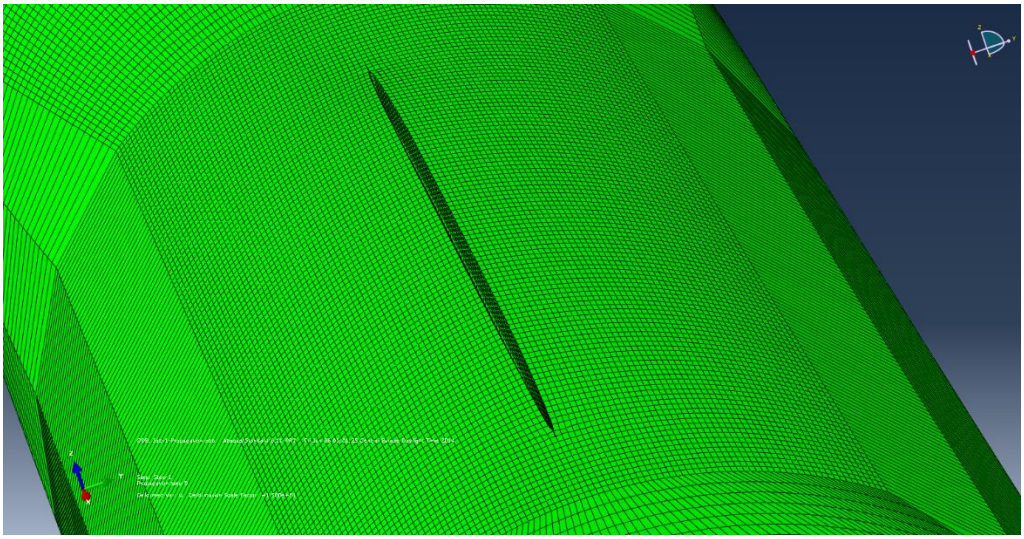

Figure 6-51: Appearance of the network in the first step of "opening" the crack

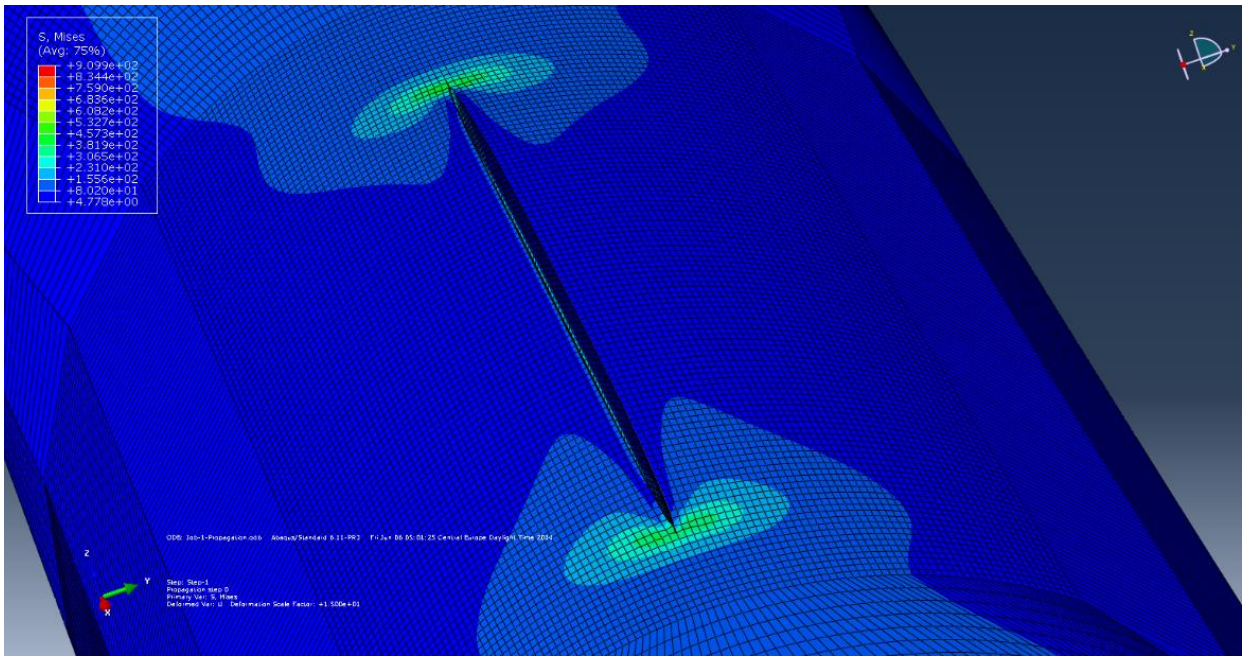

Figure 6-52: The first step - opening the crack and von Mises stresses at the top of the crack

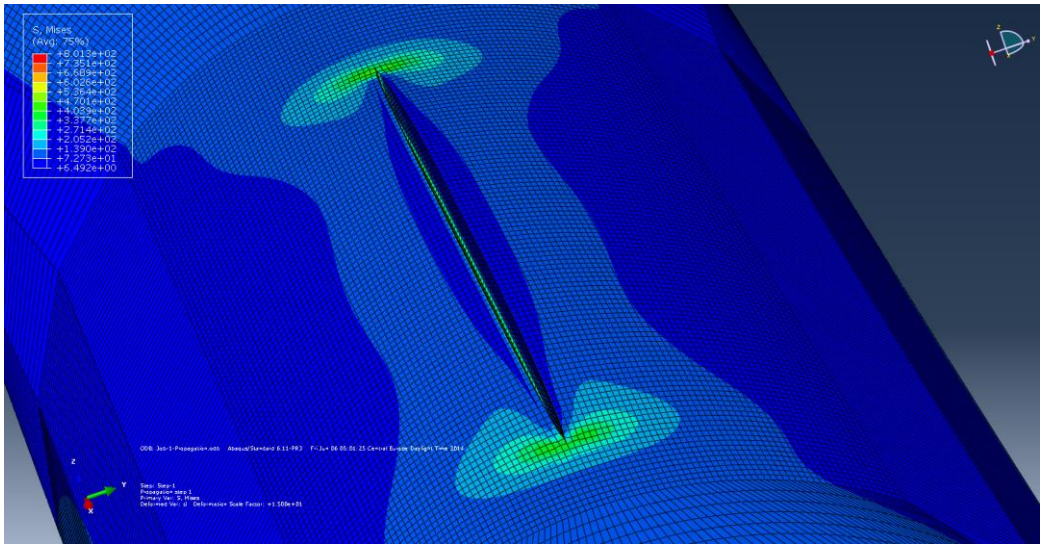

Figure 6-53: Second step and von Mises stresses at the crack tip

The crack grew in-depth in the first 6 steps, while the length of the initial surface crack 2a = 200 mm did not change. ***Figure 6***-54 shows an open initial crack 200 mm long and a newly formed through a crack on the inner half of the wall, 25.88 mm long in the seventh propagation step.

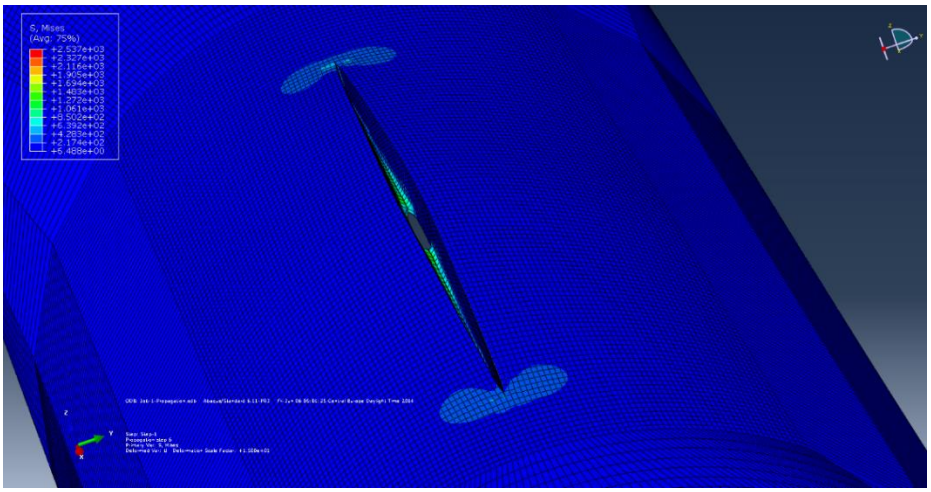

Figure 6-54: The crack becomes transient and von Mises stresses at the crack tip

The appearance of the pipe from the inside and von Mises stress in the area around the crack in steps 1, 2, and 3 are shown in ***Figures* 6.55-6.57**. In ***Figure 6***.57, in the third step, a crack appeared on the inside of the pipe, 68.24 mm long, but the crack had not yet opened. In the seventh step, a crack was opened on the inside of the pipe. ***Figure 6.58*** shows a newly formed through the crack on the inner half of the wall, 25.88 mm long. Further growth of plain flowed in the axial direction along the inner half of the pipe wall thickness. Following the direction of the outer axial initial crack (the appearance of the crack on the inside is shown in step 23 in ***Figure 6.59***, the length of the "open" crack was 2c = 120 mm).

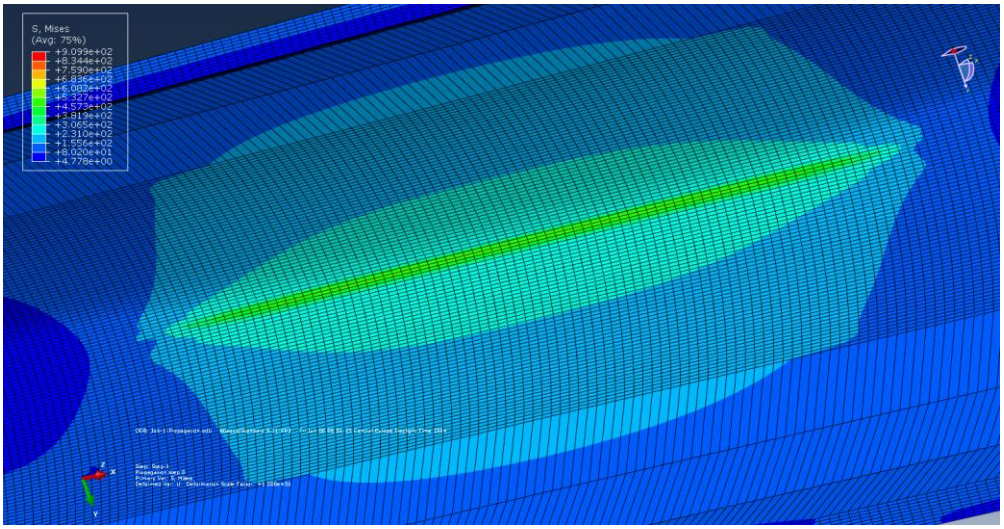

Figure 6-55:First step - crack opening and von Mises stresses around the crack (view from inner sides)

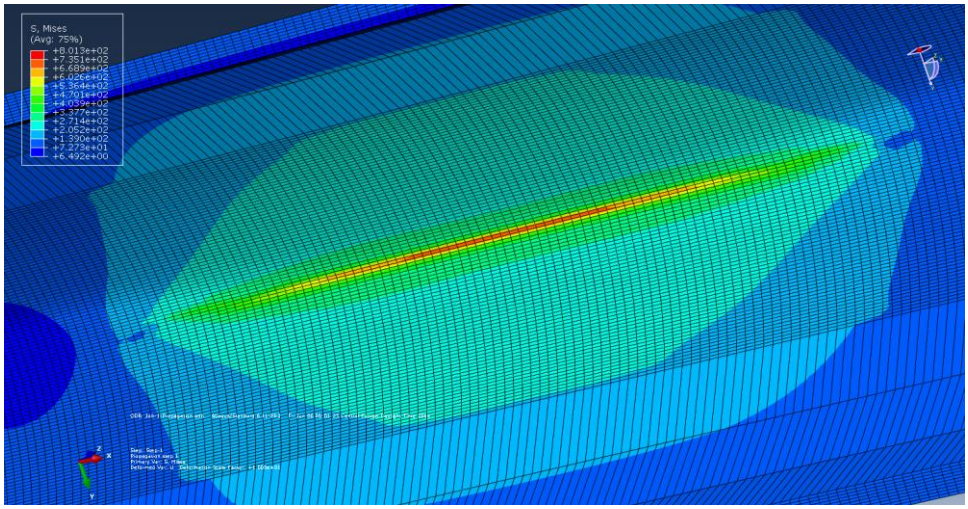

Figure 6-56: Second crack propagation step and von Mises stresses (inside view)

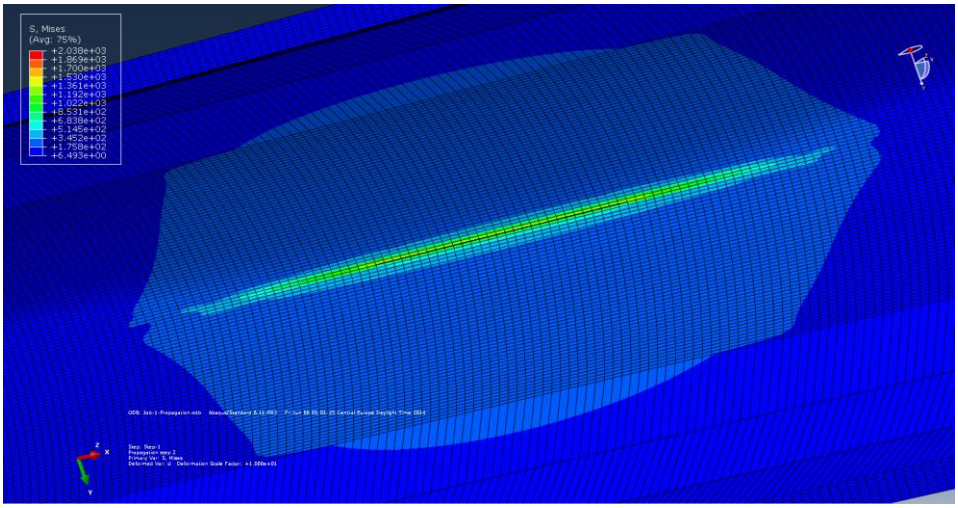

Figure 6-57: The third step - the appearance of a crack on the inside of the pipe

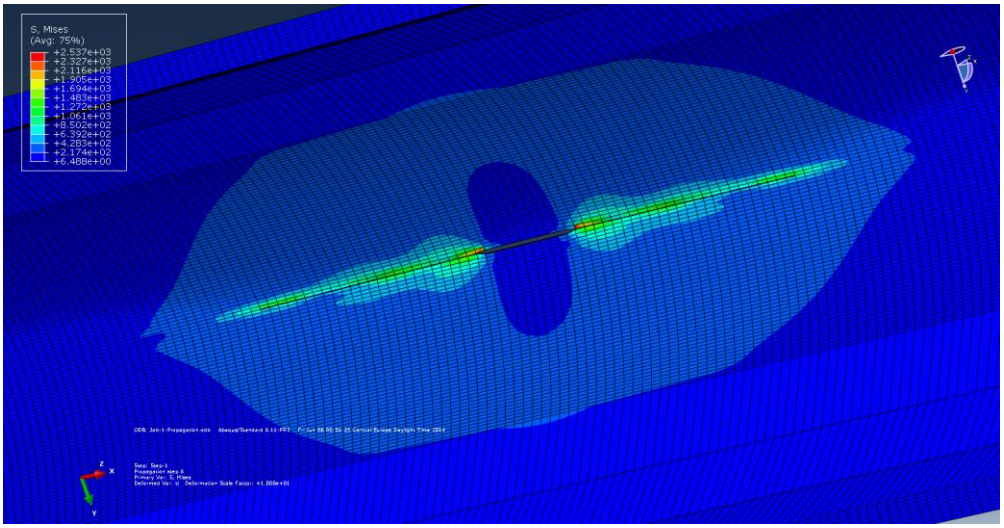

Figure 6-58: Appearance of the crack from the bottom in the seventh step (the crack "passes" through the wall of the pipe) and von Mises stresses around the crack

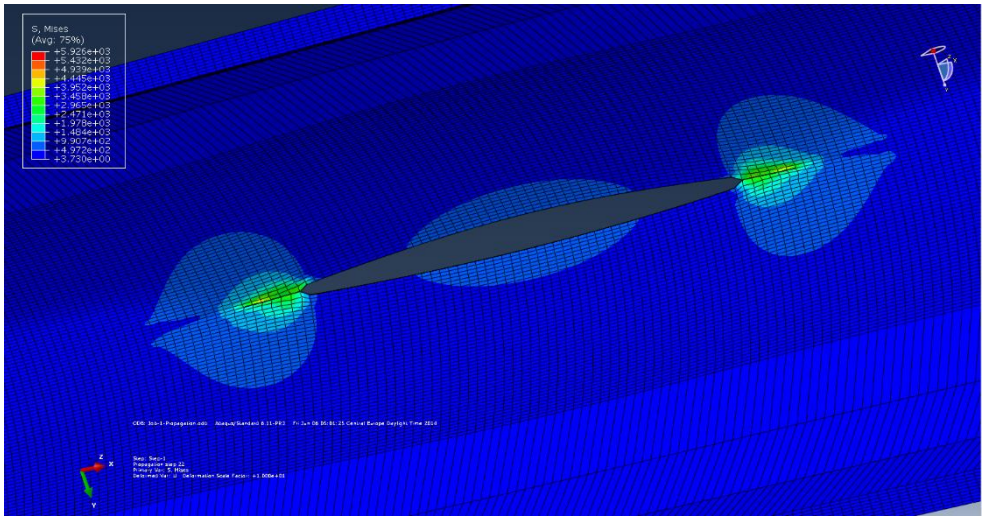

Figure 6-59: Appearance of the crack on the inside of the pipe and von Mises stresses in the 23rd propagation step

Figure 6.60 shows the appearance of the crack in the 24-propagation step (outside view), where it can be seen that the crack still grows only in the inner half of the pipe wall, and the initial crack length of 200 mm remains unchanged. This growth trend continues until step 66 (Figure 6-62), when the crack on the inside of the pipe reaches the length of the outside initial cracks of 200 mm. The front of the crack now extends over the entire thickness of the pipe wall.

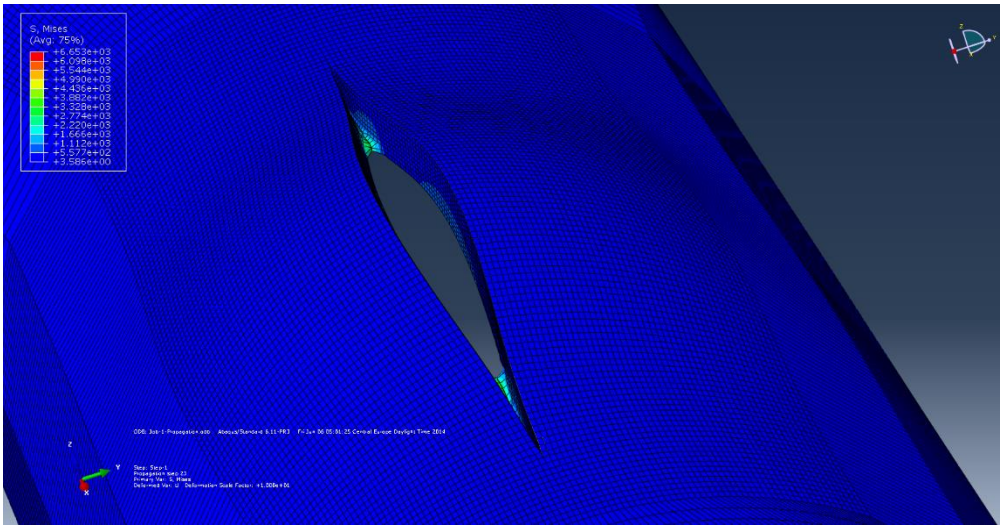

Figure 6-60: Step 24 crack propagation

Figures 6.61-6.63 show steps 66, 67, and 69 in which there is still no 200 mm long axial through-crack propagation. These images show the characteristic von Mises stresses around the crack. The crack occurs to grow in the axial direction as a completely transient crack, only from the 74th step of the simulation. In this period used is a slightly larger number of cycles for the crack to continue to grow because it is now growing through a complete wall thickness of 6.98mm.

Figure 6-64 shows the 100th crack propagation step in which the crack reached a length of 209.42 mm. ***Figure 6-65*** shows the total crack growth using 3D graphics.

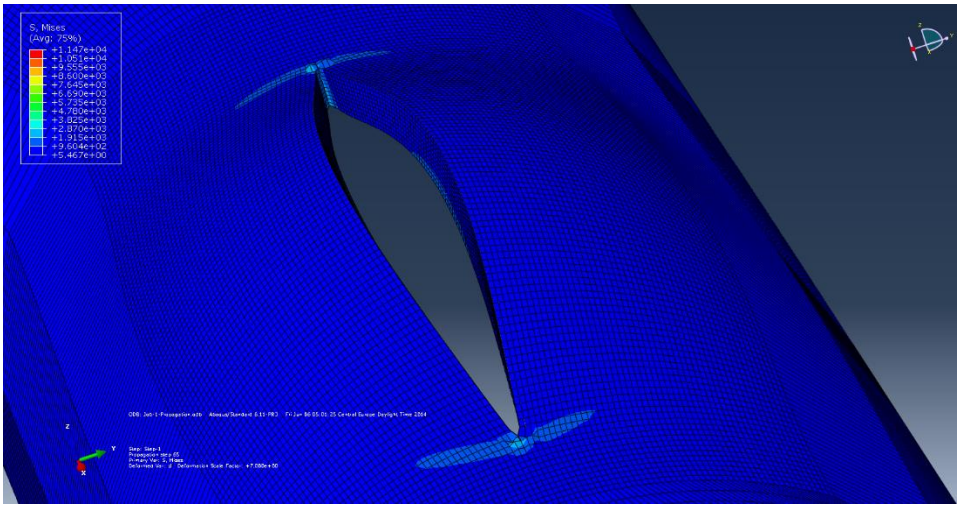

Figure 6-61: Step 66 crack propagation

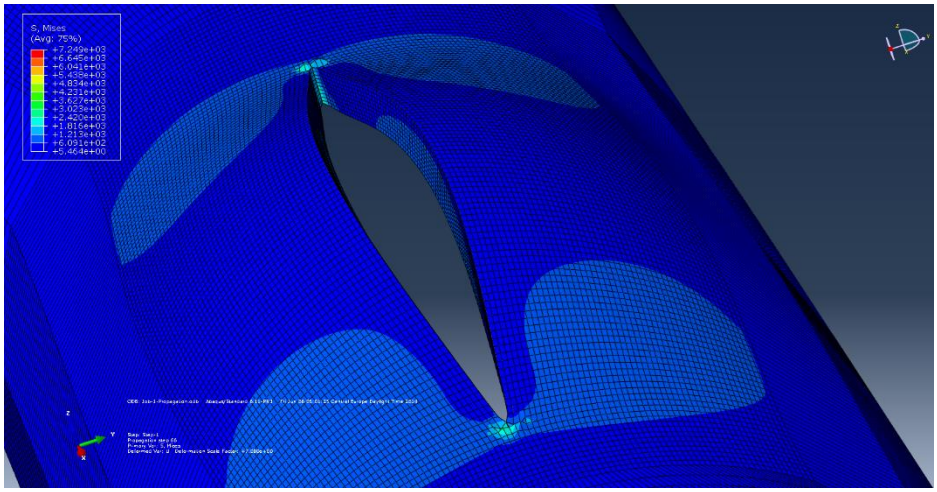

Figure 6-62: Step 67 crack propagation and von Mises stresses

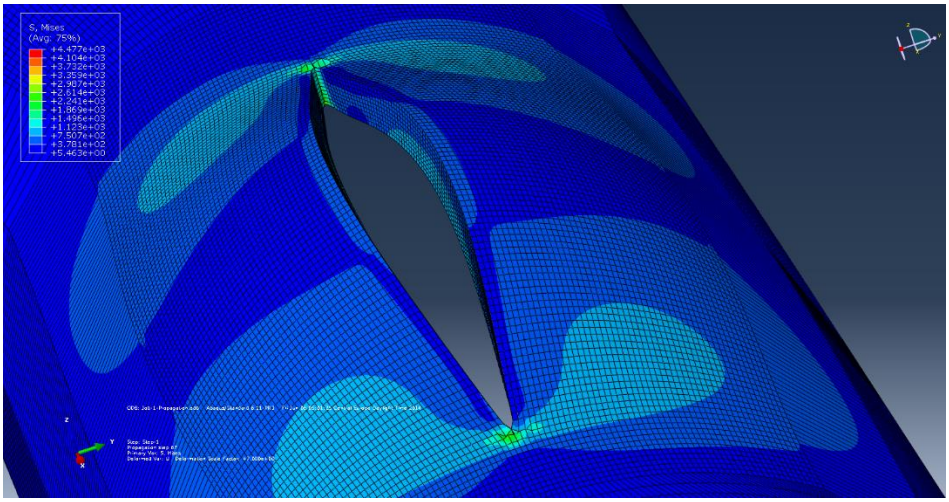

Figure 6-63: Step 69 crack propagation

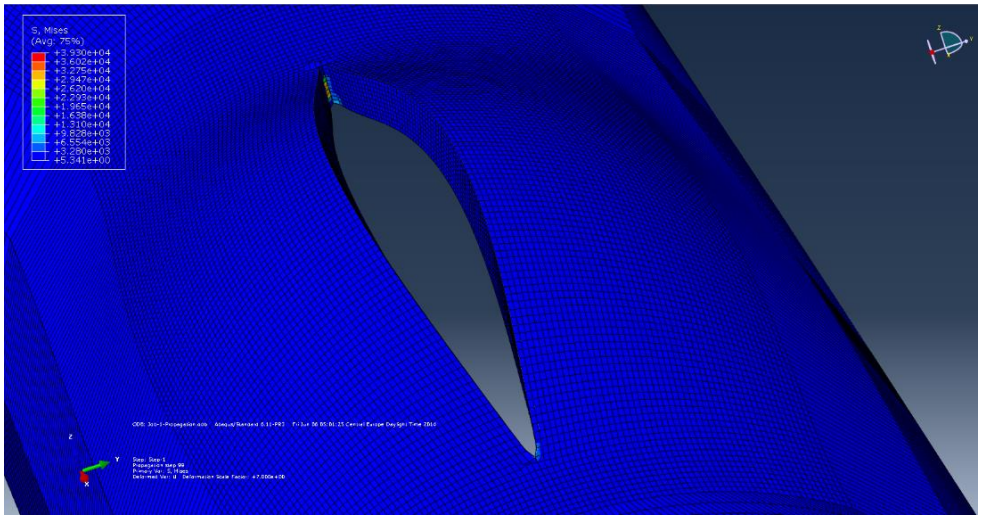

Figure 6-64: Final appearance and crack length at step 100 (total crack length is a = 209.4 mm)

Figure 6.65 shows the crack growth in the axial direction using 3D graphics.

The blue line shows the crack growth in the axial direction on the inside of the pipe wall, which starts only from the 7th step (until then, the crack grew only in the radial direction, into the depth of the pipe wall) and lasts until the 66th step, when it is equal to the outer crack length 200 mm (pink line on the graphic). Crack growth in the axial direction it begins only after the 74st step, when a transient axial crack 200 mm long grows up to a length of 209.42 mm, which it reaches in the 100th step. (in that part these two lines stand parallel to the graph).

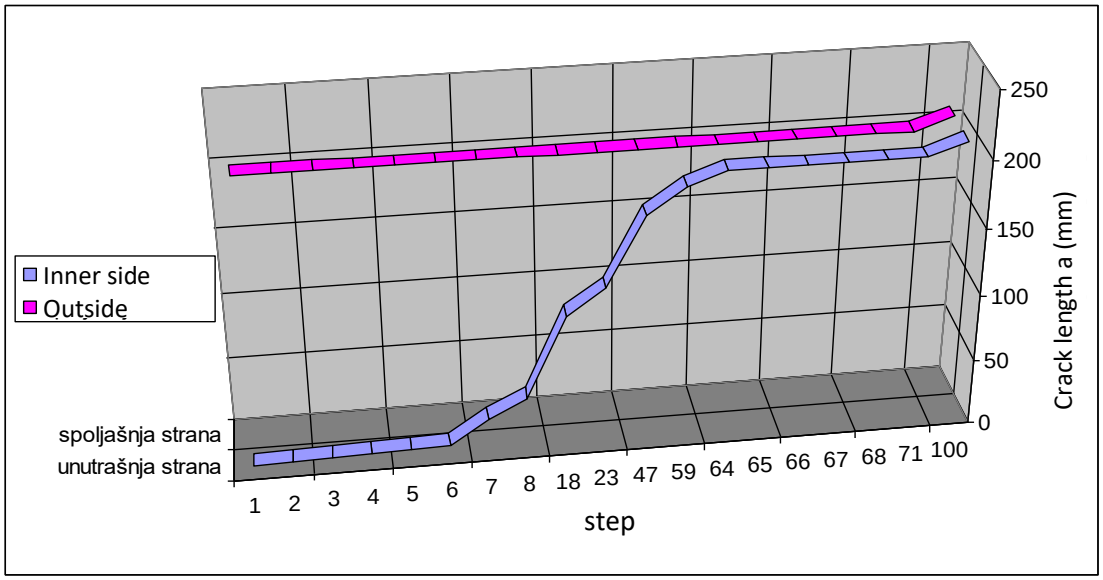

Figure 6-65: View of crack propagation during 100 steps showing crack growth in radial and axial direction

In the following, the values of the intensity factor obtained will be considered by 3D simulation stresses calculated at a large number of points along the crack front. The values of the stress intensity factor determine the appropriate degree of crack increase. This procedure was repeated 100 times, and the display of the values obtained at each step of the simulation is given in Table 6.16 The values of the stress intensity factor are shown in the last four columns, respectively, the equivalent stress intensity factor K_{eq}, and the stress intensity factors for shapes (modes) I, II, and III (K_I, K_{II}, and K_{III}) . It is obvious that the FIN values for mode I are much higher than for modes II and III. Hence, it makes sense to further predict the crack growth rate consider only the values of K_I, or even better K_{eff} because it takes into account the stress intensity factors of all three modes. ***Table 6.19*** shows the number of simulation steps, total crack length, number crack front points as well as values (minimum, maximum and mean) for the factor stress intensity mode I, K_I, and the equivalent voltage intensity factor, K_{eq}, for some characteristic simulation steps. ***Table 6.20*** Values of equivalent stress intensity factor and stress intensity factor mode I, obtained by crack propagation in some characteristic steps

Table 6-19: View the values that the software provides for each crack growth step

curves. abscissa along the crack front	*X (coord* data point front)	*y*	*z*	K_{eq}	K_I	K_{II}	K_{III}
0	50.7745	8.77E-05	69.4784	860.175	837.413	1.55444	1.65058
0.349	50.7745	8.72E-05	69.1294	859.6	837.004	1.468	1.74059
0.698	50.7745	8.68E-05	68.7804	859.072	836.648	1.38001	1.83133
1.047	50.7745	8.64E-05	68.4314	858.595	836.348	1.29048	1.92288
1.396	50.7745	8.59E-05	68.0824	858.175	836.113	1.19942	2.01528
1.745	50.7745	8.55E-05	67.7334	857.82	835.95	1.10692	2.1085
2.094	50.7745	8.51E-05	67.3844	857.54	835.868	1.01306	2.20247

Table 6-20: Values of equivalent stress intensity factor and stress intensity factor mode

			equivalent stress intensity factor [MPa(*mm)^0.5*]			*stress intensity factor* mode I, K_I [MPa(*mm)^0.5*]		
step	Crack length [mm]	The number of front points cracks	max	min	Middle value	max	min	Middle value
1	3.5	206	1870.06	856.863	1363.462	1896.53	835.868	1366.199
2	4.19	208	2194.46	880.989	1537.725	2198.72	853.959	1526.34
3	4.88	208	2431.09	916.345	1673.718	2432.93	885.092	1659.011
4	5.57	208	2727.92	921.732	1824.826	2745.87	900.343	1823.107
5	6.26	208	2813.96	921.732	1875.125	2984.54	900.343	1948.814
6	6.9	207	3367.18	960.857	2164.019	3647.07	936.596	2291.833
7	25.883	185	7433.56	798.383	4115.972	6959.8	769.833	3864.817
8	40	173	7566.9	769.35	4168.125	7639.73	740.371	4190.051
18	101.179	119	10098.7	672.668	5385.684	9770.31	629.367	5199.839
23	120	106	10565.3	736.698	5650.999	10176.3	679.722	5428.011
47	171.769	60	10918.9	3146.38	7032.64	10498.1	2982.88	6740.49
59	190.593	45	7859.79	5479.08	6669.435	7337.13	3747.14	5542.135
64	200	45	7431.78	5903.18	6667.48	7710.26	5916.5	6813.38
71	200	49	7314.96	6272.92	6793.94	7060.96	6277.72	6669.34
100	209.417	50	7341.33	6323.69	6832.51	7201.13	5681.02	6441.075

Change of equivalent stress intensity factor K_{eq} during 100 steps propagation is shown in ***Figure 6.66*** In the first 6 steps of propagation, while the crack grows in the radial direction, the values of K_{eq}, gradually increase, while there is a large jump in values K_{eq}, in the seventh step, when the

crack became transient, that is, it opened in the axial direction from the inside of the pipe. Further gradual growth is observed from this step values of K_{eq},, which after the 50th step varies significantly with the values until the last steps of propagation.

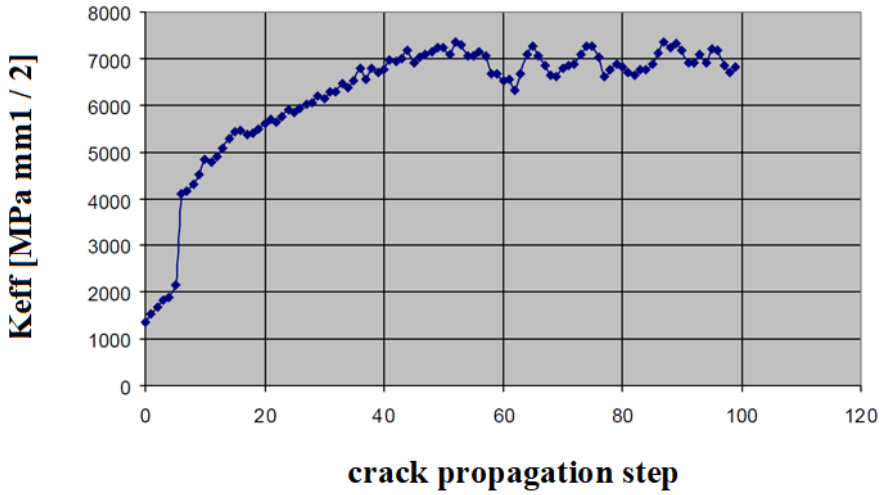

Figure 6-66: Change of the stress intensity factor K_eq during 100 crack propagation steps

The diagram in ***Figure 6-67*** shows the relationship between the number of steps and the logarithmic value of the number of cycles logN. The values for the number of cycles N are given in the logarithmic form, for better visibility of the diagram, because there is a large range between the values up to the seventh step and values after it. After the seventh step, when the crack penetrates the pipe wall, the number of cycles required for crack growth becomes significantly smaller and remains approximately the same until the last, 100th step, when the crack reaches a length of 209.42 mm.

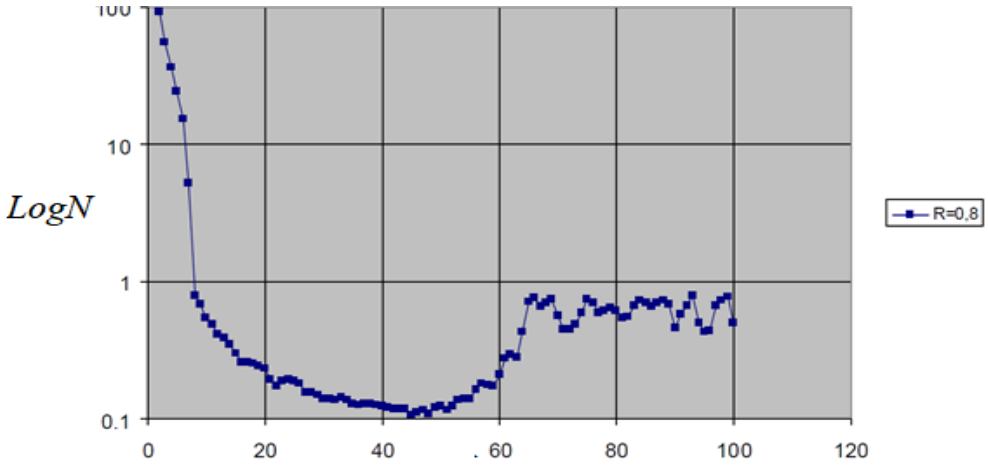

Figure 6-67: The obtained dependence between the steps and the number of cycles – logN

It is obvious that the largest number cycle requires to increase the crack in the first six steps until it breaks through the wall of the pipe because of the crack it grows simultaneously in the radial (in the depth of the wall) and in the axial direction. This is evidenced by data on the number of crack front

points ***Table 6-20*** of which there are 206 to 208 in the first 6 steps, and from the seventh step, this number decreases to 187 and continues to decrease, until the internal and external (initial) cracks are "equalized", the front of the crack does not become perpendicular to the wall of the pipe, when there are less than 50.

When the crack penetrates the pipe wall, in the seventh step, it becomes an axial through crack 25.88 *mm* long (on the inside of the wall) and continues to grow only in the axial direction, following the external initial crack. it is for her further growth requires a significantly smaller number of cycles, as shown in the diagram in ***Figure 6.67***. The number of cycles is first in a slight decline (somewhere up to the 40th step) and then in a slight increase, only to start (around the 64th step). From the 60th step, the internal crack "reached" external and now axial through crack continues to grow in the axial direction. Total the number of cycles for the crack to grow from an initial length of 200 mm and a depth of 3.5 mm to a final length of 209.42 mm was 258 cycles, of which part of the crack growth until it becomes transient 25.88 mm long (seventh step) it consumes the largest part, 229.3 cycles. ***Figure 6.68*** shows the propagation of the crack into the depth of the pipe wall in the first 6 steps, until the crack became transient. The diagram in ***Figure 6.69*** shows the obtained dependence the total crack length a and the number of cycles N required for the crack to grow to a final length of 209.42 mm for all 100 propagation steps. The blue line indicates the crack that occurs on the inside of the pipe wall, which grows in the radial direction until the sixth step, and then begins to develop very quickly in the axial direction to a length of 200 mm (from 25.88 mm to 200 mm required is only about 225 cycles). After that the crack growth is somewhat slower, up to a length of 209.42 mm (only about 30 cycles are required)

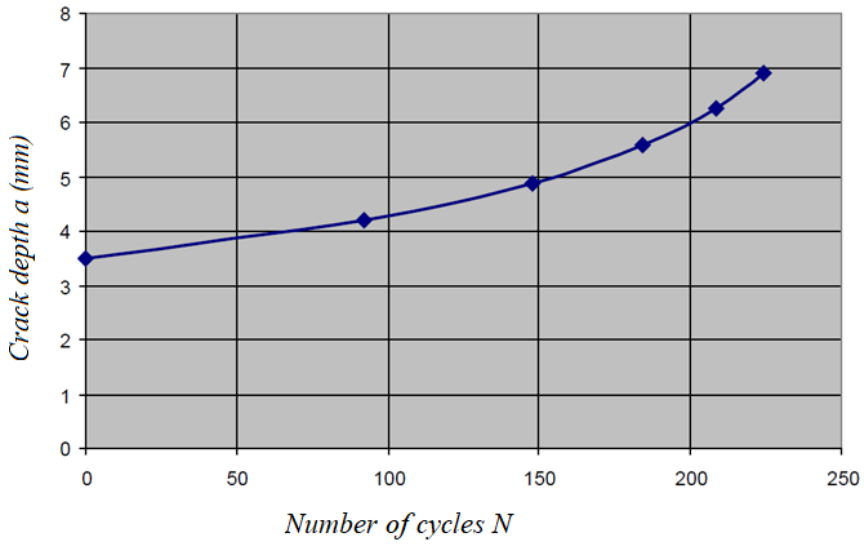

Figure 6-68: Propagation of a crack into the depth of the pipe wall (first 6 steps) to penetration

It is obvious that the largest number of cycles was needed for the crack to rise in the first seven steps, until it broke through the wall of the pipe, because then the crack front was the largest. The pink line in the diagram in ***Figure 6.69*** represents an initial axial crack 200 mm long on the outside of the wall.

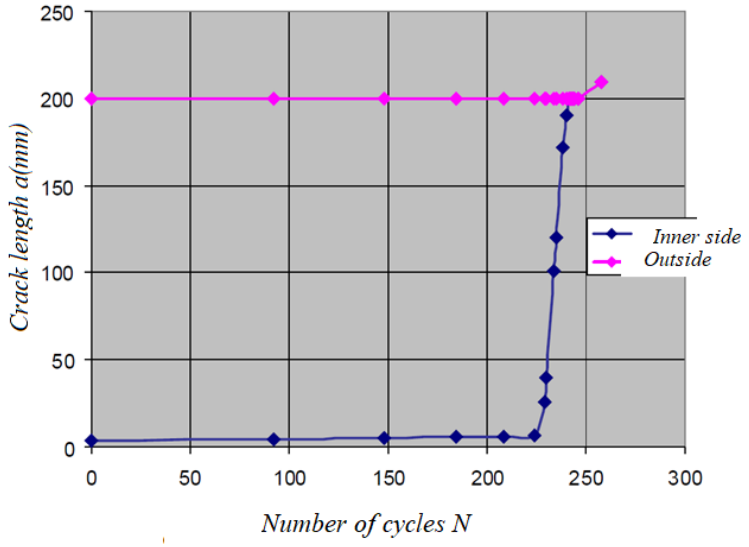

Figure 6-69: Dependence of crack length a and number of cycles N for 100 propagation steps

Crack remains the same length until the 71st step, after which it propagates as a completely crack passing in the axial direction to a length of 209.42 mm in the 100th step.

The value of the equivalent stress intensity factor K_{eq} as a function of crack length a are shown in ***Figure 6.70*** The K_{eq} growth trend is obvious with increasing crack length a, the biggest jump is between the 6th and 7th step, when the crack opens.

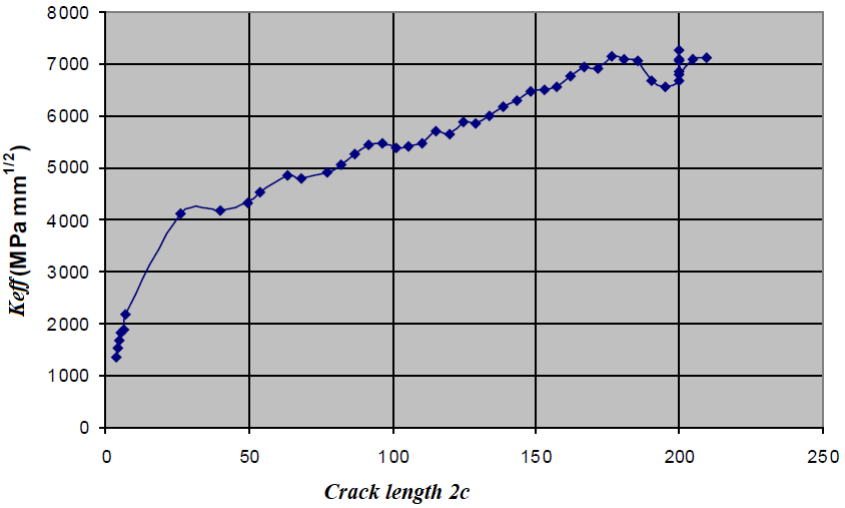

Figure 6-70: Values of the equivalent stress intensity factor Keq as a function of crack length a

Figures 6.71-6.76 show a crack in a pipe in several characteristic steps of propagation, where, in addition to the network of finite elements in the area around the crack, see also stress state around it. ***Figures 6.71-6.73*** show the crack immediately before and after the moment of its penetration through the wall (steps 6, 7 and 8). ***Figure 6.74*** shows the appearance of a crack in 64th step, when the crack in the inner part of the pipe reached the length of the initial 200 mm external cracks, and in ***Figure 6.76*** cracks in the 100th step. For the same initial external damage, length 2c = 200mm, and depth a = 3.5mm, a simulation was done for new and material from exploitation, as well as for two values of stress ratio R = 0.8 and R = 0.7. The simulation was done for 24 steps of crack propagation. ***Figure 6.77*** shows the results of crack growth as a function of the number of cycles N for new material and for stress ratio R = 0.8 and R = 0.7. A much shorter life (almost 5 times) is obvious for the stress ratio R = 0.7 in relation to R = 0.8. When it comes to material from exploitation, this influence is even more pronounced ***Figure 6.78***, where the number of cycles to crack penetration is 16 times smaller.

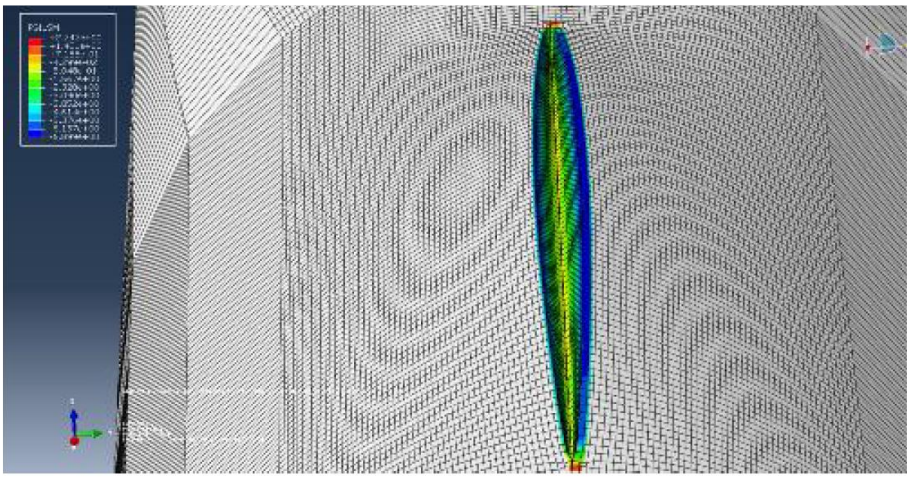

Figure 6-71: Crack in the sixth step and stress distribution

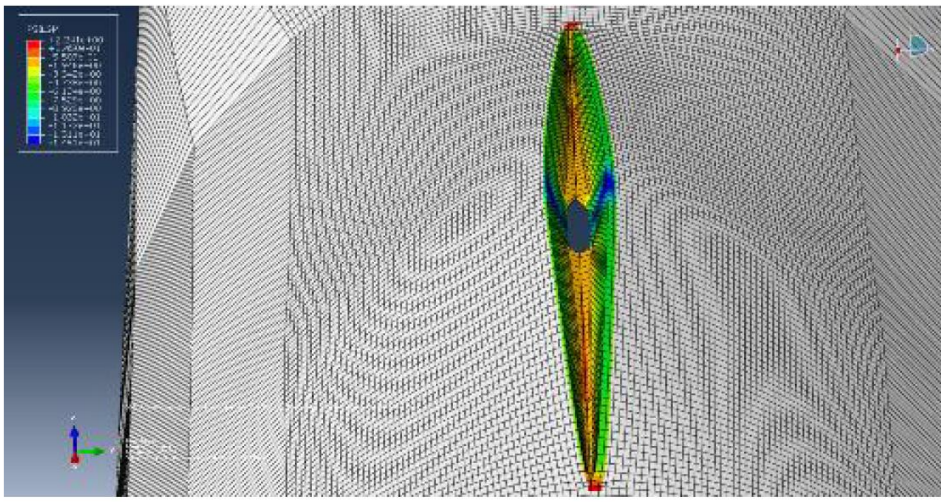

Figure 6-72: Crack in the seventh step and stress distribution

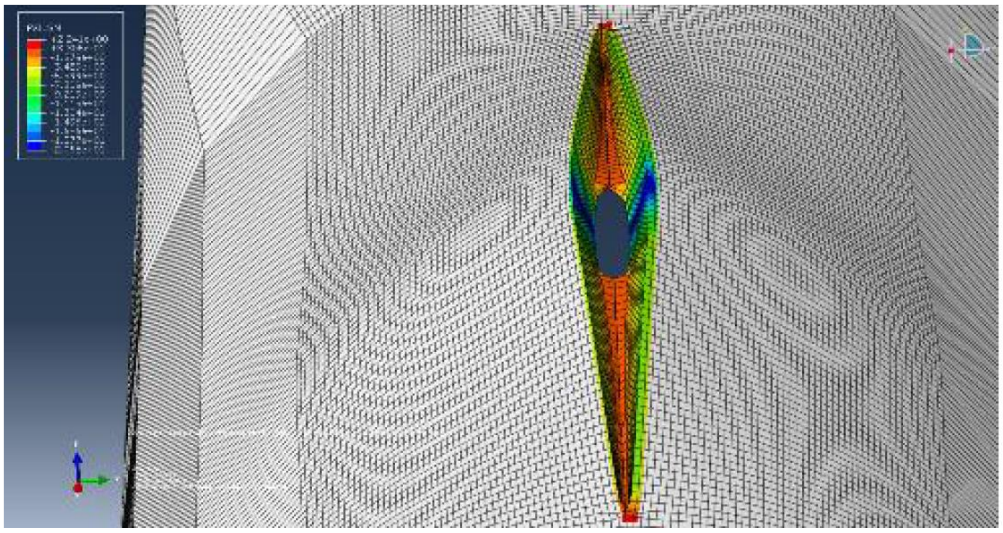

Figure 6-73: Crack in the eighth step and stress distribution

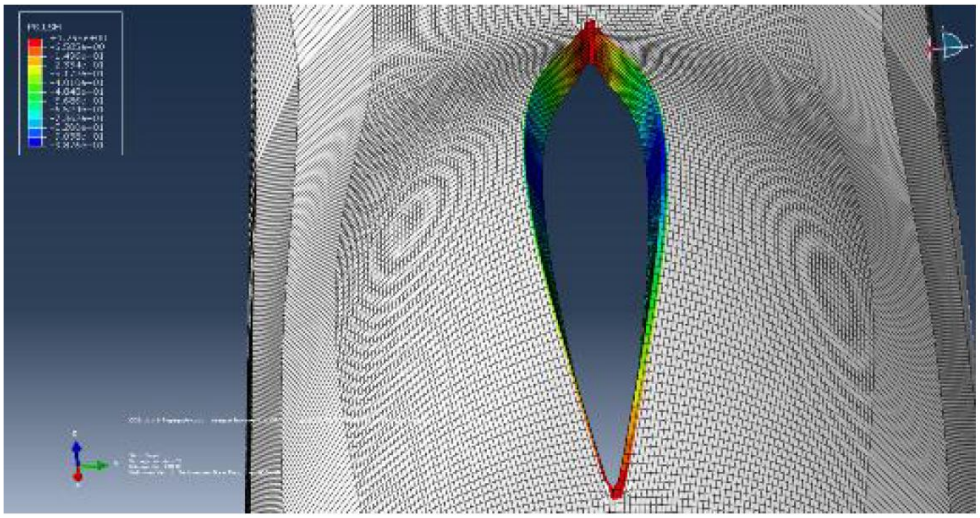

Figure 6-74: Crack in step 64 and stress distribution

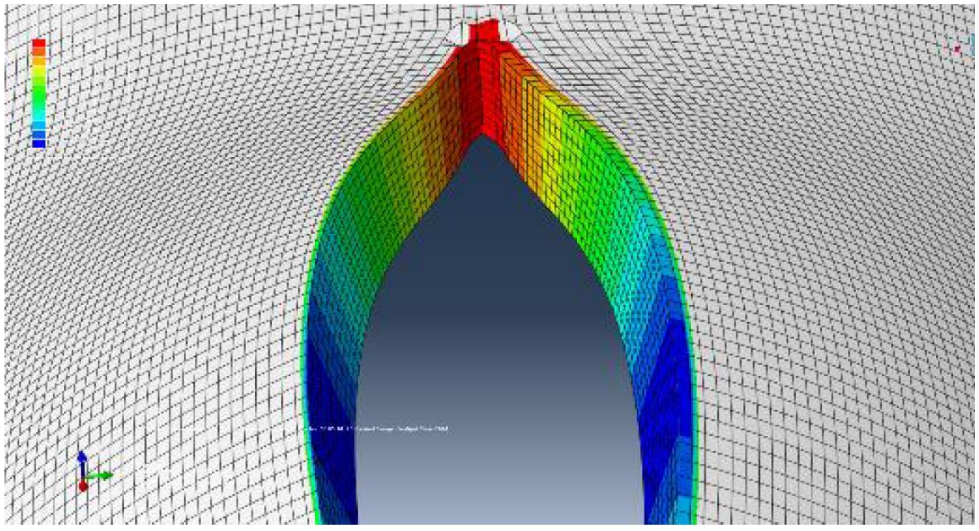

Figure 6-75: Crack in step 64 and stress distribution (zoomed view)

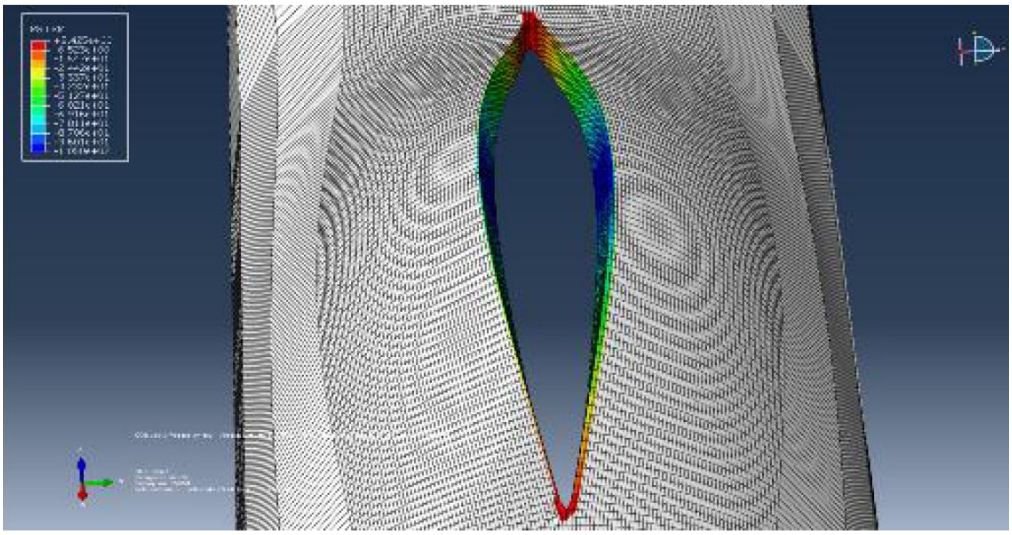

Figure 6-76: Crack in step 100 and stress distribution (zoomed view)

This is certainly in favor of the fact that there was a degradation of material from exploitation, and that it is completely expected that the crack growth will then be faster. However, realistically speaking, at this magnitude of damage, these are the values of the number of cycles N that have a purely theoretical significance, because in practice both cases there was a crack opening for a very small number of cycles, almost instantaneously. However, the results obtained are worthy of attention.

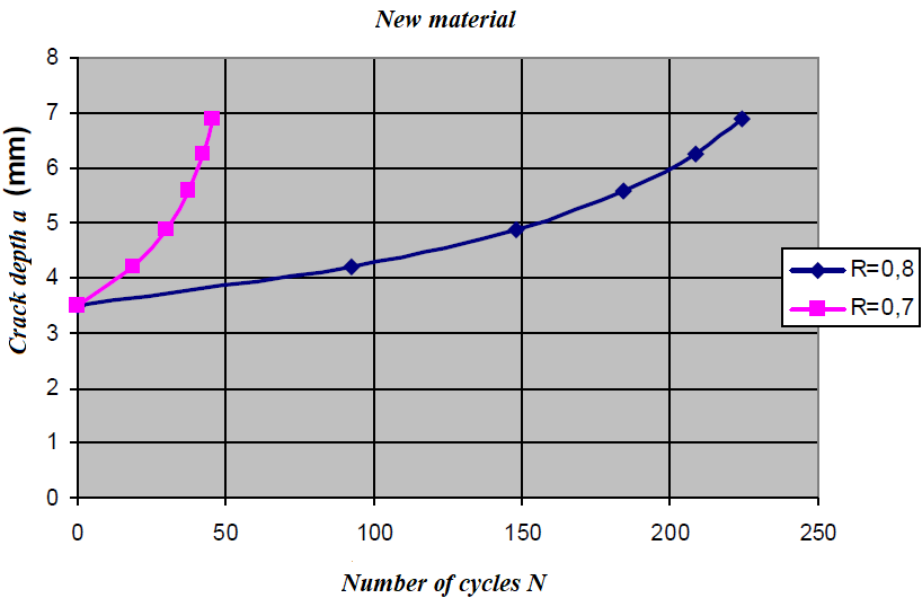

Figure 6-77: Influence of stress range and stress ratio on service life; new material

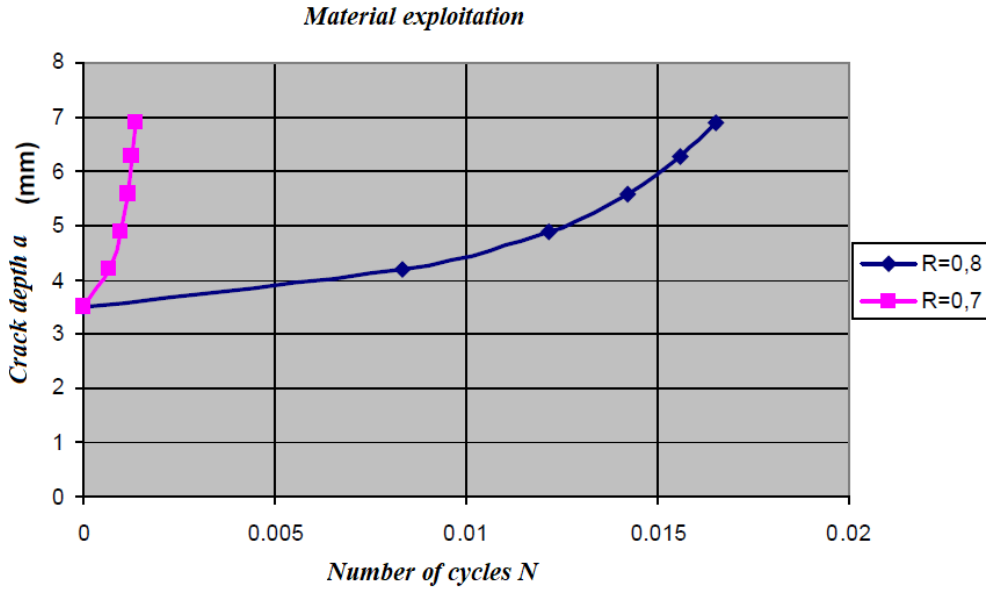

Figure 6-78: Influence of stress range and stress ratio on service life; exploited material

Another influential parameter was considered through the simulation, and that is the initial depth cracks. For an initial crack depth of $a = 2mm$ and a crack length of $2c = 200mm$ it was done 3D simulation in 30 steps of crack propagation for stress ratio $R = 0.7$. Pipe wall penetration occurred n step 25 results obtained compared to initial depth Cracks of a = 3.5 mm and crack lengths of $2c = 200mm$, are shown in ***Figure 6.79***

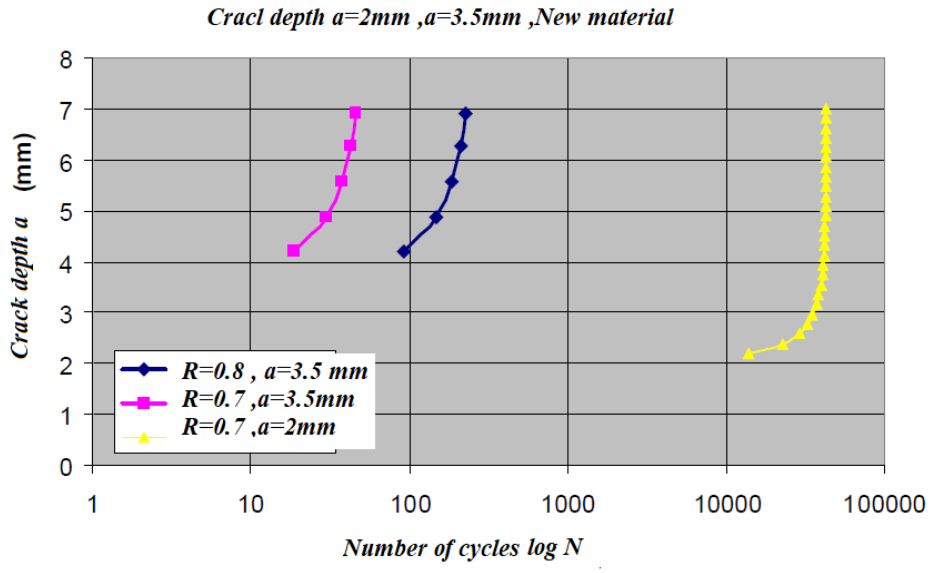

Figure 6-79: Influence of initial damage depth and stress quotient on fatigue life; new material

In the case of the initial crack depth a = 2mm, the predicted fatigue life is 42635 cycles until the crack penetrates. This is 947 times longer than for the initial depth of a = 3.5mm and the same stress ratio R = 0.7.

It was compared through 3D simulation and the influence of the initial crack on the outer and the inside of the pipe wall for the remaining century. The simulation was done for the internal initial

Crack depth a = 2 mm, length 2c = 200 mm, and stress ratio R = 0.7 in 30 steps. The penetration of the crack through the pipe wall occurred in the 25th step of the simulation in both cases, and when it did, the crack was outside and inside, but with a different number of cycles. For the case when the initial crack was from the outside, the penetration occurs after 42635 cycles, and when it was from the inside side, 80113.9 cycles were required. In the presented, it can be seen that, for these given conditions, the initial crack on the outside of the pipe gives twice the shorter life than on the inside. And as expected because the material on the inside of the pipe is significantly less exposed to stretching than that on the outside, which is even more pronounced with pipes with a thicker wall. Addiction results crack depths to penetration and the required number of cycles N, are shown in ***Figure 6.80***.

.

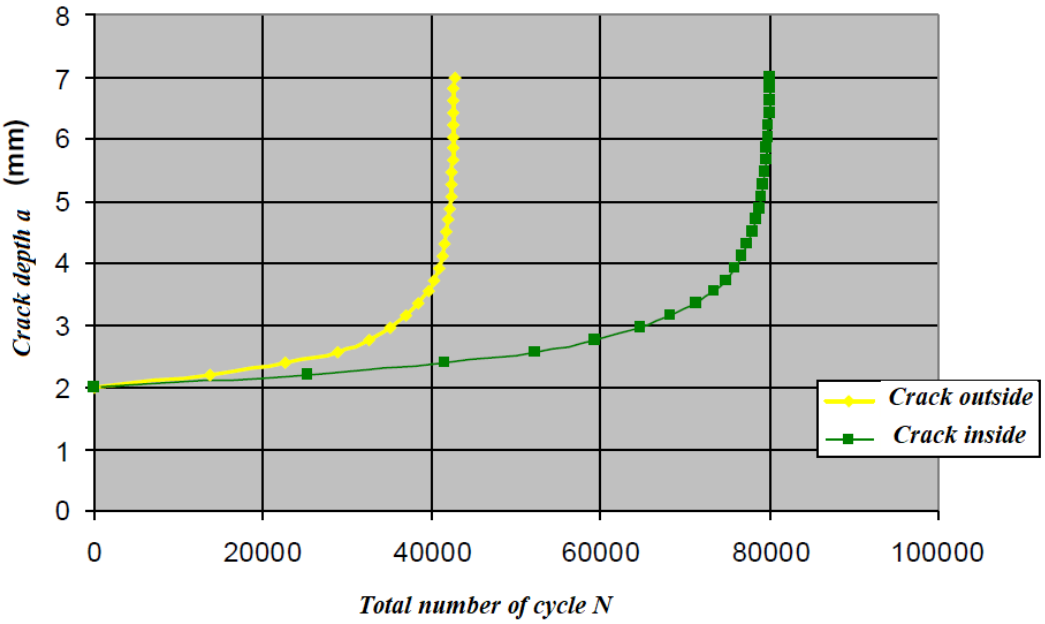

Figure 6-80: Influence of the initial crack on the outside and inside of wall on the fatigue life at a = 2 mm, 2c = 200 mm and R = 0.7

Figures 6.81-6.84 show, for illustration purposes, the von Mises stresses that occur on the pipe in the first propagation step and the step when the crack becomes transient. By comparison.

Figures 6.82 and ***6.52*** (initial crack is of the same length but greater depth, a = 3.5 mm) have completely different distribution of stresses in the pipe wall and around the crack itself can be observed

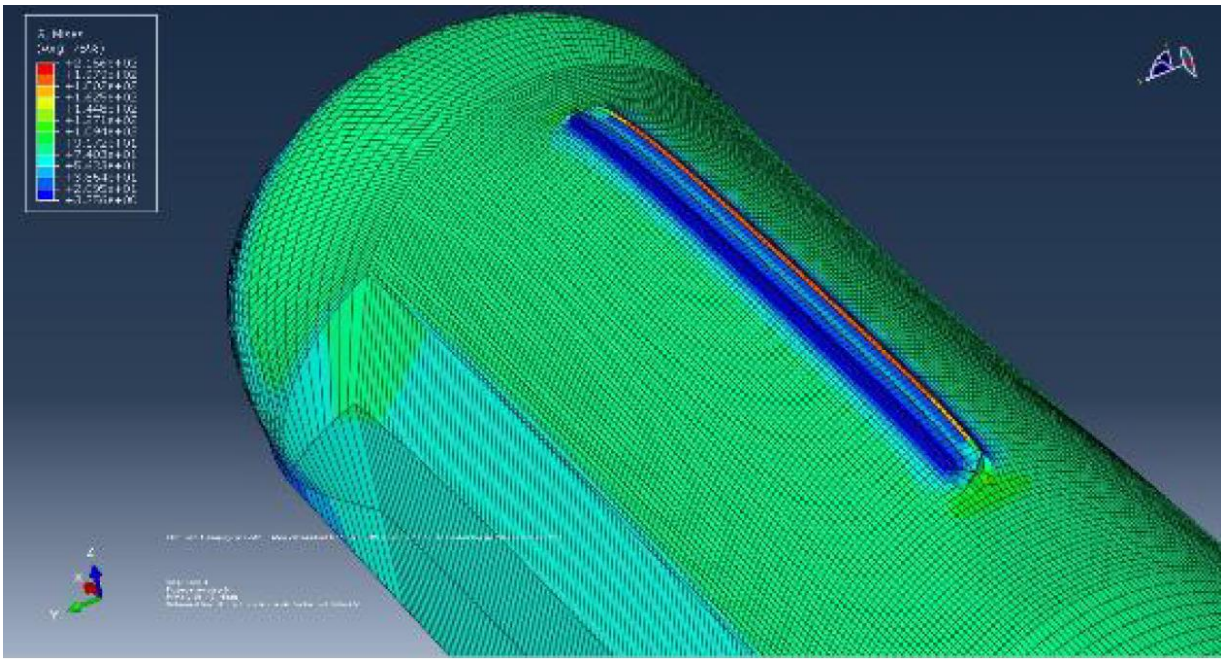

Figure 6-81: First step of the simulation and von Mises stresses; initial crack depth a = 2 mm,

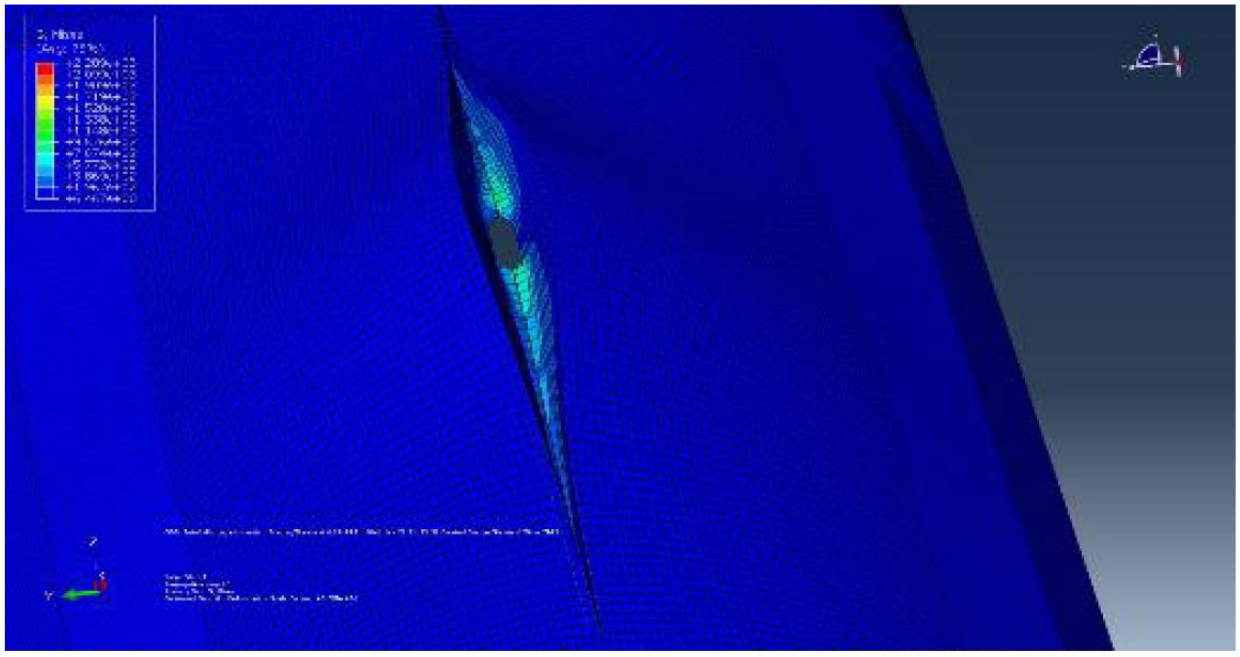

Figure 6-82: Propagation step 25- penetration, from von Mises stresses; a = 2mm

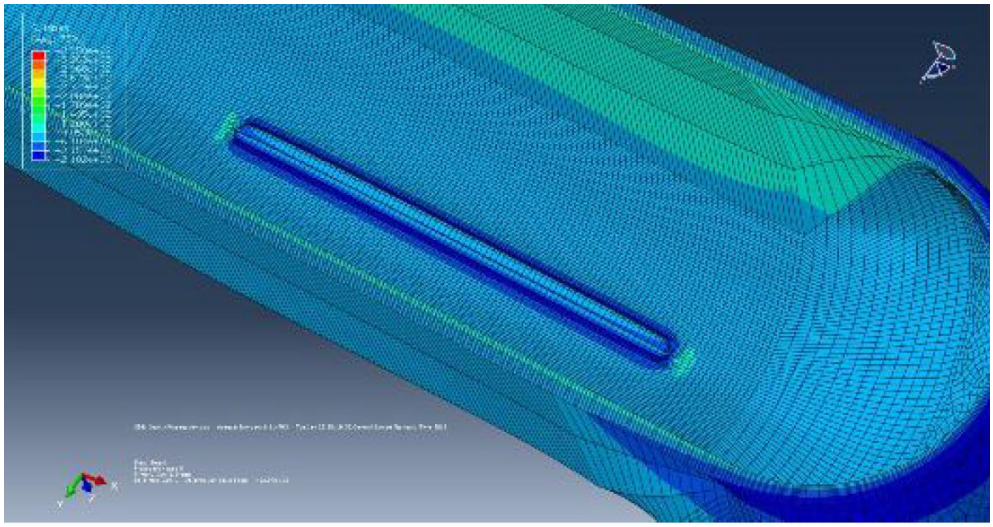

Figure 6-83: First step, von Mises stresses; a = 2mm on the inside of the pipe

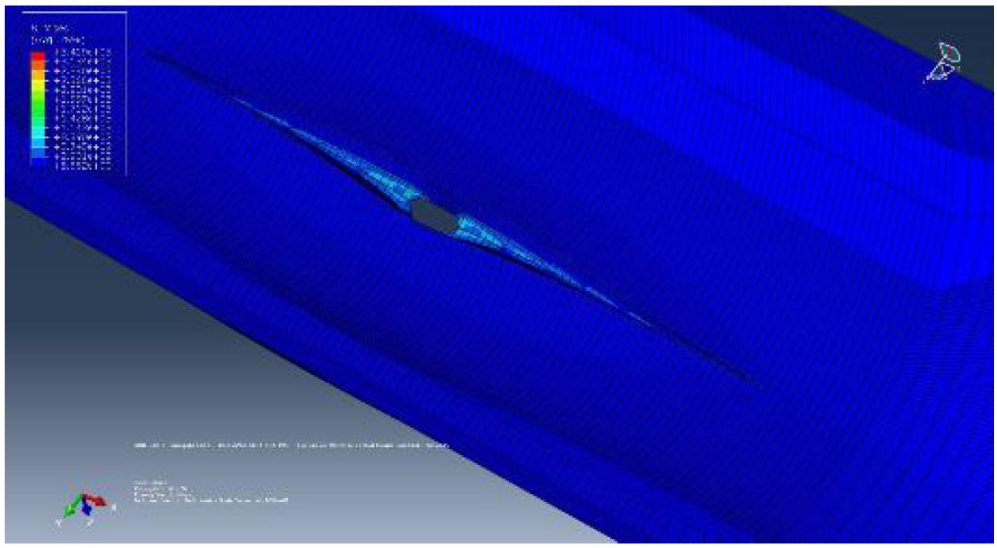

Figure 6-84: Step 25 - penetration, from Mises stresses; a = 2mm, inner side of the pipe

The influence of the initial crack length will be considered below. In the previous one's simulations, the initial crack was in the axial direction of length 2c = 200mm, which is quite a large length and it can be seen that pipe failure occurs extremely quickly. For consideration fatigue behavior for different crack dimensions, both in depth and in length, was taken the initial crack length of 2c = 14mm. Depth at the beginning of the simulation was a = 2mm. The simulation was done in 50 steps because it was estimated that by then the crack would open (penetrate through the pipe wall), which happened in the 32nd step. Obtained data which showing the influence of crack length in the axial direction are shown in ***Figure 6.85***. The contribution to a smaller initial crack length, at which the fatigue life is 9.4 times longer (401 104.3 cycles) than at length 2c = 200mm (42 635 cycles).

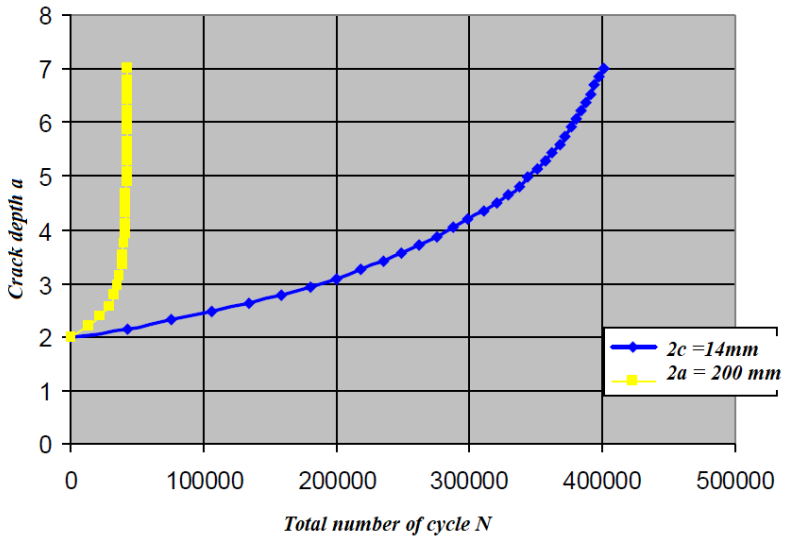

Figure 6-85: Influence of crack length in axial direction at initial crack depth a = 2mm and for two values of crack length in axial direction: 2c = 14mm and 2c = 200mm; Ratio R = 0.7.

A simulation for a crack of length 2a = 14 mm and depth a = 2 mm was also done for two values of stress quotients R = 0.7 and R = 0.8, and this effect is shown in ***Figure 6.86***. at R = 0.8 to crack opening takes 1964394 cycles, which is 4.9 times longer than for the same crack and ratio R = 0.7. ***Figure 6.87*** shows the dependence of the number of cycles (log N) for the propagation steps and the initial one crack with dimensions a = 2 mm and 2c = 14 mm, for R = 0.7

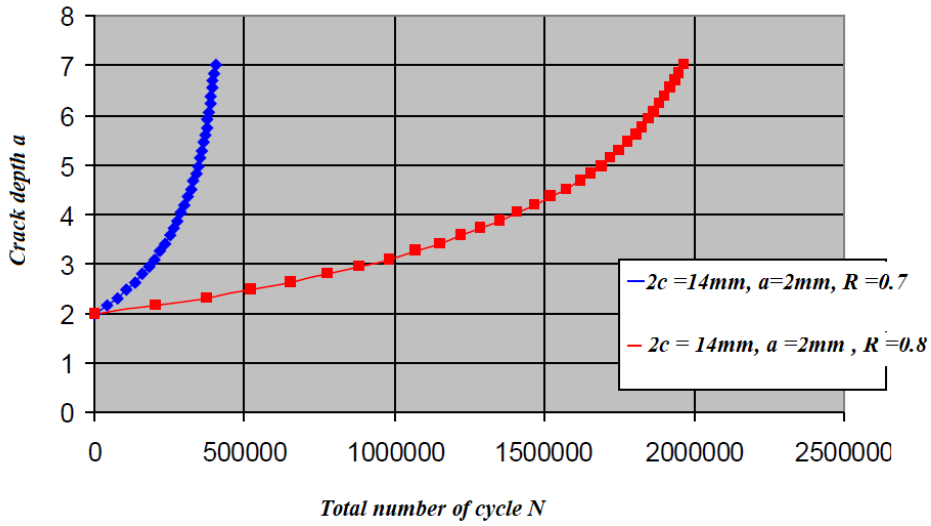

Figure 6-86: Influence of stress Quotient R at initial crack depth of a = 2mm and length cracks in the axial direction 2c = 14mm

As can be seen, the number of cycles N is gradually decreasing with increasing number of steps, which goes to contribution to the fact that the crack grows evenly in all directions, until it breaks through the wall, and after that.

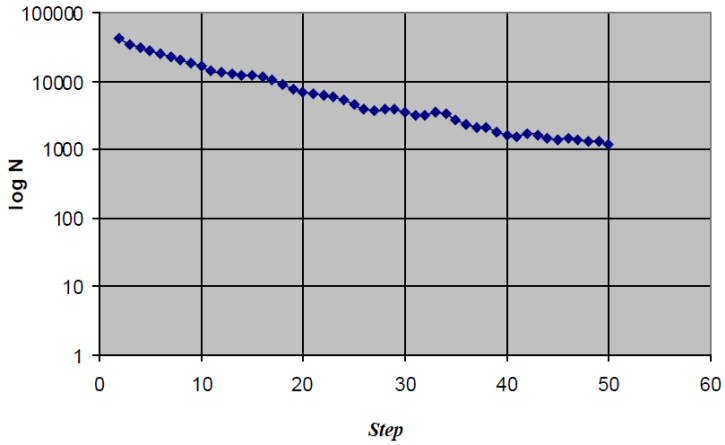

Figure 6-87: Obtained number of cycles (log N) for propagation steps at initial dimensions

Figures 6.88-6.93 show the appearance of the network and the stresses around the crack of initial dimensions 2c = 14mm and a = 2mm in several characteristic propagation steps.

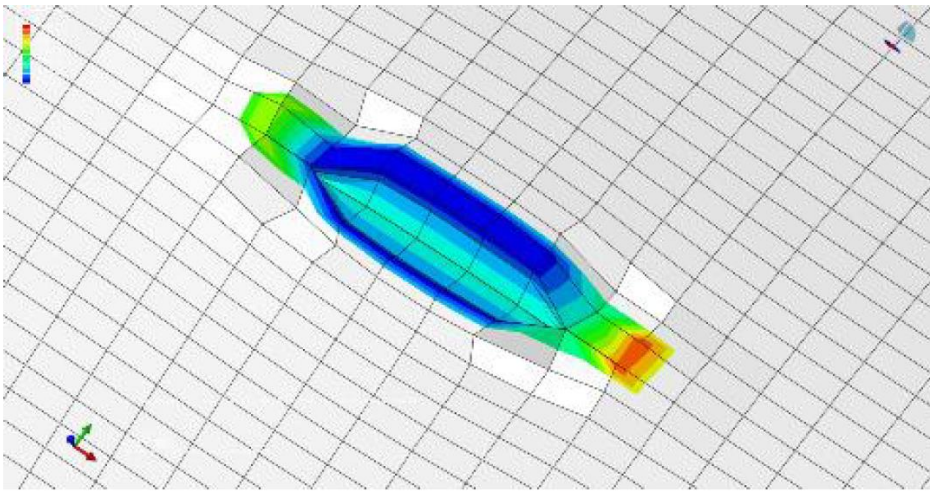

Figure 6-88: Propagation step1 - crack opening

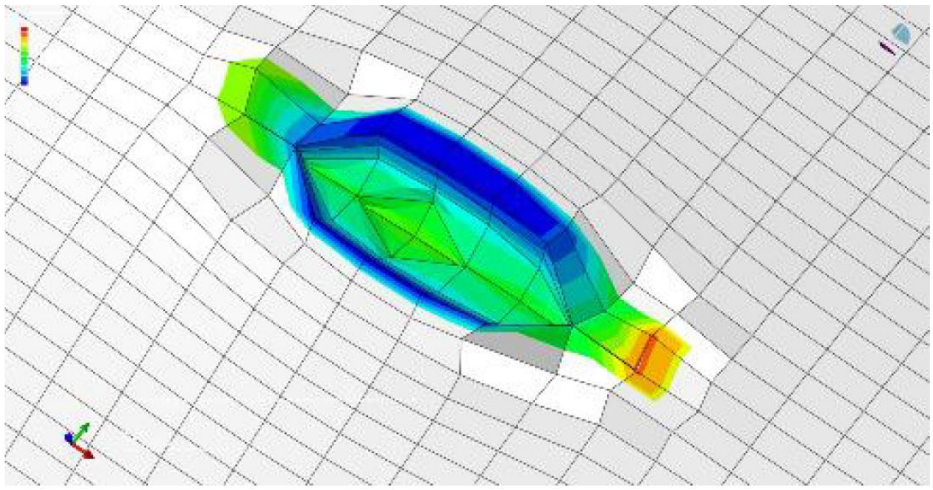

Figure 6-89: Propagation step 4

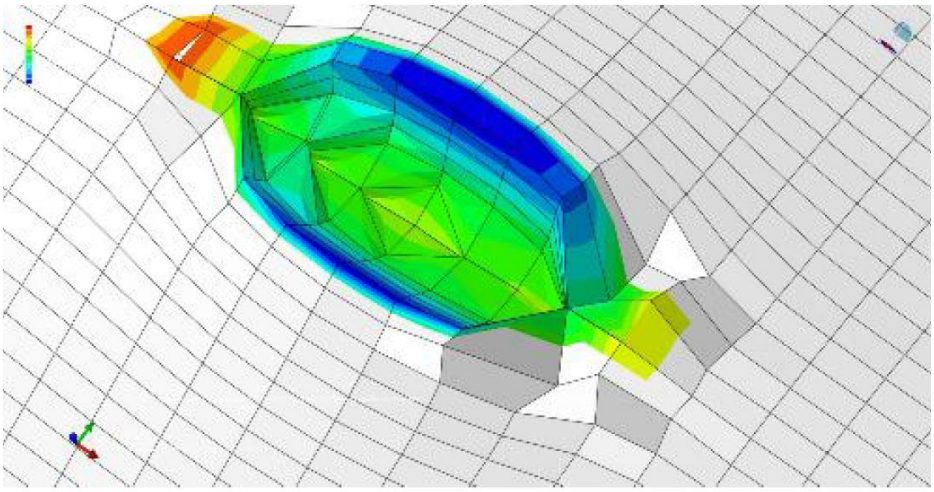

Figure 6-90: Propagation step 12

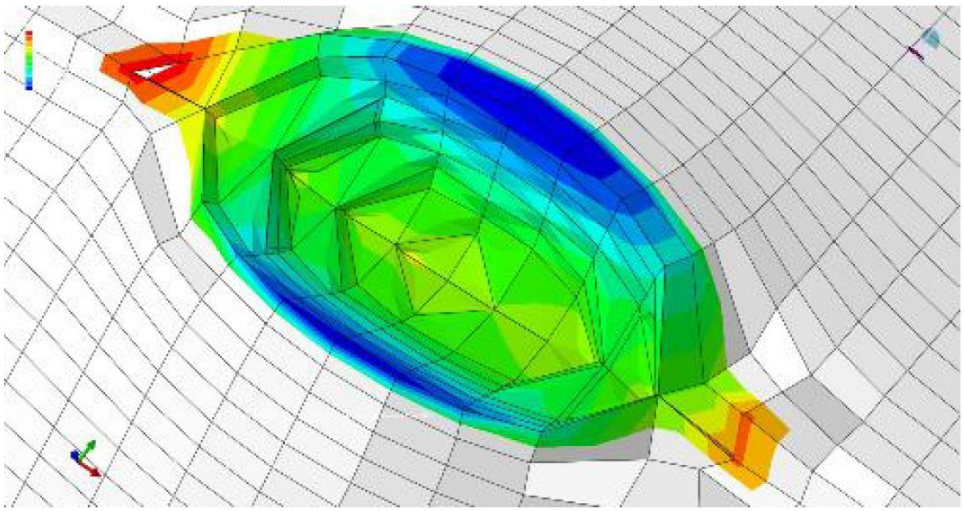

Figure 6-91: Propagation step 27

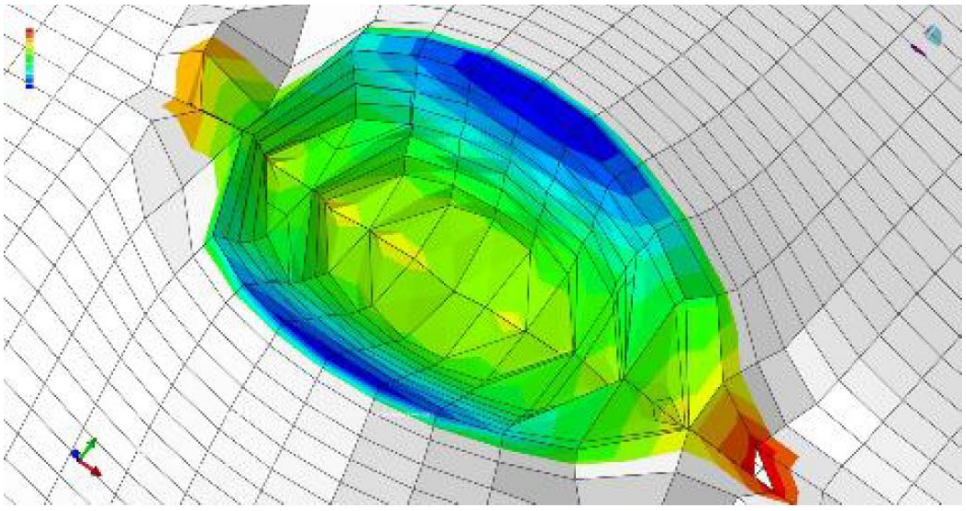

Figure 6-92: Propagation step 31

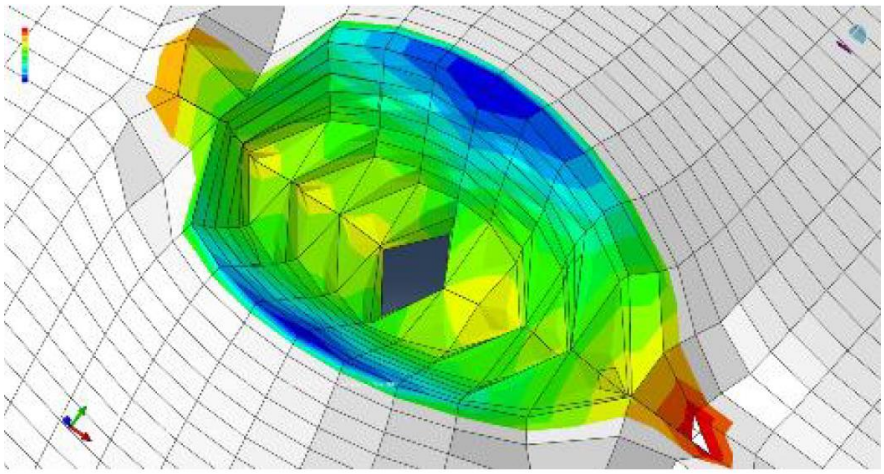

Figure 6-93: Propagation step 32 - crack penetration through the pipe wall

Figure 6.94 shows the comparative results of the obtained fatigue life predictions for different lengths (in the axial direction) of the initial pipe damage and two values of the stress ratio R, A similar trend can be observed when it comes to the influence of voltage range and magnitude damage to the remaining life which is that the change in the voltage range has a more significant impact than the reference value of external damage. Of course, the number of cycles is significantly smaller here, because it is a simulation done for real construction and 3D crack.

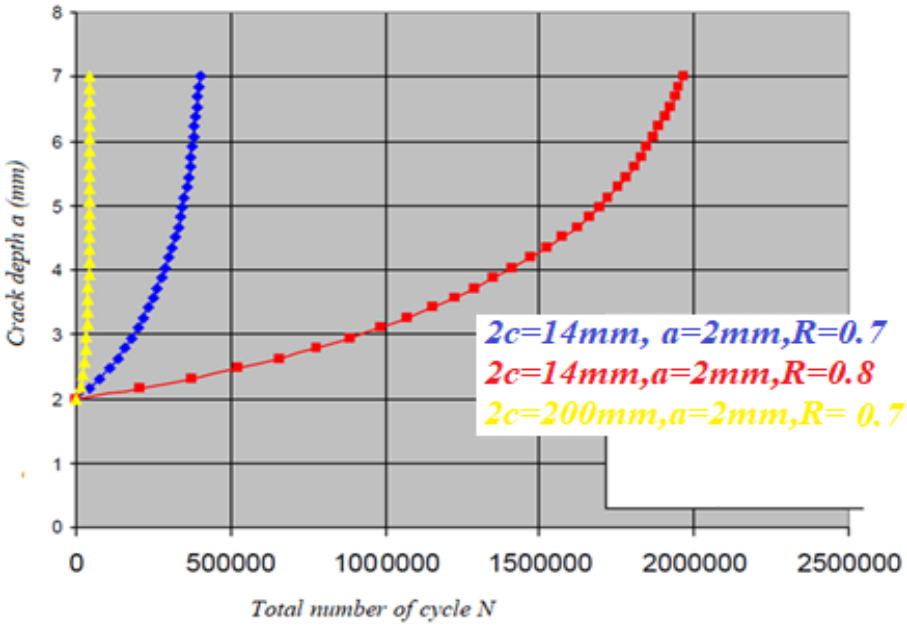

Figure 6-94: Comparative results of obtained fatigue life predictions for different lengths (in axial direction) of the initial pipe damage and two values of the stress ratio R.

The results presented here show the possibility of applying the Extended Finite Element Method (XFEM), as method, in a three-dimensional simulation of fatigue crack growth on pipe type geometry. The problem of integrity and resistance assessment according to the fatigue fracture of welded pipes made of high strength steel can be successful using the extended finite element method.

Of course, the results presented here are a contribution to the idea that extensive, time- consuming, expensive, and very often difficult to perform experimental tests can be effectively replaced by numerical simulations.

7 CONCLUSION

Functionality and safety in operation are two important requirements for successful construction, in addition to the requirement of design strength, risk of fracture must be considered, which largely depends on the properties of the welded joints as potential defect zone. The fatigue life of the structure includes a period of gradual accumulation of crack-like damage in the material of the structural element under conditions of dynamic loading. This period represents the process of formation and growth of the fatigue crack, until the final loss of the structure due to fracture. 90% of defects need not be repaired, but just more carefully monitored. The decision was made by the authorities (DOT) who concluded that ”fracture mechanics is an acceptable basis for allowable exception form the standards and rule since it was proved by conservative approach of fracture mechanics that these defects will not cause failure”, the reasoning that if the crack driving force (crack driving force at its maximum) is smaller than fracture toughness (fracture toughness at its minimum), failure will not occur. Based on this reasoning, other procedures were introduced, e.g. FAD, which combines brittle fracture with plastic collapse, in a relatively simple way. The achieved scientific level of fracture mechanics has been essential for accepting its principles and parameters in structural integrity, life assessment this approach is beneficial even in a design stage, from here it was introduced the concept of safe-fail design, instead of the safe- life approach, by assumption, assume crack existence, and prove safe-fail life of a component, using the following reasoning: if NDT has not found any cracks, then one can assume that the presence of small crack size, and can calculate the number cycles for such a crack, period of time needed for the crack to grow up to the critical value, evaluated according to LEFM rules. Based on the initial crack length and Paris law, i.e. The relation between fatigue crack growth rate and stress intensity factor amplitude was used Paris law, to calculate the remaining life of the component but direct integration of Paris law provides a conservative estimate of residual life and probability of failure since it can handle only simple geometry, Another problem is the effect of geometry factor Y (a/W), since it might need small steps in the direct integration process to accommodate significant changes in its value during crack growth and change of its length. for more precise analysis of complex geometries, FEM and XFEM. should be used. From all presented results following conclusions can be drawn:

- The problem of integrity and resistance assessment according to the fatigue fracture of welded pipes made of high strength steel can be successful using the extended finite element method. The results presented here are a contribution to the idea that extensive, time-consuming,

expensive, and very often difficult to perform experimental tests can be effectively replaced by numerical simulations. This dissertation aimed to investigate the behavior in case of fatigue damage of welded pipes made of API J55 steel. By applying the parameters of mechanics fracture, obtained on the basis of experimental research, an assessment of the remaining century of protective welded pipes with external axial surface crack, made of API J55 steel. The influence of stress range and the longitudinal axial crack was analyzed at the same time with crack depth on the remaining fatigue life, and it is shown that is more influence of the stress range and surface crack dominant compared of the obvious depth of damage. , it can be concluded that it is for this species problems, in cases where there is a crack of a certain depth in the structural element, it is more important to monitor the load range and surface crack also in addition to monitor the depth this explains why the tube collapsed in a shorter time than expected.

- The obtained results show the efficiency of the application of the extended finite element method - XFEM (Extended Finite Element Method), in a three-dimensional simulation of fatigue crack growth by comparing the numerical and experimental results for a test pipe made from the same material API J55, was successfully verified in determining fatigue life.
- The fatigue life is more sensitive to changes in the stress range and axial surface crack than the values of the depth crack. The presence of deep cracks in the case of stable pressures with small longitudinal cracks takes a longer time to penetrate the wall and even with the happening of leaks it continues in service and failure may in the expected time designed for the pipe or longer.
- The total failure probability, as a function of the fraction of crack length (surface crack) , that was noticed from results obtained from XFEM method and that was close with the experimental and also from the analytical method, demonstrated the effect of crack length on collapsing velocity and thus fatigue life.
- occur leak probability when crack breaks through the wall but there no failure and the pipe continue to serves for the expected period in case the initial longitudinal cracks are small, this explains the failure of the pipe after 8 years before the expected time.
- Comparing results obtained directly by applying Paris law on the model of a standard Charpy specimen made of API J55 steel, one can see that the agreement with XFEM and experimental method is good, we note that the results obtained from the analysis are very closed to the results obtained by the experiment, and the slight difference was due to the difference in Δa, which leads to an effect in values the geometry coefficient constant Y (a/W) the user in direct integration of Paris law.

- The geometry coefficient constant Y (a / W) the user in direct integration of Paris law one of the main reasons that lead to the difference in results.
- The difference in the results between the analytical and numerical methods in a pipe model goes back to the part regarding of the longitudinal axial crack analysis, in the three-dimensional simulation the length of the crack was calculated after the crack penetrates the wall by increasing length until it reaches failure, but in the analytical method using the Paris equation it starts from c to the point of failure c_c.
- Risk based approach is an engineering tool for assessment of structural integrity, based on the risk matrix presentation as the most suitable for managers to make decisions, even difficult ones.
- Decisions that are made based on an engineering assessment of structural integrity (and later, structural life), this is the point where managers and engineers meet from two different directions, one being the decision-making process, the other being providing reliable technical data. At this point, engineers have to provide all the evidence and data to those who have to decide. The problem here is that managers do not understand technical data, so the statement like "K_I is half the value of K_{IC}" means practically nothing to them. herein lies the importance of using a risk matrix
- Analysis solutions for axial surface defects versus XFEM data available shows that Newman solutions were very closed compared with API 579-1 / ASME FFS-1 and BS 7910.

7.1 Recommendation for future work

- More precise methods like FEM and experiment are more expensive, especially the later ones, but often inevitable in the case of complicated components. Probably the best approach would be to adopt a two-phase decision-making process, with the first one based on a simple engineering approach, based on analytical tools, and then, if needed, more sophisticated numerical and / or experimental analysis, in the second phase.
- We can use analytical methods when having uncomplicated geometric shapes to be obtained results in a short time instead of applying expensive experiments or by applying XFEM, where it is necessary to model a test tube, generate a network, and then define the load, boundary conditions.
- The existence of a database of data obtained from experiments, realistic events, and numerical results and arranging them in matrices that help in calculating the life expectancy by analytical methods without the need to conduct costly experiments especially if the geometric shape is uncomplicated and by knowing the percentage of error between the analytical methods,

experimental methods and numerical methods that are inferred comparison with the data base, and put that percentage of error the form of a factor, the results will be more accurate.

References

[1] American Petroleum Institute, “Specification for Casing and Tubing - Purchasing Guidelines,” vol. API 5CT, no. July 2011, 2006.

[2] H. Iqbal, S. Tesfamariam, H. Haider, and R. Sadiq, “Inspection and maintenance of oil & gas pipelines: a review of policies,” *Struct. Infrastruct. Eng.*, vol. 13, no. 6, pp. 794–815, 2017, doi: 10.1080/15732479.2016.1187632.

[3] H. A. Gabbar and H. A. Kishawy, “Framework of pipeline integrity management,” *Int. J. Process Syst. Eng.*, vol. 1, no. 3/4, p. 215, 2011, doi: 10.1504/ijpse.2011.041560.

[4] J. . V. A. W. Dawotola, P.H.A.J.M van Gelder, “Risk Assessment of Petroleum Pipelines using a combined Analytical Hierarchy Process - Fault Tree analysis,” *Proc. 7th Int. Probabilistic Work. Fac. Civ. Eng. Geosci. Delft Univ. Technol. Stevinweg 1, 2628CN Delft, Netherlands*, vol. 13, no. 2006, pp. 491–501, 2009.

[5] I. M. Program, “Mechanical Damage,” *Dev. Agric. Eng.*, vol. 8, no. C, pp. 260–283, 1986, doi: 10.1016/B978-0-444-99523-0.50017-9.

[6] M. J. (Kiefner and A. I. . Rosenfeld, “Factors to consider when evaluating damage to pipelines,” *Oil Gas J.*, vol. 2, no. September, 2002.

[7] M. Science, “High Frequency Induction Welding & Post-Welding Heat Treatment of,” no. June, 2011.

[8] B. J. Wright and E. H. Equipment, “Optimizing Efficiency in,” no. December, 1999.

[9] L. Forschungsverbund, J. I. Asperheim, P. Das, B. Grande, D. Hömberg, and T. Petzold, “Numerical simulation of high-frequency induction welding in longitudinal welded tubes,” no. 2600, 2020.

[10] P. M. Rr, “MICROSTRUCTURAL CHANGES IN THE FORGE WELD AREA DURING HIGH-FREQUENCY ELECTRIC RESISTANCE WELDING,” vol. 1, pp. 59–62, 2016.

[11] G. P. Kelkar, “WJM Technologies,” no. 562, pp. 1–5.

[12] M. Coramik and Y. Ege, “Discontinuity inspection in pipelines: A comparison review,” *Meas. J. Int. Meas. Confed.*, vol. 111, no. July, pp. 359–373, 2017, doi: 10.1016/j.measurement.2017.07.058.

[13] “Crack propagation analysis of welded joints by numerical and experimental investigations Diplomarbeit FAHEEM SHAH,” 2015.

[14] B. Ernst and W. Jensen, “Master Thesis Numerical Analysis of Crack Propagation Fracture Mechanics and Numerical Programming,” no. June, 2015.

[15] “FATIGUE LIFE ASSESSMENT OF DAMAGED INTEGRAL SKIN – STRINGER PANELS INTEGRALNIH OPLATA- UZDUŽNICI PANELA,” 2018.

[16] T. Edition, *Thir d Edition MECHANICS FRACTURE Fundamentals and Applications*. .

[17] C. Ruggieri and F. Dotta, "Numerical modeling of ductile crack extension in high pressure pipelines with longitudinal flaws," *Eng. Struct.*, vol. 33, no. 5, pp. 1423–1438, 2011, doi: 10.1016/j.engstruct.2011.01.001.

[18] J. Catalán Castilla *et al.*, "FATIGUE CRACK GROWTH IN HYDROGEN PIPELINE STEELS," vol. ثقثق ث, no. ثقثقثق ثق, p. ثقثقثقثقثق, 2018.

[19] J. . N. and J. I.S. Raju, "Stress-Intensity Factors for Internal and External Surface," *J. Press. Vessel Technol.*, vol. 1, no. 1982, pp. 3–8, 2016.

[20] J. W. O. Pan, "FRACTU RE M EC HAN I CS AND FATIGUE CRACK PROPAGATION JWO PAN AND SHIH-HUANG LIN UNIVERSITY OF MICHIGAN 6."

[21] P. Moore and G. Booth, "Weld fatigue assessment," *Weld. Eng. Guid. to Fract. Fatigue*, pp. 175–184, 2015, doi: 10.1533/9781782423911.2.175.

[22] "Chapter_9e_Fatigue." .

[23] P. D. studen University of Belgrade, Innovation Centre of the Faculty of Mechanical Engineering, Belgrade, Serbia 2) University of Belgrade, Faculty of Mechanical Engineer- ing, Serbia, asedmak@mas.bg.ac.rs 3) Omsknefttimproekt, filijala Balkans, Belgrade, Serbia 4) U, "SAF€RA – EUROPEAN PROJECT ON INDUSTRIAL SAFETY Originalni," *Экономика Региона*, vol. 12, no. 1990, pp. 12–30, 2012.

[24] O. D. V. C. Legure, "A. Sedmak 1 , K. Č oli ć 2 , Z. Burzi ć 3 , S. Tadi ć 2," vol. 10, no. 2, pp. 161–164, 2010, [Online]. Available: https://pdfs.semanticscholar.org/43d1/ddf22148487aee1251a08092a097b23a0cff.pdf?_ga=2.41821280.336854893.1585487159-1172291687.1585487159.

[25] R. Jovicic and S. Sedmak, "Quality assurance of storage tanks after in-service crack repairs," no. July 2016, 2013.

[26] T. Golubovic, A. Sedmak, V. Spasojevic Brkic, S. Kirin, and E. Veg, "Welded joints as critical regions in pressure vessels – Case study of vinyl-chloride monomer storage tank," *Hemijska Industrija*, vol. 72, no. 4. pp. 177–182, 2018, doi: 10.2298/HEMIND171009006G.

[27] "RISK ANALYSIS IN STRUCTURAL INTEGRITY," vol. 10, no. 2, p. 2002, 2002.

[28] A. P. Institute, "API RP 581 Risk-based Inspection Methodology, Api 581," no. September, p. 306, 2016.

[29] M. L. Ivana Vučetić, Snezana Kirin, Aleksandar Sedmak, Tamara Golubović, "SOME ACHIEVEMENTS IN RBIM IMPLEMENTATION ACCORDING TO RIMAP APPROACH," vol. 15, no. 2, pp. 79–84, 2015.

[30] I. Vučetić, S. Kirin, A. Sedmak, T. Golubović, and M. Lazić, “Risk management of a hydro power plant – fracture mechanics approach,” *Tehnicki Vjesnik*, vol. 26, no. 2. pp. 428–432, 2019, doi: 10.17559/TV-20180618102041.

[31] R. Zaidi *et al.*, “Risk assessment of oil drilling rig welded pipe based on structural integrity and life estimation,” *Eng. Fail. Anal.*, vol. 112, , p. 104508, 2020, doi: 10.1016/j.engfailanal.2020.104508.

[32] R. T. Selvan and N. A. Siddqui, “Risk Assessment of Natural Gas Gathering Station & Pipeline Network,” *Int. J. Theor. Appl. Mech.*, vol. 12, no. 2, pp. 227–242, 2017.

[33] T. Golubovic, A. Sedmak, V. Spasojevic Brkic, S. Kirin, and E. Veg, “Welded joints as critical regions in pressure vessels – Case study of vinyl-chloride monomer storage tank,” *Hem. Ind.*, vol. 72, no. 4, pp. 177–182, 2018, doi: 10.2298/HEMIND171009006G.

[34] P. N. Botsaris, A. D. Naris, and G. Gaidajis, “A risk based inspection (rbi) preventive maintanance programme: A case study,” *Eng. Asset Lifecycle Manag. - Proc. 4th World Congr. Eng. Asset Manag. WCEAM 2009*, no. September, pp. 902–911, 2009, doi: 10.1007/978-0-85729-320-6_102.

[35] B. B. C. srl Vittorio Colombo, Cristina Panizza and I. Milan, “Corrosion and Asset Integrity Management in Oil and Gas Production, Process, Transportation and Storage Facilities,” *J. Chem. Inf. Model.*, vol. 53, no. 9, pp. 1689–1699, 2019.

[36] E. Dzindo, S. Sedmak, Z. Radakovic, and I. Cvetkovic, “Crack growth resistance of weldment constituents,” *Procedia Struct. Integr.*, vol. 13, pp. 420–423, 2018, doi: 10.1016/j.prostr.2018.12.070.

[37] I. Površinskih and Z. Prslina, “STUDY OF SURFACE FATIGUE CRACKS,” vol. 6, no. 3, pp. 97–110, 2006.

[38] L. Milović *et al.*, “Determination of fatigue crack growth parameters in welded joint of HSLA steel,” *Struct. Integr. Life*, vol. 11, no. 3, pp. 183–187, 2011.

[39] A. Sedmak, “Fracture and fatigue behavior of NIOMOL 490K welded joint,” January 2008, 2015.

[40] A. T. Submitted, I. N. Partial, F. Of, T. H. E. Requirements, T. H. E. D. Of, and B. O. F. Technology, “Development of Exponential Model To Find Fatigue Crack Growth and Residual Life for Constant Amplitude Loading Development of Exponential Model To Find Fatigue Crack Growth and Residual Life for,” pp. 1–40.

[41] J. P. GEORGE E. DIETER, “Mechanical Metallurgy.” .

[42] A. T. Submitted *et al.*, “Prediction of Fatigue Crack Propagation Life in Single Edge Notched Beams Using Exponential Model . a Thesis Submitted in Partial Fulfillment of Prediction of Fatigue Crack Propagation Life in Single Edge Notched Beams Using,” no. 211, 2013.

[43] R. G. Bundynas and J. K. Nisbett, “Chapter 6: Fatigue Failure Resulting from Variable Loading,” *Shigley’s Mech. Eng. Des.*, no. 8, pp. 273–349, 2015.

[44] J. Marques, “Stress Ratio Effects on the fatigue Properties of Biaxially Loaded Tubular FRP-Specimens – Experimental Study by Jorge Marques Matriculation number: 4345066 Th,” no. 6, 2013.

[45] J. C. Lippold, *Welding Metallurgy and Weldability*. John Wiley & Sons, Inc., Hoboken, New Jersey.

[46] R. O. RITCHIE, “Mechanisms of fatigue-crack propagation in ductile and brittle solids R.O.,” © *2000 Kluwer Acad. Publ. Print. inthe Netherlands. Mech.*, doi: 10.1088/1009-0630/14/2/06.

[47] M. C. Niu, *Airframe Stress Analysis and Sizing (2nd Ed 1999)*. 1999.

[48] R. I. Stephens, “Fatigue Design Criteria,” *Encycl. Mater. Sci. Technol.*, pp. 2910–2918, 2001, doi: 10.1016/b0-08-043152-6/00518-0.

[49] C. Outline, *12 Fatigue and Fracture*. 2014.

[50] E. Puntel, G. Bolzon, and V. E. Saouma, “Fracture mechanics based model for joints under cyclic loading,” *J. Eng. Mech.*, vol. 132, no. 11, pp. 1151–1159, 2006, doi: 10.1061/(ASCE)0733-9399(2006)132:11(1151).

[51] C. S. and M. M. G Pluvinage*, J.Capelle**, “DOMAIN FAILURE ASSESSMENT DIAGRAMS FOR DEFECT ASSESSMENT OF GAS PIPES.” .

[52] P. G. Kossakowski, “Assessment of Material Behaviour and Structural Integrity of Engineering Structures Based on R6 Procedure,” *Adv. Mater. Sci.*, vol. 13, no. 4, pp. 25–32, 2014, doi: 10.2478/adms-2013-0017.

[53] M. Bergman, “Stress Intensity Factors for Circumferential Surface Cracks in Pipes,” *Fatigue Fract. Eng. Mater. Struct.*, vol. 18, no. 10, pp. 1155–1172, 1995, doi: 10.1111/j.1460-2695.1995.tb00845.x.

[54] X. Wang and S. B. Lambert, “Weight functions and stress intensity factors for semi-elliptical cracks in T-plate welded joints,” *Fatigue Fract. Eng. Mater. Struct.*, vol. 21, no. 1, pp. 99–117, 1998, doi: 10.1046/j.1460-2695.1998.00472.x.

[55] Y. J. Kim, N. S. Huh, and Y. J. Kim, “Reference stress based elastic-plastic fracture analysis for circumferential through-wall cracked pipes under combined tension and bending,” *Eng. Fract. Mech.*, vol. 69, no. 3, pp. 367–388, 2002, doi: 10.1016/S0013-7944(01)00074-1.

[56] Y. J. Kim, J. S. Kim, Y. J. Park, and Y. J. Kim, “Elastic-plastic fracture mechanics method for finite internal axial surface cracks in cylinders,” *Eng. Fract. Mech.*, vol. 71, no. 7–8, pp. 925–944, 2004, doi: 10.1016/S0013-7944(03)00159-0.

[57] J. S. Park, S. J. Kim, K. H. Kim, S. H. Park, and C. S. Lee, “A microstructural model for predicting high cycle fatigue life of steels,” *Int. J. Fatigue*, vol. 27, no. 9, pp. 1115–1123, 2005, doi: 10.1016/j.ijfatigue.2005.01.013.

[58] A. Fatemi, Z. Zeng, and A. Plaseied, “Fatigue behavior and life predictions of notched specimens made of QT and forged microalloyed steels,” *Int. J. Fatigue*, vol. 26, no. 6, pp. 663–672, 2004, doi: 10.1016/j.ijfatigue.2003.10.005.

[59] X. Wu, Y. Katada, S. G. Lee, and I. S. Kim, “Hydrogen-involved tensile and cyclic deformation behavior of low-alloy pressure vessel steel,” *Metall. Mater. Trans. A Phys. Metall. Mater. Sci.*, vol. 35 A, no. 5, pp. 1477–1486, 2004, doi: 10.1007/s11661-004-0256-8.

[60] S. T. Method, “Standard Test Method for Measurement of Fracture Toughness 1,” no. February, 2017, doi: 10.1520/E1820-16.

[61] ASTM E647−13, “Standard Test Method for Measurement of Fatigue Crack Growth Rates,” *Am. Soc. Test. Mater.*, pp. 1–50, 2014, doi: 10.1520/E0647-15E01.2.

[62] Ž. Šarkoćević, M. Arsić, A. Sedmak, B. Međo, and M. Mišić, “Assessment of the integrity of welded pipes,” *Zast. Mater.*, vol. 55, no. 3, pp. 287–292, 2015, doi: 10.5937/zasmat1403287s.

[63] A. Sedmak, “Numerical analysis of surface crack problems in pressure vessels,” no. January 2004, pp. 26–31, 2018.

[64] L. L. Vulićević, M. Arsić, Ž. Šarkoćević, A. Sedmak, and M. Rakin, “Structural life assessment of oil rig pipes made of API J55 steel by high frequency welding,” *Teh. Vjesn.*, vol. 20, no. 6, pp. 1091–1094, 2013.

[65] F. A. June, “the Extended Finite Element Method in Fatigue Life Predictions of Oil Well Welded,” 2015.

[66] Ž. Šarkoćević *et al.*, “Damage level estimate of API J55 steel for welded seam casing pipes,” *Strojarstvo*, vol. 51, no. 4, pp. 303–311, 2009.

[67] S. Kirin, A. Sedmak, R. Zaidi, A. Grbović, and Ž. Šarkočević, “Comparison of experimental, numerical and analytical risk assessment of oil drilling rig welded pipe based on fracture mechanics parameters,” *Eng. Fail. Anal.*, vol. 114, p. 104600, 2020, doi: 10.1016/j.engfailanal.2020.104600.

[68] J. C. Newman and I. S. Raju, “Stress-intensity factors for internal surface cracks in cylindrical pressure vessels,” *J. Press. Vessel Technol. Trans. ASME*, vol. 102, no. 4, pp. 342–346, 1980, doi: 10.1115/1.3263343.

[69] X. W. & S. B. Lambert*, “Stress intensity factors and weight functions for longitudinal semi-elliptical surface cracks in thin pipes Department,” *ht. J. Pres. Vex. Pip.*, vol. 25, no. 3, pp. 291–304, 1996, doi: 10.1046/j.1460-2695.2002.00502.x.

[70] T. L. Anderson and G. Glinka, “A closed-form method for integrating weight functions for part-through cracks subject to Mode I loading,” *Eng. Fract. Mech.*, vol. 73, no. 15, pp. 2153–2165, 2006, doi: 10.1016/j.engfracmech.2006.04.027.

[71] I. O. for Standardization, “BS 7910:2005 Guide to methods for assessing the acceptability of flaws in metallic structures,” vol. 3, 2005.

[72] D. A. Osage and J. L. Janelle, “API 579-1/ASME FFS-1 2007 - A joint API/ASME Fitness For Service standard for pressurized equipment,” *Am. Soc. Mech. Eng. Press. Vessel. Pip. Div. PVP*, vol. 1, pp. 777–791, 2008, doi: 10.1115/PVP2008-61796.

[73] R. C. Cipolla and D. R. Lee, “Pvp2012-78187 for Circumferential Id Surface Flaws in Cylinders in,” pp. 1–13, 2012.

[74] P. Institute, D. C. 20005407. 1220 L Street, Northwest Washington, 202-682-8000, and Date:, *API 579: Fitness For Service Engineering*. 2016.

[75] P. Vessel, P. Codes, R. C. Cipolla, and D. R. Lee, “Aptech Engineering Services Principal Engineer,” vol. 480, pp. 1–12, 2016.

[76] “ElliptCylindZheng (1).pdf.” .

[77] M. El-Sayed, A. E. El Domiaty, and A. H. I. Mourad, “Fracture Assessment of Axial Crack in Steel Pipe under Internal Pressure,” *Procedia Eng.*, vol. 130, pp. 1273–1287, 2015, doi: 10.1016/j.proeng.2015.12.297.

[78] Ľ. Gajdoš and M. Šperl, “Application of a fracture-mechanics approach to gas pipelines,” *World Acad. Sci. Eng. Technol.*, vol. 73, no. 1, pp. 480–487, 2011.

[79] A. Keprate, R. M. Chandima Ratnayake, and S. Sankararaman, “Minimizing hydrocarbon release from offshore piping by performing probabilistic fatigue life assessment,” *Process Saf. Environ. Prot.*, vol. 106, pp. 34–51, 2017, doi: 10.1016/j.psep.2016.11.019.

[80] A. M. C. R. S. S. Keprate, “A SURROGATE MODEL FOR PREDICTING STRESS INTENSITY FACTOR: AN APPLICATION TO OIL AND GAS INDUSTRY Arvind,” no. June, pp. 2016–2018, 2017, doi: 10.1115/omae2017-61091.

[81] P. M. S. and T. W. THORPE, “A CRITICAL REVIEW OF CRACK TIP STRESS INTENSITY FACTORS FOR SEMI-ELLIPTIC CRACKS*,” *Fatigue Fract. Eng. Mater. Struct.*, vol. 4, no. 4, pp. 291–309, 1981, doi: 10.1111/j.1460-2695.1981.tb01127.x.

[82] R. W. Bourga, “COMPARISON OF BS 7910 AND API 579-1/ASME FFS-1 SOLUTIONS WITH REGARDS TO LEAK-BEFORE-BREAK Renaud,” *July 17-21, 2016, Vancouver, Br. Columbia, Canada PVP2016-63876*, pp. 1–21, 2016.

[83] L. L. Vulićević, A. Rajić, A. Grbović, A. Sedmak, and Ž. Šarkočević, “Fatigue life prediction of casing welded pipes by using the extended finite element method,” *Frat. ed Integrita Strutt.*, vol. 10, no. 36, pp. 46–54, 2016, doi: 10.3221/IGF-ESIS.36.05.